Updating the Ionospheric Propagation Factor, M(3000)F2, Global Model using the Neural Network Technique and Relevant Geophysical Input Parameters

---

A thesis submitted in partial fulfilment of the
requirements for the degree of

MASTER OF SCIENCE

---

of

RHODES UNIVERSITY

By

Samuel Iyen Jeffrey Oronsaye

June 2012

Abstract

This thesis presents an update to the ionospheric propagation factor, M(3000)F2, global empirical model developed by Oyeyemi et al. (2007) (NNO). An additional aim of this research was to produce the updated model in a form that could be used within the International Reference Ionosphere (IRI) global model without adding to the complexity of the IRI. M(3000)F2 is the highest frequency at which a radio signal can be received over a distance of 3000 km after reflection in the ionosphere. The study employed the artificial neural network (ANN) technique using relevant geophysical input parameters which are known to influence the M(3000)F2 parameter. Ionosonde data from 135 ionospheric stations globally, including a number of equatorial stations, were available for this work. M(3000)F2 hourly values from 1976 to 2008, spanning all periods of low and high solar activity were used for model development and verification.

A preliminary investigation was first carried out using a relatively small dataset to determine the appropriate input parameters for global M(3000)F2 parameter modelling. Inputs representing diurnal variation, seasonal variation, solar variation, modified dip latitude, longitude and latitude were found to be the optimum parameters for modelling the diurnal and seasonal variations of the M(3000)F2 parameter both on a temporal and spatial basis.

The outcome of the preliminary study was applied to the overall dataset to develop a comprehensive ANN M(3000)F2 model which displays a remarkable improvement over the NNO model as well as the IRI version. The model shows 7.11% and 3.85% improvement over the NNO model as well as 13.04% and 10.05% over the IRI M(3000)F2 model, around high and low solar activity periods respectively. A comparison of the diurnal structure of the ANN and the IRI predicted values reveal that the ANN model is more effective in representing the diurnal structure of the M(3000)F2 values than the IRI M(3000)F2 model. The capability of the ANN model in reproducing the seasonal variation pattern of the M(3000)F2 values at 00h00UT, 06h00UT, 12h00UT, and 18h00UT more appropriately than the IRI version is illustrated in this work.

A significant result obtained in this study is the ability of the ANN model in improving the post-sunset predicted values of the M(3000)F2 parameter which is known to be problematic to the IRI M(3000)F2 model in the low-latitude and the equatorial regions. The final M(3000)F2 model provides for an improved equatorial prediction and a simplified input space that allows for easy incorporation into the IRI model.

Dedication

This research is dedicated to Dr Austin Uwumagbe and family for their love, support, inspiration, and understanding.

Acknowledgement

I remain grateful to God for without him I will not be alive, and for granting me the opportunity to undergo a master's program in South Africa.

I appreciate the National Astrophysics and Space Science Programme (NASSP) for awarding me the bursary to undertake this program. Many thanks to the NASSP administrator, Mrs Nicky Walker, for her kind gesture and assistance. I sincerely appreciate the support and cooperation of my NASSP classmates and friends, Mr Michael Afful, Mr Temwani J. Phiri, and Mrs Doreen Agaba.

My profound gratitude goes to my supervisors Prof Lee-Anne McKinnell and Dr John Bosco Habarulema for their continuous guidance, support, and for seeing me through this research, despite their busy schedule. Thanks to Dr Pierre Cilliers and Dr Elijah Oyeyemi for their kind assistance. I acknowledged and appreciate the constant motherly advice, care and support from Mrs Anita Engelbrecht. I am grateful to the South African National Space Agency (SANSA) Space Science team for creating the enabling environment for my research program. The warm hospitality, encouragement, and support granted me is highly acknowledged. I appreciate the support of Nichkolas Ssessanga (gwebev), Electom Matandirotya, Matamba Tshimangadzo, Lotz Stephan, and Vumile tyalimpi for their unwavering assistance and support. I appreciate my fellow SANSA Space Science students for the quality period we spent together, you guys made me feel at home during my stay here at SANSA.

My unmitigated indebtedness goes to my family and relatives especially the families of Dr Austin, the Oronsayes, and the Uwumagbes, for their unwavering love, patients, support, and assistance. I sincerely appreciate my best friend, Ms Hilda John for her love, care and patients.

May the good Lord reward you all.

Table of Contents

List of Figures

List of Tables

Chapter 1

Introduction

1.1 Introduction to the Project

This project aims to provide an update to the M(3000)F2 ionospheric model developed by Oyeyemi et al. (2007) as an option for the M(3000)F2 parameter model within the International Reference Ionosphere (IRI). M(3000)F2 is a propagation factor for high frequency (HF) radio propagation in the ionosphere. The model is essentially a computer programme for reproducing the M(3000)F2 parameter at any geographical location and time. The model required should provide an accurate and reliable prediction of the M(3000)F2 ionospheric parameter at any given location on the globe under all geophysical conditions.

The ionosphere is the ionised region of the upper atmosphere. Its importance ranges from the transmission and attenuation of radio signals passing through it. Ionospheric models are important in HF radio propagation and also assist in characterising ionospheric parameters. Bradley and Dick (1997) noted that ionospheric models are vital for communication operations as well as radio wave propagation for calculating communication paths, and planning HF radio wave propagation circuits. The interest in the M(3000)F2 parameter arises from its role in HF communication and frequency planning.

1.2 International Reference Ionosphere (IRI)

The successful use of the ionosphere in HF radio communication requires a proper understanding of the ionospheric parameters. The essential parameters for HF radio propagation in the ionosphere are M(3000)F2, the critical frequency (foF2), and the peak height (hmF2) of the F2 region of the ionosphere, which are well represented by global ionospheric models (e.g. Bilitza et al., 1997). Over the years, several models (Fox and McNamara, 1988, Rush et al., 1989, Bradley, 1999, Bilitza, 1990, Bilitza et al., 1997, Poole and McKinnell, 2000, Tulunay et al., 2000, Liu et al., 2004) for specifying and forecasting the behaviour of ionospheric parameters have been developed. The most widely used of these models is the International Reference Ionosphere (IRI) model. The IRI model is a global model which was initiated by the International Union of Radio Science (URSI) and the Committee on Space Research (COSPAR) in the late sixties, and provides a wide range of atmospheric and ionospheric parameters, including electron and ion densities, and temperatures. The purpose was to institute an international standard for the specification and

prediction of ionospheric parameters, using world-wide data obtained from ground-based as well as satellite observations (Bilitza, 2006). The IRI model is updated periodically as a result of the emergence of new data, instruments and new research ideas from various research groups across the globe. These periodic updates of the IRI model have led to the improvement of several versions of the model (Bilitza and Reinisch, 2007).

The inspiration behind the IRI model is the important role of the ionospheric parameters, such as foF2, hmF2, M(3000)F2, Total Electron Content (TEC) etc., in ionospheric studies and HF radio propagation. The updated version of the M(3000)F2 model developed in this work is expected to be included within the IRI as an option for global M(3000)F2 prediction.

1.3 Project Motivation

The F2 region of the ionosphere exhibit both spatial and temporal variations. This variation is due to the vertical and horizontal winds associated with global thermospheric circulation (see Rishbeth, 1967 and 1998). In the past, global models for predicting the parameters associated with this region were developed using numerical mapping from a theoretical approach (e.g. Fox and McNamara, 1988; Rush et al., 1989;Bilitza, 2002). A major deficiency of existing models has always been the lack of representation of the southern hemisphere and the ocean areas, where measurements were not available. A paucity of real measured data has posed significant challenges in modelling attempts. Hence numerical methods have been employed to generate artificial data for areas where data is scarce, particularly for the development of a global map of the F2 region parameters (see Bilitza 2002). Thus, the IRI model provides a better representation of the northern hemisphere where data were available than the southern hemisphere. The current M(3000)F2 global model that is used within the IRI community was developed by the International Radio Consultative Committee (CCIR), now called International Telecommunication Union (ITU). The model is based on the 12-month running average sunspot number R_{12}, geographical coordinates and universal time for reproducing M(3000)F2 for a particular region (CCIR report, 1967). Though the model has been successful, it has been found to be inaccurate in reproducing M(3000)F2 values in some cases. For instance, the model does not reproduce the sharp post-sunset drop in the M(3000)F2 parameter (see Obrou et al., 2003; Adeniyi et al., 2003; Zhang et al., 2004 and 2007) which is a prominent feature of the low-latitude region and the equatorial ionosphere.

In an attempt to provide a more accurate and representative M(3000)F2 prediction, Oyeyemi et al. (2007) developed a global model for predicting the M(3000)F2 parameter using the neural network technique. The model successfully predicted M(3000)F2, but the equatorial

region was still under represented. Based on these considerations, the primary motivation for this work was to provide an update to the work of Oyeyemi et al. (2007), by developing additional solutions to improve performance, as an option for the IRI M(3000)F2 module using the neural network technique. This newly developed version of the neural network M(3000)F2 model should also be adaptable to be included as a module in the IRI model.

Neural networks are capable of modelling non-linear dynamical processes, which is a prominent feature of the ionosphere; and the technique does not require artificial data in order to generalise. Therefore, neural networks can be seen as an alternative to classical methods for forecasting the M(3000)F2 variable.

1.4 Objectives

The main objective of this thesis is to provide an update to the M(3000)F2 model as discussed earlier; It will serve as a global model for predicting the M(3000)F2 at any particular place and time. Geophysical parameters and available global data are employed in updating this model, with the application of the neural network technique.

Another goal of this study was to produce a robust model that would take care of the inadequacies of the previous model, to reproduce the diurnal structure of the M(3000)F2 parameter for the low-latitude region and the equatorial ionosphere which is problematic for the current IRI model.

1.5 Overview of the Thesis

This thesis is structured into five chapters, including this one. Chapter 2 discusses the background theory relevant to the development of a M(3000)F2 model. The ionosphere (including the M(3000)F2 parameter) and the relevant theory of the neural network technique (which was employed in this work) are discussed in Chapter 2.

Chapter 3 introduces M(3000)F2 modelling and the database used. The parameters used as input variables to the neural network, the procedure for training the network, as well as the optimum input variable used for the global modelling of M(3000)F2 are discussed.

Chapter 4 presents the development of the M(3000)F2 global model, including the selection of the optimum network. The performance of the model is compared with the current IRI M(3000)F2 model as well as with the work of Oyeyemi et al. (2007). The diurnal and seasonal variation of the M(3000)F2 predicted by the new model is compared with the values predicted by the IRI version.

Chapter 5 summarises the result and offers recommendation for future work.

Chapter 2

Background Theory

This chapter presents the relevant ionospheric and neural network theory that are of importance to M(3000)F2 modelling. Since M(3000)F2 is closely related to the ionospheric foF2 parameter which represents the maximum electron density, the ionopheric structure will be described in some detail.

2.1 Review of the Ionosphere

The high variability of the ionosphere has significant effect on the M(3000)F2 parameter. The ionosphere is the ionised region of the upper atmosphere which consists of free electrons and positive ions in an electrically neutral medium. It extends from ~60 km up to above ~1000 km. The free ions are mainly formed as a result of the interaction between solar radiation and gas molecules. These free ions control the conductivity and electrical property of the medium (Hunsucker and Hargreaves, 2003), and they are the cause of the reflection or bending of radio signals occurring at certain critical frequencies in the ionosphere. These critical frequencies vary with the intensity of ionisation. The higher the density of the electrons, the higher the frequencies that can be used for radio wave propagation. The abundance of these charged particles in the ionosphere affects the M(3000)F2 parameter considerably, and account for its practical importance in HF radio wave communications.

The electron density of the ionosphere undergoes strong daily variation due to sunrise and sunset. The ionosphere also varies with season, solar cycle, latitude, and geomagnetic activity; and responds to the variation in the neutral part of the upper atmosphere (i.e. the thermosphere). Thus, the ionosphere is a highly variable and non-linear medium, which responds to changes in various geophysical parameters on different time scales (Rishbeth and Garriott, 1969).

2.1.1 Layers of the Ionosphere

Apart from the fact that the ionospheric electron density is of great practical importance in HF propagation as discussed above, it is also useful for characterizing the structure of the ionosphere. The electron density of the ionosphere varies considerably with height. Consequently, the ionosphere is classified into three regions: the lower ionosphere, the

bottomside ionosphere, and the topside ionosphere. The bottomside ionosphere is described in terms of four regular regions (D, E, F1 & F2) according to their chemical composition, sources of ionization, altitude, and their degree of variability. HF radio waves are propagated over a long distance due to the reflection in this ionised region of the atmosphere. The E, F1, and F2 regions are responsible for the reflection or bending of HF radio signals, and allow for long-distance transmission between terrestrial terminals. Figure 2.1 illustrates the various regions of the ionosphere.

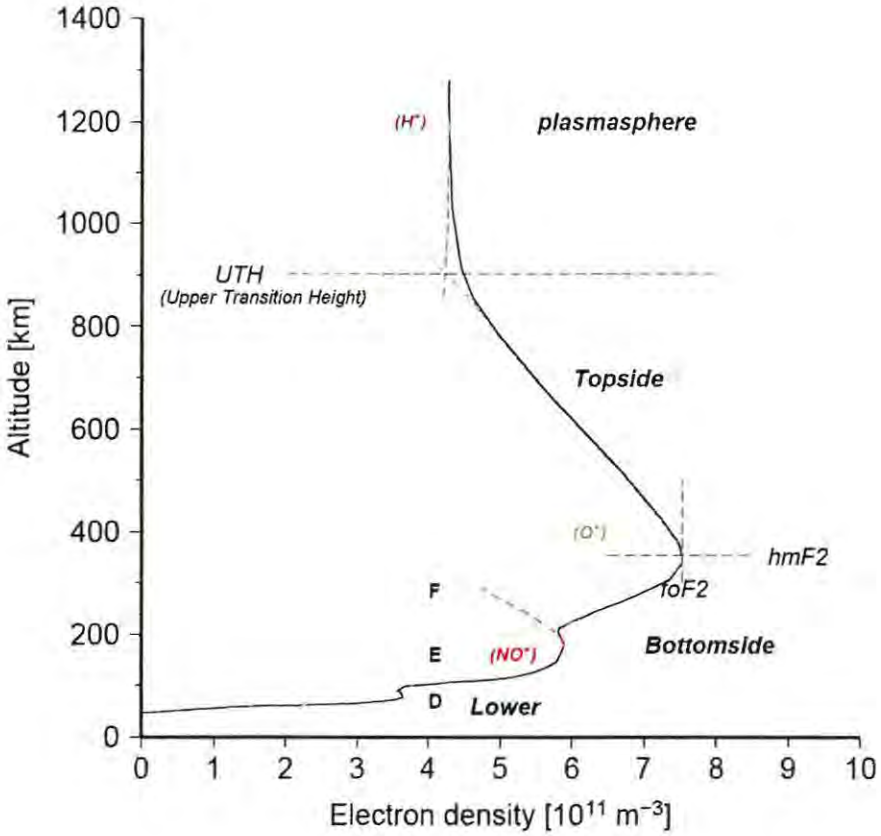

Figure 2.1: A schematic illustration of plasma density profile of the ionosphere as a function of altitude (Adapted from Sibanda, 2010).

2.1.1.1 The D Region

This is the lowest region of the ionosphere, which exists at an altitude range of about 50 km up to ~90 km (Rishbeth and Garriott, 1969). The density of the particles in the region is relatively high, and causes a lot of collision between the particles. These particles are formed as a result of the interaction of solar X-rays and cosmic rays with the gas molecules in the region. Another source of ionisation within the D region is solar Lyman α which ionises only nitric oxide (NO), a trace constituent in the region (Rishbeth and Garriott, 1969). The density of gas in this region suggests that most of these charged particles collide with particles and

recombine quickly. This implies that after sunset, the electron density decreases, and subsequently, the region disappears, hence it is called a day-time layer. As the altitude of the D region increases, the collision frequency decreases exponentially. The D region is responsible for the absorption or attenuation of HF radio signals at 10 MHz and below (Bonnet and Woltjer, 2008).

2.1.1.2 The E Region

Immediately above the D region is the E region, which is produced by soft X-rays, and extends from about 105 km up to ~160 km, with an electron density of several times 10^{11} m^{-3} (10^5 cm^3) (Hunsucker and Hargreaves, 2003). The gas in this region is relatively less dense, and the ionisation is much stronger than the D region. Due to the rarefied nature of the gas in this region, there are minimal collisions of ions and electrons, leading to a population of molecular ions (O^+ and NO^+). The E region undergoes strong daily variation, and longitudinal variation. This region is present throughout the day, and weakly ionised after sunset, with an electron density of about $5x10^9$ m^{-3} (against $10^{11}m^{-3}$ during the day) (Hunsucker and Hargreaves, 2003). Since the electron density of the E region is drastically reduced after sunset, the E layer is sometimes referred to as a day time layer. The E region acts mainly as an attenuator, and reflects HF radio signals with frequencies less than 10 MHz. The E layer has a negative effect on high frequencies as a result of its partial attenuation factor (Bonnet and Woltjer, 2008).

A phenomenal anomaly which occurs in the E region is irregular, cloud-like patches of unusual intense ionisation known as sporadic E (E_s). The factor responsible for this anomaly is not well known; instabilities in the equatorial electroject have been linked to its major cause (Hunsucker and Hargreaves 2003). The occurrence of E_s cannot be predicted, but is known to change with latitude. This anomaly, which is seen on an ionogram as an echo at constant height that extends to a higher frequency than is usual for the E region (Hunsucker and Hargreaves, 2003), seems to have a close link with the aurora borealis or northern lights in the northern latitudes. Piggott and Rawer (1972) should be consulted for comprehensive classification of Es. E_s tends to be regular at low latitudes, and is a frequent occurrence during the day with intensity high enough to cause the reflection of HF radio waves.

2.1.1.3 The F Region

The highest region of the bottomside ionosphere is the F region. The very low attenuation, high electron density, and high reflective/refractive nature of the F region makes it a very important region for HF radio propagation. This property of the F2 region has a significant

influence on the M(3000)F2 parameter, and is the subject of this work. The F region extends from about 150 km up to ~600 km (Rishbeth and Garriott, 1969). Below the height of about 180 km, the F region is predominantly dominated by NO+ ions. The behaviour of the F region can be characterised as photochemical equilibrium similar to that of the E region (see Hunsucker and Hargreaves 2003). The daytime electron density of the F region is about 10^{12} m^{-3} at an altitude range of about 300 km to 400 km. The region terminates where O^+ reduces considerably and H^+ becomes dominant. The formation of this region is a result of the interaction of extreme ultraviolet radiation with atomic oxygen. The F region splits into two layers (F1 and F2) during the day, and recombines after sunset. The F1 layer reaches its maximum ionisation at local midday, and subsequently merges with the F2 layer after sunset. The peak frequency of the F1 layer also possesses variations similar to that of the F2 layer. Among the F2 layer parameters is the M(3000)F2 (the subject of this work) which is discussed below.

M(3000)F2 Parameter: M(3000)F2 parameter is an ionospheric variable which depends on the dynamical processes of the ionosphere. M(3000)F2 is defined as the ratio of the maximum usable frequency at a distance of 3000 km to the F2 layer critical frequency, foF2. This parameter represents the optimum frequency at which to broadcast a signal that is to be received at a distance of 3000 km, the parameter is given by the equation:

$$M(3000)F2 = MUF(3000) / foF2 \qquad 2.1$$

where MUF(3000) is the maximum usable frequency at which a radio wave can be reflected and received at a horizontal distance of 3000 km (Liu et al., 2008). M(3000)F2 is related to the peak height of the F2 region, hmF2, of the ionosphere. The parameter, hmF2 can be obtained from its anti-correlation with M(3000)F2, using the formula:

$$hmF2 = \frac{1490}{M(3000)F2 + CF} - 176 \qquad 2.2$$

where CF is a correction factor which accounts for the effects of the E-layer (Bilitza et al., 1979).

Apart from the importance of the M(3000)F2 parameter for frequency planning and radio communication applications, it is also important for ionospheric research owing to its close correlation with hmF2 (Bilitza et al., 1979), hence the need for an accurate model for

predicting the M(3000)F2 parameter. Effort has been made by various groups (see Bilitza, 2006) to update the general IRI model, but there has not been significant progress in M(3000)F2 modelling due to the good performance of the M(3000)F2-based hmF2 model (Bilitza, 2002). The resolution attained with the current model is not enough to reproduce small-scale spatial and temporal variations. This thesis presents an update of the M(3000)F2 global model, using available data from ionosonde stations worldwide.

2.1.2 Ionospheric Variations

The ionosphere owes its formation to the sun, which suggests that the ionosphere is influenced by a number of factors including solar radiation, solar wind, geomagnetic activity etc. The ionosphere varies with time of the day, season, and position on the surface of the earth. The electron density in the ionosphere is generally highest in summer, in the middle of the day, and near the equator (McNamara, 1991). Ionospheric variations can be classified as follows:

2.1.2.1 Diurnal Variation:

The diurnal variation of the ionosphere occurs as a result of the earth's rotation about its axis, giving rise to sunrise and sunset. The critical frequencies of the various regions of the ionosphere vary according to the solar zenith angle. The solar zenith angle is the angle between the line from the observer to the position directly overhead (the zenith) and the line from the observer to the sun (McNamara, 1991). The structure and electron density of the ionosphere (D, E, and F regions) depend on the time of the day and solar zenith angle. In particular, the F2 region peak electron density will vary with the time of day according to the solar zenith angle over a given geographical location (McNamara, 1994). The peak electron density is usually higher during the day and drops rapidly at night. At sunrise, solar radiation results in the production of electrons in the ionosphere. Consequently, the electron density increases rapidly and maximum is reached at local noon. Immediately after local noon, electron loss due to recombination begins to occur, hence the frequencies begin to drop and the D, E, and F1 layers disappear after sunset. The F2 region survives the night, which makes HF communication possible throughout the entire day.

2.1.2.2 Seasonal Variation:

It is well established that spatial and temporal variations are phenomenal features of the ionosphere. The seasonal variation of the ionosphere is directly related to the solar zenith angle which varies as a result of the changes in the position of the sun. The electron densities

of the ionospheric layers are higher in summer than in winter. However, this is not always true in the mid-latitude areas; the peak frequency of the F2 layer (foF2) in the mid-latitude region is sometimes lower during the day in summer than in winter. This unexpected difference is known as the mid-latitude seasonal anomaly (see McNamara, 1991). This irregularity in the mid-latitude area is due to seasonal changes in the chemical composition of the atomic-to-molecular ratio (i.e. ratio of [O]/[N2] greater in winter than summer) of the neutral atmosphere. This variation in chemical composition is as a result of vertical and horizontal winds associated with global thermospheric circulation (King and Smith, 1968; Duncan, 1969; Wright, 1963; Rishbeth and Setty, 1961; Rishbeth, 1998).

2.1.2.3 Variation with Solar Activity

A sunspot is a phenomenal feature on the surface of the sun which is used as a measure of solar activity. It appears as an irregularly shaped, dark region on the surface of the sun and it is believed to be formed by violent eruptions in the sun. Sunspots are characterised by a very strong magnetic field. The sunspot number is a parameter that is mostly used in describing the solar activity as it relates to the ionosphere. Various groups (e.g. McNamara, 1991; Bilitza, 2000; Forbes et al., 2000; Richard, 2001; Rishbeth and Mendillo, 2001; Sethi et al., 2002; Liu et al., 2003; Williscroft and Poole, 1996) have shown the linear dependence of the monthly median values of the peak frequencies of the ionosphere on the monthly average value of the sunspot number. A general cycle of sunspot occurrence, usually referred to as sunspot cycle, has a minimum and maximum period which usually occurs every 11 years. The electron density of all the ionospheric layers increases during the period of maximum sunspot activity. As a result of this increase in electron density, absorption in the D region increases and the peak frequencies of E, F1 and F2 regions are greater. Therefore, in general during solar maximum, higher operating frequencies must be used for long distance HF communication.

2.1.2.4 Variation with Geomagnetic Activity:

Geomagnetic variations in the ionosphere occur as a result of current flowing above the earth's surface. This current is triggered by ultraviolet radiation from the sun, and causes thermal convection in the ionosphere (McNamara, 1991). The geomagnetic field variation varies according to local solar and lunar time; this variation is referred to as solar (Sq) and lunar (L) daily magnetic variation (see Rishbeth and Garriott, 1969).

Apart from the variation in the ionosphere discussed above, another unpredictable geomagnetic activity is the occurrence of a geomagnetic storm. It occurs as a result of the

interaction between the solar wind and earth's magnetic field. During a geomagnetic storm, the F2 layer is unstable leading to rapid fading of HF radio signals (Rishbeth and Garriott, 1969). McNamara (1991), Lui et al., (2003) and Rishbeth, (1969) should be consulted for more detail and other forms of ionospheric variation.

2.2 Artificial Neural Network

Artificial neural networks (hereafter referred to as ANN) have been employed in this work. The application of ANN in ionospheric research stems from its high performance in predicting and modelling non-linear parameters. The use of the ANN technique is stimulated by its dexterity in predicting non-linear processes. Previous works have demonstrated the application of the ANN technique in modelling different ionospheric parameters. For instance, the ANN technique has been used successfully for single station and regional modelling of foF2 and M(3000)F2 variables (e.g. Xenos, 2002; Williscroft and Poole, 1996; Lamming and Cander, 1999; Wintoft and Cander, 1999; Tulunay et al., 2000). Recently, Yilmaz et al. (2009) and Habarulema et al. (2011) applied the ANN technique in TEC modelling and mapping. An ANN is a massively parallel distributed processor made up of simple processing units which has a natural propensity for storing experimental knowledge and making it available for use (Haykin, 1994). An ANN has the ability to generalise from a set of training patterns, when familiarised with input patterns that are similar but not identical, with the parameters with which the ANN was trained. An ANN finds its applications in medicine, business, speech production, pattern recognition, control systems, speech recognition and ionospheric predictions (Fausett, 1994; Haykin, 1994). The basic unit of an ANN responsible for its effective performance in a wide range of applications is the neuron (units). The major components of an artificial neuron are discussed in following subsections.

2.2.1 Major Components of an Artificial Neuron

Fausett (1994) established that an artificial neuron is a processing unit connected to another neuron within the network which performs the function of adding up the output of a neuron or other neurons in the network. It is a hypothetical model of a biological neuron which represents an ingredient common to all ANNs. This commonality makes it possible to share theories and learning algorithm in different applications of neural networks (Haykin, 1994).
Figure 2.2 is a model of an artificial neuron. It consists of a set of synapses or connecting links, an adder for summing the input signals, and an activation function. This model forms the basis for designing a neural network.

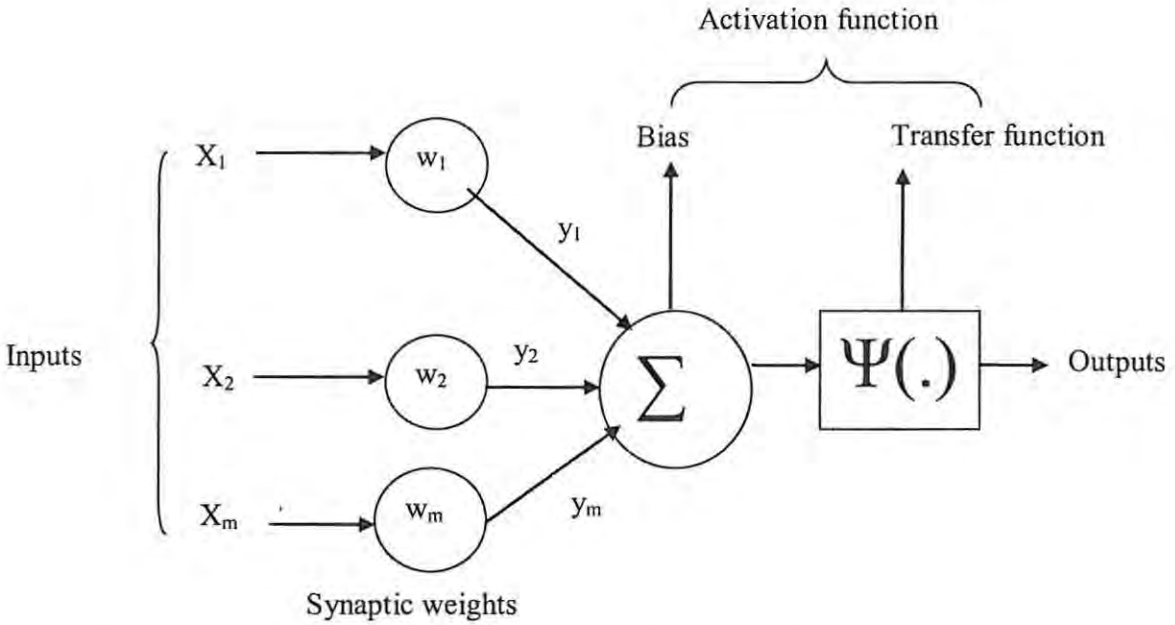

Figure 2.2: Components of an Artificial Neuron (Adapted from Haykin, 1994)

The figure illustrates the relationship between the inputs (X_1, X_2 ...X_m), the synaptic weights (w_1, w_2 ...w_m), the strength of the output signals (y_1, y_2.... y_m), the summing function, activation function and the output node of an artificial neuron.

2.2.1.1 Weighting Factor

The weight represents information used by the network to solve a problem. It is a representation of the amount of the effect that a synaptic input has on the overall response of a neuron (Wells, 2003). The weights are associated with each unit and determine the strength of the output signals from the input units X_1, X_2,....,X_m according to the relation:

$$y_m = X_m w_m \qquad 2.3$$

Some inputs are more essential than others, such that they possess a considerable effect on the processing elements as they blend to produce a neural response. It should be noted that the weights, which fall within the range of $-1 \leq w \leq 1$ are usually initialized and randomly chosen at the beginning of the ANN training (see Fausett, 1994; Haykin, 1994). This is done to ensure the proper generalisation of the network.

2.2.1.2 Activation Function

The activation function consists of two functions: the summing function and the transfer function (Enquist and Ghirlanda, 2005). The summing function combines all the input units into a single value. It is the first step in a processing element's operator. The inputs and corresponding weights are vectors which can be added algebraically.

The transfer function computes the value from the result of the summing function. In other words, the result of the summing function, which is usually the weighted sum, is transformed into a working output via an algorithm process known as the transfer function. It can be categorised into three: sigmoid, linear, and hyperbolic functions. The type of problem to be solved determines the choice of the type of transfer function to be employed. For the purpose of this work, the sigmoid function was employed due to the fact that the value of the function and its derivative at a point reduces the computational burden during training (see Fausett, 1994).

As noted by Berry and Linoff (1997), the sigmoid function is a squashing (limiting) function, because it is both continuous and differentiable. Thus, it provides linear, near-linear and non-linear approximates for a given set of inputs. The sigmoid function is of the form:

$$S_a(x) = \frac{1}{1+\exp(-ax)} \qquad 2.4$$

Another form of sigmoid function (bipolar sigmoid function) which is commonly used is given by:

$$S_a(x) = \frac{2}{1+\exp(-ax)} - 1 \qquad 2.5$$

This function is closely related to the function tanh(x) according to the relation.

$$\tanh(x) = \frac{e^{x} - e^{-x}}{e^{x} + e^{-x}} \qquad 2.6$$

where S_a is the sigmoid function, x is the training pattern, and a is the slope parameter; different slopes are obtained by varying the parameter a (see Haykin, 1994). Figure 2.2 is a graphical representation of the log-sigmoid and tanh-sigmoid function.

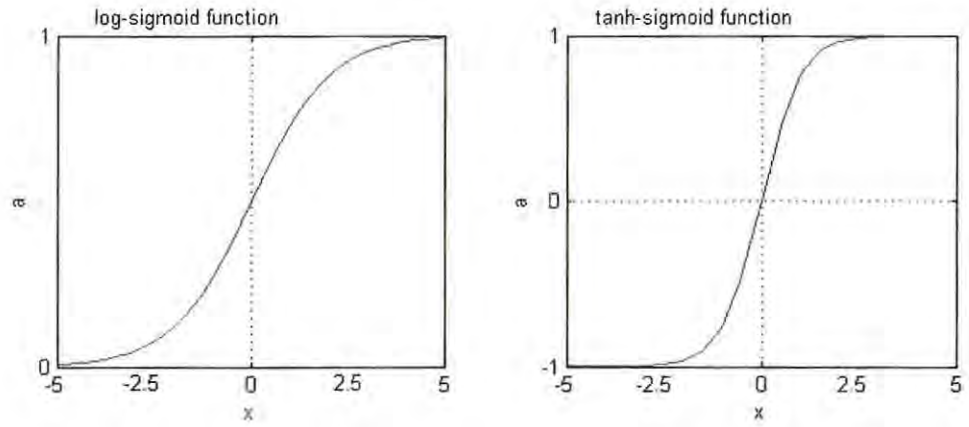

Figure 2.3: Graphical representation of log-Sigmoid tanh-sigmoid functions (Adapted from Haykin, 1994).

2.2.1.3 The Bias

Bias is the complexity restriction which the ANN architecture imposes on the degree of fitting accurately to the target function (Geman et al., 1992). Over-fitting is a major problem that usually arises in connectionist learning by an ANN. This means that the learned function fits very closely to the training data, but does not generalise properly. This implies that it cannot model the unseen data for the same task well enough. Since the idea behind the learning mechanism of ANN is attaining good generalisation; a balanced bias is required to eliminate the problem of over-fitting. The bias, which is associated with each of the hidden and output units, provides a threshold for the activation of the units.

2.2.2 Architecture of an Artificial Neural Network

The organisation of neurons and the connection patterns within and between the layers of neural network is called the neural network architecture. The neurons are simply visualised as being arranged in layers; and as such, units in the same layer behave the same way. The primary factor that determines the behaviour of units in an ANN is its activation function, and the pattern of weighted connections over which it sends and receives signals (Fausett, 1994). An ANN architecture is made up of a collective number of units. It should be noted that the units possess a common activation function and a common pattern of connections to other units. The number of units employed in training a neural network depends on the volume of data involved.

An ANN is often categorised into single layer or multilayer networks. For the purpose of this work, a multilayer feed-forward network architecture was employed. It consists of one or more layers (hidden layers) of computational nodes sandwiched between the input and the

output units. The input units in this case are geophysical and ionospheric parameters which are known to influence M(3000)F2, while the output unit is the M(3000)F2 parameter. The input space parameters to the ANN are considered in Chapter 3. Figure 2.4 is a schematic diagram of a simple multilayer feed forward network.

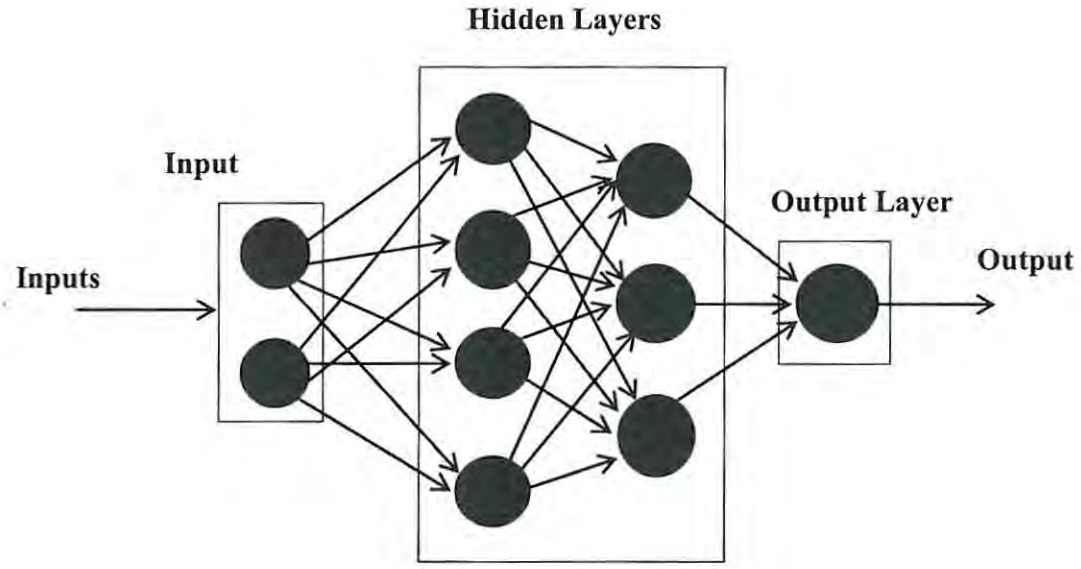

Figure 2.4: A schematic diagram of a simple multilayer feed-forward network

The procedure for applying the feed forward network is such that the input training pattern is fed to the input neurons (X_a, a =1... m) which send the signal to the neurons in the hidden layer. The neurons in the hidden layer (Z_b, b = 1... n) compute the weighted sum of the input patterns according to the relation:

$$(Z_b)^{in} = v_{ob} + \sum_{a=1}^{m} x_a v_{ab} \qquad 2.7$$

Where v_{ob} is the bias on the hidden neuron m and v_{ab} is the connection weight between input neuron a and hidden neuron b. The hidden neuron computes the input pattern by applying the activation function $Z_b = f((Z_b)^{in})$ and forwards it to the neuron in the output layer. The neurons in the output layer (y_m, m = 1... p) compute the weighted sum of the input patterns such that:

$$(y_m)^{in} = k_{om} + \sum_{b=1}^{n} Z_b k_{bm} \qquad 2.8$$

Where k_{om} is the bias on the neuron m, and k_{bm} is the connection weight between the hidden neuron b and output m. The output pattern is computed using the function $y_m = f((y_m)^{in})$ by applying its activation function (see Fausett, 1994).

2.2.3 The Back-propagation Algorithm

Following Paul Werbos' (1974) development of the back-propagation algorithm, and its subsequent application by Rumelhart in the 1980s, the back-propagation algorithm has been widely employed in solving diverse ionospheric problems (e.g Lamming and Cander, 1999; Wintoft and Cander, 1999; Lundestedt et al., 2002; Vandegriff et al., 2005; Leandro and Santos, 2007, Yilmaz et al., 2009, Habarulema and McKinnell, 2012). To train a network for the purpose of performing a specific assignment, the weights of each unit must be modified in such a way that the error between the desired output and actual output is reduced to its lowest minimum. This mechanism requires the computation of how the error varies as each weight is varied (increased and decreased). The back-propagation algorithm uses a gradient-decent method in minimizing the total squared error between generated values and the desired output (Fausett, 1994). The blending of the weights, which reduces the error function is considered to be the solution to the learning problem (Rojas, 1996). The general idea of the back-propagation algorithm is to reduce the error, until the network learns the training data.

The back-propagation of errors in the network is such that the output neurons compute the error information, the weight correction, as well as the bias correction term; and then transfer the error information term to the neurons in the hidden layer when the target pattern corresponding to the input training pattern is presented according to the following relations:

$$\delta_m = (t_m - y_m) f'((y_m)^{in}) \tag{2.9}$$

$$\Delta k_{bm} = \alpha \delta_m Z_b \tag{2.10}$$

$$\Delta k_{om} = \alpha \delta_m \tag{2.11}$$

where δ_m is the error information term, Δk_{bm} is the weight correction term, Δk_{om} is the bias correction term, and α is the learning parameter. The neurons in the hidden layer perform the computation of the error information term. This term is the result of the addition of the derivative of the activation function and the δ_m (see Fausett, 1994).

For the purpose of this work, feed-forward multilayer network architecture, with a standard fully connected back-propagation algorithm was employed. The network was trained in

topological order using randomized weights. Topological order in this case implies that the input training pattern presented to the input layer propagates forward to the hidden layer until the activation gets to the output layer (Zell et al., 1998).

2.2.4 Training the Artificial Neural Network

An ANN has a salient feature of learning from its environment and improving its performance through the training process over time with some prescribed conditions. In other words, the ANN is designed in such a way that the application of a set of inputs produces the desired set of outputs. To achieve this, the network is trained to learn the relationship between the given set of inputs and the expected outputs. The training algorithm is categorised into two: supervised (associative) learning and unsupervised (self-organisation) learning algorithms (Haykin, 1994).

A supervised back-propagation learning algorithm was employed in this research. A Neural network software package, version 4.2 of the Stuttgart Neural Network Simulator (SNNS, 1995a) was used. The software was developed by the University of Stuttgart Institute for Parallel and Distributed High Performance Systems, and is available on the Internet (SNNS, 1995b). The software uses a binary sigmoid function as its default neuron activation function for the neuron input-output mapping processes (see Zell et al., 1998).

2.3 Summary

This chapter offered a brief discussion of the ionosphere and its structure. The formation of the charged particles in the ionosphere and their role in HF propagation and ionospheric research was briefly discussed. A synoptic treatment of the M(3000)F2 parameter which is the subject of this research, as well as the ionospheric variations which are known to affect the M(3000)F2 variable was also presented here.

The relevant theoretical background of the ANN that was employed in this research was also presented in this chapter. The components of the ANN as well as the network architecture were considered. It was established that a feed-forward multilayer network architecture, with a standard fully connected back-propagation algorithm was employed in this work. The training procedure was briefly discussed.

The Application of the relevant aspects of ANN in modelling the M(3000)F2 parameter is discussed in the following chapter.

Chapter 3

Preliminary Study of M(3000)F2 Modelling

3.1 Introduction

Ionospheric parameters, such as foF2, hmF2, and M(3000)F2 are important tools for HF communication and frequency planning. In the past, effort has been made by various groups (e.g. Williscroft and Poole, 1996; Fuller-Rowell, 2000; Bilitza, 1990 and 2001) in developing a tool for predicting these ionospheric parameters. Some authors (Piggott and Rawer, 1972 and 1978; Bradley and Dudeny, 1973; Bilitza et al., 1979, Fox and McNamara, 1988; Fuller-Rowell, 2000; Bilitza, 1990 and 2001) employed standard procedures by fitting mathematical functions to a combination of measured and theoretical data of these variables representing these ionospheric parameters.

M(3000)F2 is a parameter which depends on the F2 region of the ionosphere. This region is complex, owing to the complicated nature of its dynamical processes. To effectively manage these processes so that this parameter can be applied for practical purposes, a reliable and accurate modelling technique is required. Zang et al. (2010) used an empirical orthogonal function expansion method for modelling M(3000)F2 and hmF2 for a single station. Recently, Oyeyemi et al. (2007) employed the ANN technique for modelling the M(3000)F2 parameter on a global scale. The same procedure was employed in this thesis to update and improve the M(3000)F2 model developed by Oyeyemi et al. (2007). This updated M(3000)F2 model was developed as a possible option for incorporating into the IRI global model. This chapter presents a preliminary study of M(3000)F2 global modelling.

3.2 Data Used

Archived daily hourly values of M(3000)F2 obtained from ionospheric stations worldwide were used in this work. The data ranges from 1976 to 2008, covers periods of both quiet and disturbed solar and geomagnetic activity; and is spread across low, mid and high latitude regions. The data is not evenly distributed as a result of inadequate distribution of ionospheric stations across the globe. However, tremendous effort has been made to ensure that the available data is well utilized. The data was obtained from 135 ionospheric stations across the globe via the Space Physics Interactive Data Resource (SPIDR) website.

Table A.1 in Appendix A lists all the stations that were available for this work. Figure 3.1 shows the distribution of ionosonde stations from which M(3000)F2 data was obtained. The stations are grouped into different intervals according to their latitude (0° - 10°, 11° - 20°, 21°–30°, 31° - 40°, 41° - 50°, 51° - 60°, 61° - 70°, and 71° - 80°).

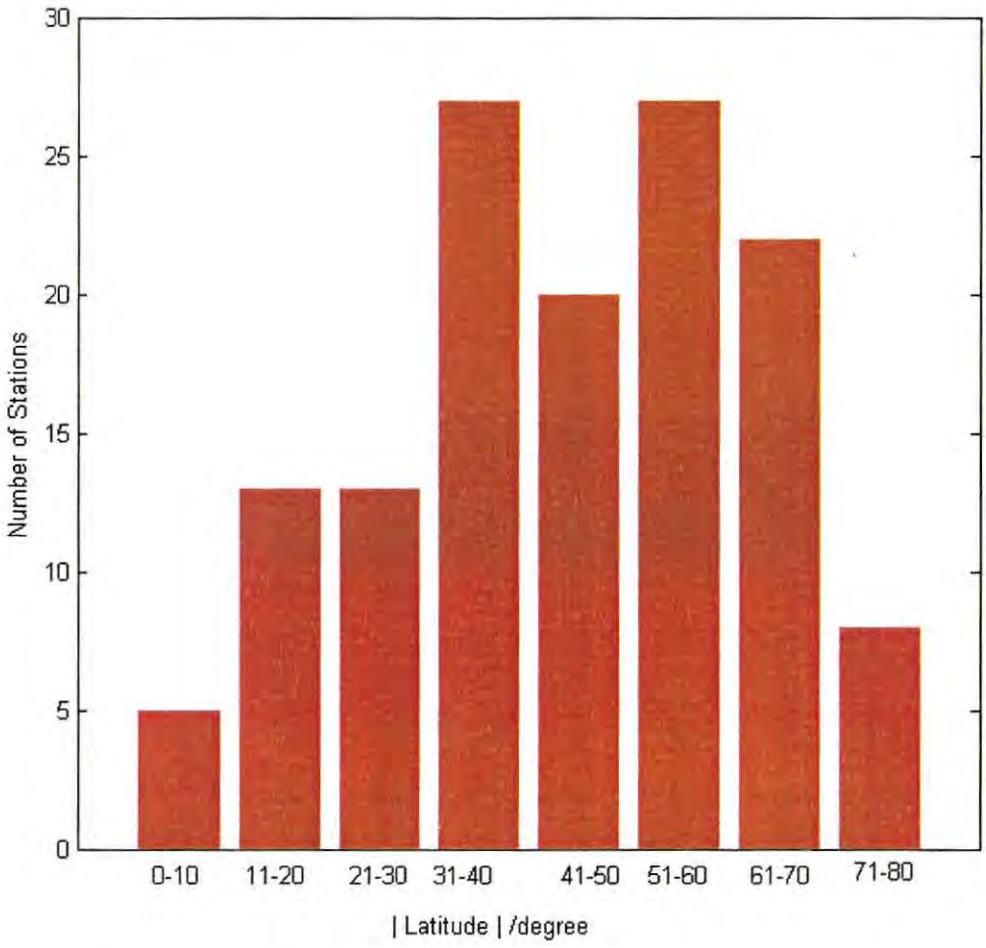

Figure 3.1: Latitudinal distribution of ionosondes providing M(3000)F2 data.

To classify the stations according to geographical regions, the latitude ranges were grouped as follows: low latitude region (latitude 0° to 20°), mid-latitude region (latitude 21° to 50°) and high latitude region (latitude 51° and above). Figure 3.2 shows the distribution of ionosonde stations according to their geographical regions. The equatorial stations in this case, were considered to be stations within the latitude range of 0° to 10°. The grouping of these stations according to their latitude is such that it covers both sides of the equator.

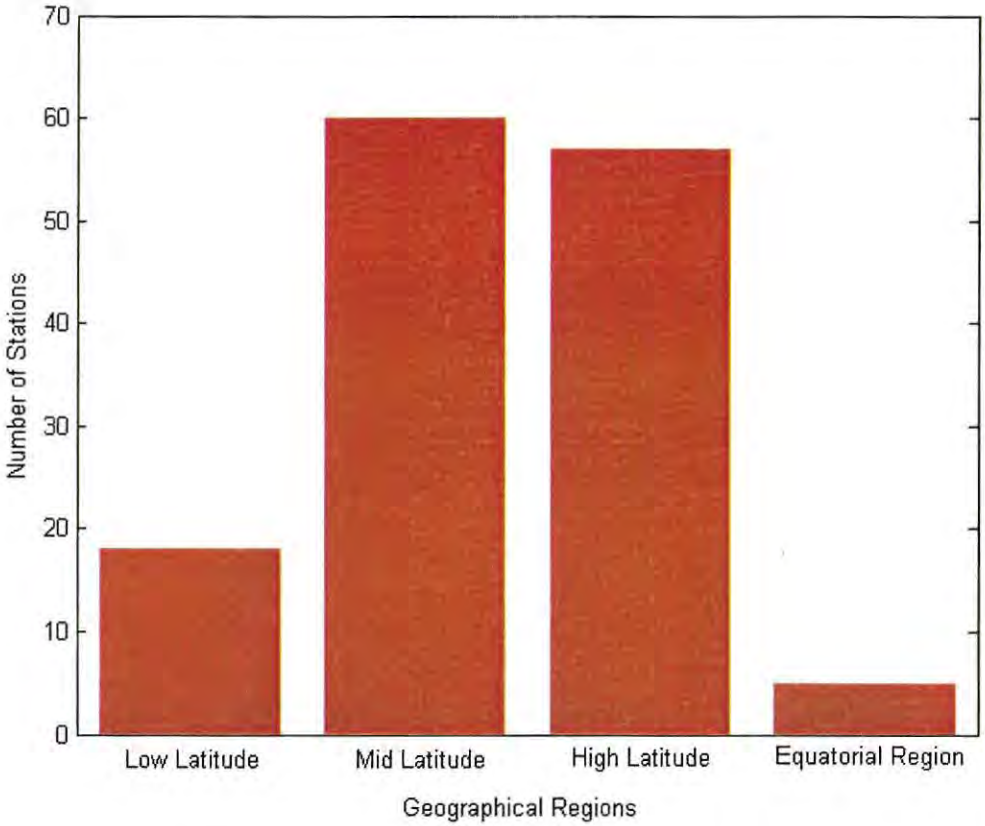

Figure 3.2: Geographical distribution of ionosonde stations providing M(3000)F2 data.

3.3 Input Parameters

The variability of the F2 region of the ionosphere has a direct influence on the M(3000)F2 parameter. As a prerequisite for neural network training for prediction purposes, input parameters which have a significant effect on the output parameters are required. As discussed in section 2.2, the F2 region of the ionosphere is vulnerable to a number of influences such as solar radiation, solar wind, and geomagnetic activity. The selection of input variables for this work was based on those known to have an influence on the M(3000)F2 parameter, as well as on the earlier work of Oyeyemi et al. (2007), and the requirements of the IRI.

The variability of the F2 region with solar activity, magnetic activity, latitude and longitude has been discussed extensively in the existing literature (e.g. Hargreaves, 1979; Rishbeth and Garriott, 1969; McNamara, 1994). M(3000)F2 is similarly influenced by these factors. The contribution and importance of these sources in modelling foF2 have been discussed in detail (see McKinnell, 1996; Williscroft and Poole, 1996; Wintoft and Cander, 1999; McKinnell

and Poole, 2000). Oyeyemi et al., (2007) also took into account the role of these sources in modelling the M(3000)F2 parameter. The input parameters to the neural network for the purpose of this work are discussed in the following section.

3.3.1 Diurnal Variation

The diurnal variation of the F2 region of the ionosphere is well understood. Rishbeth and Garriott (1969) demonstrated that foF2 reaches its minimum in the early hours of the morning, increases rapidly after sunrise as a result of photoionisation, attains its maximum at local noon, and gradually decreases to its minimum after sunset due to recombination. Consequently, the hour of the day (HR in universal time) was used as input variable of the neural network to represent the diurnal variation of M(3000)F2. The choice of this parameter is also based on the work of Williscroft and Poole (1996), McKinnell and Poole (2000) and Oyeyemi et al. (2007). Oyeyemi (2005) noted that the choice of the solar diurnal cycle as a representative of diurnal variation is based on the fact that its power amplitude (order of $5x10^9$) is considerably higher compared to the solar semidiurnal cycle (order of $7.5x10^7$) and lunar semidiurnal cycle (order of $10x10^4$). Williscroft and Poole (1996) established that in order to see 00h00 and 23h00 as two adjoining hours, the HR should be divided into its cyclic components according to the equations:

$$HS = \sin\left(\frac{2\pi \times HR}{24}\right) \tag{3.3}$$

$$HC = \cos\left(\frac{2\pi \times HR}{24}\right) \tag{3.4}$$

where HS and HC are the sine and cosine components of HR.

3.3.2 Seasonal Variation

There are significant spatial and temporal variations in the F2 region of the ionosphere. Among these variations is the seasonal variation which can be represented by the day of the year. The M(3000)F2 parameter experiences the seasonal variation and responds to changes in the day of the year. In this work, the day number (DN) represents the day of the year and ranges in value from 1 to 365 or 366 for leap years. The DN was included as an input parameter to the neural network and, as such, provided information on the seasonal variation of M(3000)F2. As noted by Williscroft and Poole (1996), 31 December and January 1 are numerically far apart, making it difficult for the neural network to see them as two adjoining days. As a result, DN was divided into its cyclic components according to the following:

$$\mathrm{DNS} = \sin\left(\frac{2\pi \times \mathrm{DN}}{365}\right) \tag{3.10}$$

$$\mathrm{DNC} = \cos\left(\frac{2\pi \times \mathrm{DN}}{365}\right) \tag{3.11}$$

where DNS and DNC are the sine and cosine components of DN.

The solar zenith angle plays a significant role in the seasonal variation of the F2 region of the ionosphere (see Rishbeth and Garriott, 1969; McNamara, 1991). As a result, the solar zenith angle (chi) was included in the input space of the neural network to also provide information on the seasonal variation of M(3000)F2. Oyeyemi (2005) pointed out that the inclusion of chi rather than latitude and longitude would remove the empty space in the input data that may arise as a result of geographical clustering of ionospheric stations. The values of chi were generated with respect to geographical location using equations 3.5 to 3.7, as described in Rishbeth and Garriott (1969).

$$\cos(\mathrm{chi}) = \sin(\theta)\sin(\delta) + \cos(\theta)\cos(\delta)\cos(\lambda_s - \lambda_g) \tag{3.5}$$

Where λ_s is the subsolar longitude and is given by:

$$\lambda_s = 15\mathrm{UT} - 180 \tag{3.6}$$

δ is the subsolar latitude, i.e. the angle between the earth-sun line and the equatorial plane called the declination angle, which is given as:

$$\delta = 23.45\sin\left[\frac{360}{365}\left(\mathrm{DN} + 284^{\circ}\right)\right] \tag{3.7}$$

λ_g is the geographical longitude, θ is the geographical latitude, UT is the universal time, and DN is the day of the year.

Following the argument by Williscroft and Poole (1996), as discussed in Section 3.3.1, chi was split into its cyclic components by the equations:

$$\mathrm{SCHI} = \sin\left(\frac{2\pi \times \mathrm{chi}}{360}\right) \tag{3.8}$$

$$CCHI = \cos\left(\frac{2\pi \times chi}{360}\right) \quad 3.9$$

where SCHI and CCHI are the sine and cosine components of chi.

3.3.3 Solar Cycle Variation

Several authors (Jones and Gallet, 1962 and 1965; Rush et al., 1983 and 1984; Williscroft and Poole, 1996; Forbes et al., 2000; Sethi et al., 2002; Liu et al., 2003) have shown the dependence of the electron concentration of F2 region on solar activity.

The solar indices R_{12} (12-month running mean of sunspot number), F10.7 (solar flux), P10.7 (index of solar radio wave radiation), SF81 (81 days running mean of daily F10.7), and SG12 (global ionospheric index based on ionosonde) are all measures of solar activity. For the purpose of this work, some of these parameters were considered as measure of solar cycle variation in the input space of the ANN. Since the aim was to improve on the existing M(3000)F2 model developed by Oyeyemi et al. (2007), a preliminary investigation was undertaken to determine the most suitable parameter for representing solar cycle variation in the network. The final parameter had to also be in line with the parameters used in the IRI model to avoid additional complexity in the model.

3.3.4 Geomagnetic Activity

Geomagnetic activity has a significant influence on the variation of the F2 region of the ionosphere (see McNamara, 1991). This is a short-term variation which can prove challenging to model. For the purpose of this work, the ap index (A16) was included as an input variable to the neural network to account for geomagnetic activity. A16 is a 2-day running mean of the 3-hourly ap geomagnetic index. These values are obtained from the measurements made at geomagnetic stations world-wide, and represent the variation of the geomagnetic field as a result of currents circulating in the ionosphere. The work of Oyeyemi et al. (2007) proved the relevance of this parameter as one of the input variables for the global modeling of the M(3000)F2 parameter.

3.3.5 Other Input Parameters

It is well established that the ionosphere varies considerably with longitude and latitude. Rishbeth and Garriott (1969) and McNamara (1994) pointed out that this ionospheric behaviour is due to the variation in the solar zenith angle, as well as the latitudinal

dependence of neutral wind, and its contribution to influencing the ionisation of neutral particles up and down the field lines. The need to include longitude and latitude as input parameters of the ANN arises from the fact that the use of the solar zenith angle alone may not reproduce the evening peak values seen in the measured data, as the evening peak can be very sharp and easily missed. The inclusion of latitude and longitude is consistent with the IRI models, which include these parameters as input variables.

Another input parameter which was considered is the modified dip latitude (modip). Rawer (1984) established that the F2 region and the topside ionosphere are controlled by geomagnetic field; hence a new coordinate system for modeling the F2 layer and topside ionosphere was introduced. A major drawback of the CCIR-M(3000)F2-based hmF2 model is its inability to reproduce the post-sunset peak of hmF2 which corresponds to a sharp drop in M(3000)F2 in the equatorial and low latitude regions (Adeniyi et al., 2003; Obrou et al., 2003; Zhang et al., 2004 & 2007). The inclusion of this parameter in the ANN input space should ideally assist in reproducing the post-sunset peak of hmF2 in low-latitude and equatorial regions.

The input parameters of the ANN are thus: DNS, DNC, HS, HC, SCHI, CCHI, modip, SF10.7, SF81, P10.7, SG12, A16, Long, and Lat. This gives rise to the function f such that:

$$M(3000)F2 = f(DNS, DNC, HS, HC, SCHI, CCHI, Modip, SF10.7, SF81, SG12, P10.7, A16, Long, Lat)$$

3.4 Preliminary Modelling of M(3000)F2

Considering all the input parameters described in Section 3.3, there exist the possibility of redundancy in the input space variables. For example there is multiple representation of the solar activity variation in the input parameters F10.7, SF81 and P10.7.SF81 is the 81-day running mean of F10.7, and P10.7 is an index of solar radio wave radiation which is the mean value of F10.7 and SF81. As such, determining which of these parameters is more suitable for the ANN is an important contribution of this work. The input parameters were divided into six groups, giving rise to six different networks; and training was performed with a sample of twenty selected stations. The twenty stations were randomly selected across the different geographical regions as defined in Section 3.2. These selected stations were used in order to speed up the training process. Table 3.1 shows the stations that were used for training during this preliminary stage. The input variables for the different networks are thus:

$$M(3000)F2 = f(DN, HR, CHI, Modip, SF10.7, SF81, SG12, P10.7, A16, Long, Lat) \rightarrow ANN1$$

$$M(3000)F2 = f(DN, HR, CHI, Modip, SF10.7, SF81, SG12, A16, Long, Lat) \rightarrow ANN2$$

$$M(3000)F2 = f(DN, HR, CHI, Modip, SF81, SG12, P10.7, A16, Long, Lat) \rightarrow ANN3$$

$$M(3000)F2 = f(DN, HR, CHI, Modip, SF81, SG12, A16, Long, Lat) \rightarrow ANN4$$

$$M(3000)F2 = f(DN, HR, CHI, Modip, SF10.7, SG12, A16, Long, Lat) \rightarrow ANN5$$

$$M(3000)F2 = f(DN, HR, CHI, Modip, SG12, P10.7, A16, Long, Lat) \rightarrow ANN6$$

where DN ≡ DNS & DNC; HR ≡ HS & HC; CHI ≡ SCHI & CCHI, representing the sine and cosine components of day number, hour number and chi respectively. Figure 3.3 depicts a block diagram of ANN1. The remaining networks (ANN2, ANN3, ANN4, ANN5, & ANN6) follow the same pattern, except for the difference in the solar activity parameter.

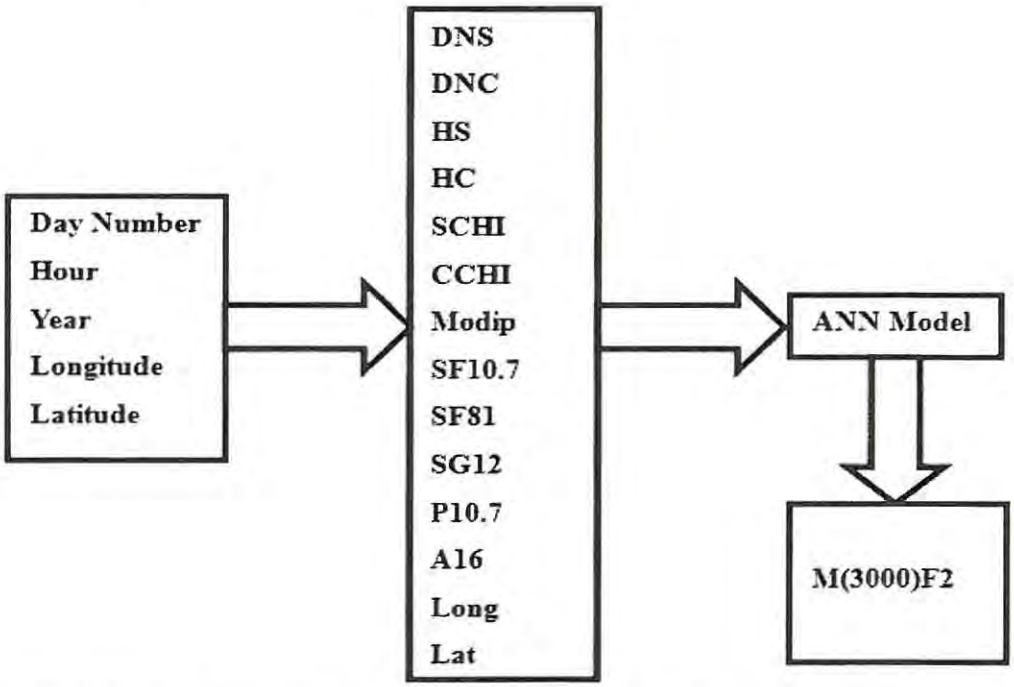

Figure 3.3: A block diagram of the inputs and output to the initial M(3000)F2 ANN 1

Table 3.1: Training stations during the preliminary stage

Name	Code	Long (°)	Lat (°)
Anyang	AN438	126.90	37.40
Ascension	AS00Q	-14.40	-7.95
Bermuda	BJJ32	-64.70	32.40
Brisbane	BR52P	152.90	-27.50
Camden	CN53L	150.70	-34.00
Casey	CW46O	110.50	-66.30
Churchill	CH958	-94.20	58.80
College	CO764	-147.99	64.92
Dakar	DKA14	-18.40	14.80
Dikson	DI373	80.40	73.50
Gakona	GA762	-145.16	62.41
Irkutsk	IR352	104.00	52.50
Jicamarca	JI91J	-76.80	-12.00
Kiev	KV151	30.50	50.50
Kiruna	KI167	20.40	67.80
Kwajalein	KJ609	167.20	9.00
Mawson	MW26P	62.90	-67.60
Puerto Rico	PRJ18	-67.20	18.50
Uppsala	UP158	17.60	59.80
Vanimo	VA50L	141.30	-2.70

3.4.1 Neural Network Architecture for M(3000)F2 Training

A feed-forward network structure was employed in modeling M(3000)F2 parameter. The feed-forward network was performed in topological order, using randomized weights with a standard, fully connected back-propagation algorithm. The number of input and output parameters was discussed in Section 3.3. There is no scientific rule for choosing the number of hidden layers and nodes. However, some researchers (Williscroft and Poole, 1996; Tulunay et al., 2000) have demonstrated the successful application of a single hidden layer neural network. In fact, Haykin (1994) and Fausett (1994) established that one hidden layer is adequate for any network architecture. Other authors favour a neural network with more than one hidden layer (e.g Lamming and Cander, 1999; Xenos, 2000). Recently, McKinnell and

Oyeyemi (2010) successfully demonstrated the application of triple hidden layer neural network for the equatorial prediction of foF2.

Following the successful application of these different number of hidden layer networks, the training process was started by arbitrarily choosing a single hidden layer network, with 10, 15 and 20 nodes respectively. The result was not satisfactory, probably due to the volume of the data involved. Hence this was followed by the training of a double hidden layer network, with nodes of 20/20, 25/20, and 35/30. A triple hidden layer network with 20/15/10 and 25/20/15 nodes was also implemented.

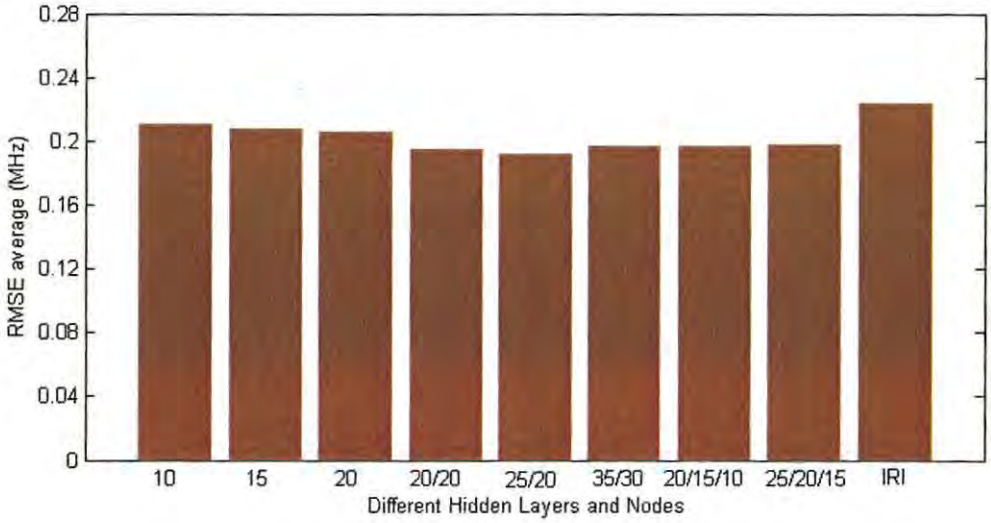

Figure 3.4: Graphical representation of the performance of the different networks trained with different neural network architectures.

The best ANN architecture was found to be the network with two hidden layers. Figure 3.4 is a bar chart illustrating the different networks. The performance of the networks was evaluated by computing the average root mean square error (RMSE), using equation 3.12.

$$RMSE_{ave} = \frac{1}{k}\sum_{j=1}^{k}(RMSE)j \qquad 3.12$$

where k represents the number of testing stations.

3.4.2 Training and Testing

The procedure for training a network is crucial to the success and optimum performance of the ANN model. The essence of this training procedure is to enable the network to actualize a satisfactory performance when presented with data that is similar but not identical to the training data set. This principle was applied in the training process of the ANN model of the M(3000)F2 parameter. Archived hourly values of M(3000)F2 from the 20 ionospheric stations listed in Table 3.1 were used to verify which of the solar flux parameters would be more appropriate for the global modelling of M(3000)F2.

For the purpose of attaining optimum performance when presented with an unseen data set, the combined data set from these stations was randomly split into training data (70%) and testing data (30%). The ANN was trained with the 70% data set, while the 30% data set was used during the testing process to make sure that the network was not being over-trained. This procedure helps the network to generalize properly when presented with data that was not used in the training process.

The training process is such that the algorithm selects the training specimen, makes forward and backward passes by adjusting the weights repeatedly, until the mean square error (MSE) difference does not vary by more than some predetermined value over a specific period. When this is achieved, the network thus has the potential for predicting satisfactorily when presented with an unseen input pattern. Hence the network is said to have attained generalization (see Oyeyemi, 2005).

The training for the different networks (ANN1, ANN2, ANN3, ANN4, ANN5 & ANN6) was done by using two hidden layers with nodes 25/20.

3.4.3 Results and Discussion

In order to evaluate the prediction performance of the six trained ANN models, observed daily hourly values of M(3000)F2 data from five ionospheric stations which were not part of the training were used. The performance of the ANN models was evaluated by comparing the RMSE values of the ANN models with the RMSE values of the IRI-2007 M(3000)F2 module. The expression for RMSE is:

$$RMSE = \sqrt{\frac{1}{N}\sum_{i=1}^{N}(M(3000)F2_{obs} - M(3000)F2_{pred})^2} \qquad 3.13$$

where N is the number of data points, $M(3000)F2_{obs}$ and $M(3000)F2_{pred}$ are observed and predicted values of the M(3000)F2 parameter respectively.

Table 3.2: Ionospheric stations used for verification (preliminary stage)

Name	Code	Long (°)	Lat (°)
Argentine Islands	AIJ6N	-64.30	-65.20
Boulder	BC840	-105.27	39.99
Grahamstown	GR13L	26.50	-33.30
Macquarie	MQ55M	159.00	-54.50
Manila	MN414	121.10	14.60

The data from the stations in Table 3.2 were used to evaluate the RMSE between the observed values and predicted values of the ANN and IRI for a period of solar maximum (1991 & 1992) and solar minimum (1987 & 1988). It should be noted that Argentine Islands is hereafter referred to as Argentine.

The comparison of the RMSE values for the different networks (ANN1, ANN2, ANN3, ANN4, ANN5 & ANN6) and the IRI model is shown in Table 3.3.

Table 3.3: Comparison of the RMSE values ofM(3000)F2 between the different neural networks and the IRI model with data from some selected stations.

Station	Long	Lat	AN1	AN2	AN3	AN4	AN5	AN6	IRI	Year
Argentine	-64.3	-65.0	0.221	0.223	0.217	0.229	0.217	0.212	0.244	1987
Boulder	-105.3	40.0	0.198	0.186	0.186	0.177	0.182	0.181	0.188	1987
Grahamstown	-26.5	-33.3	0.251	0.247	0.248	0.240	0.255	0.254	0.270	1988
Macquirie	159.0	-54.5	0.194	0.183	0.178	0.179	0.186	0.187	0.176	1987
Manila	121.0	14.6	0.227	0.218	0.219	0.220	0.221	0.224	0.255	1987
Argentine	-64.3	-65.0	0.204	0.197	0.194	0.198	0.193	0.198	0.315	1992
Boulder	-105.3	40.0	0.160	0.156	0.155	0.153	0.155	0.156	0.173	1991
Grahamstown	26.5	-33.3	0.159	0.153	0.155	0.152	0.161	0.163	0.215	1992
Macquirie	159.0	-54.5	0.159	0.162	0.160	0.173	0.169	0.170	0.196	1991
Manila	121.0	14.6	0.198	0.193	0.193	0.194	0.195	0.196	0.204	1991
	RMSEave		0.197	0.192	0.191	0.192	0.193	0.194	0.224	

The RMSE values of the different networks (Table 3.3) indicate that the ANN models perform better than the IRI M(3000)F2 model. Figure 3.5 is a graphical comparison of the

RMSE values of the IRI model and the six ANN models. The figure further illustrates the performance of the ANN over the IRI.

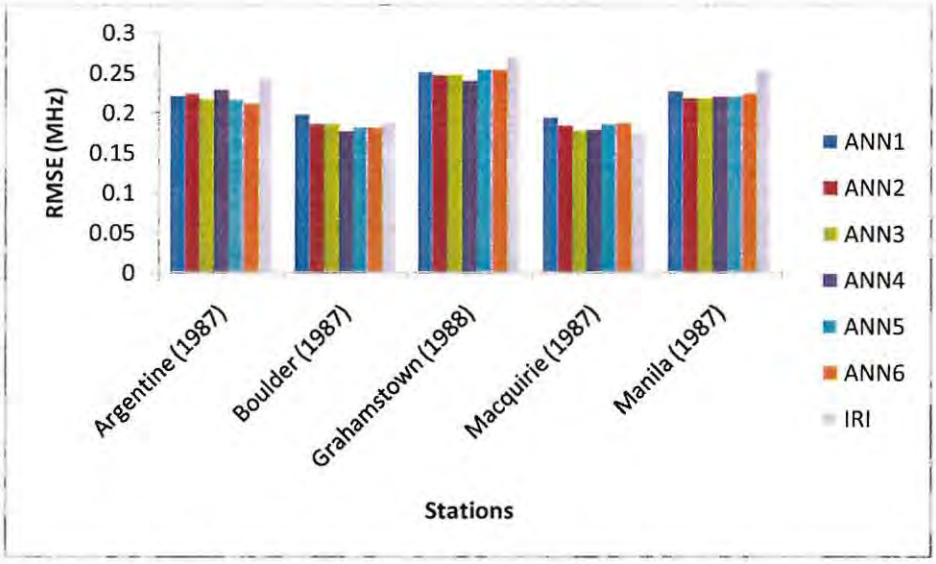

Figure 3.5: Graphical representation of RMSE values between observed M(3000)F2 and modelled values by the ANN and IRI models for some selected stations around low solar activity period.

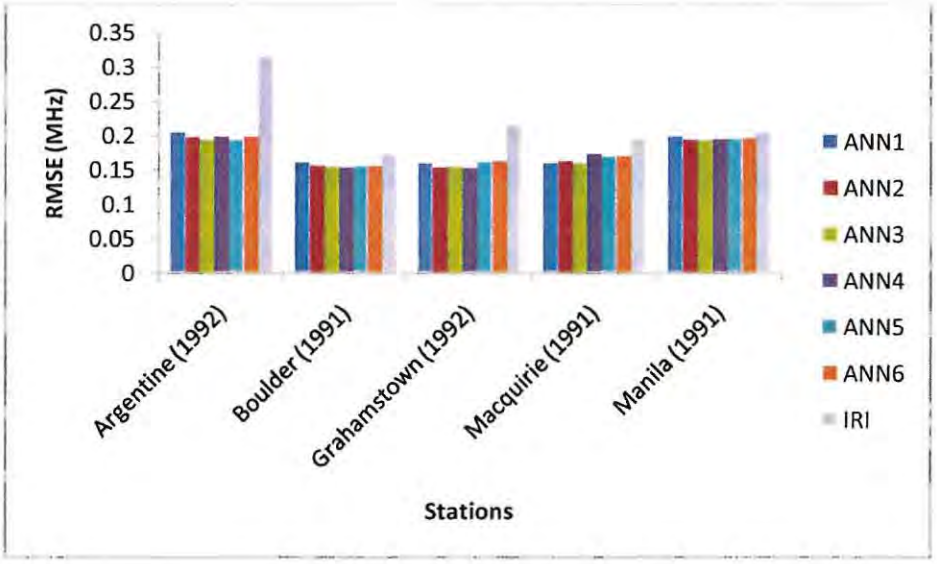

Figure 3.6: Graphical representation of RMSE values between observed M(3000)F2 and modelled values by the ANN and IRI models for some selected stations around high solar activity period.

The purpose of this preliminary stage was to ascertain which parameters would be most suitable for the global modelling of the M(3000)F2 parameter. The performance of the various networks was evaluated based on the average RMSE value. Figure 3.7 is a graphical representation of the RMSE average as evaluated using equation 3.12.

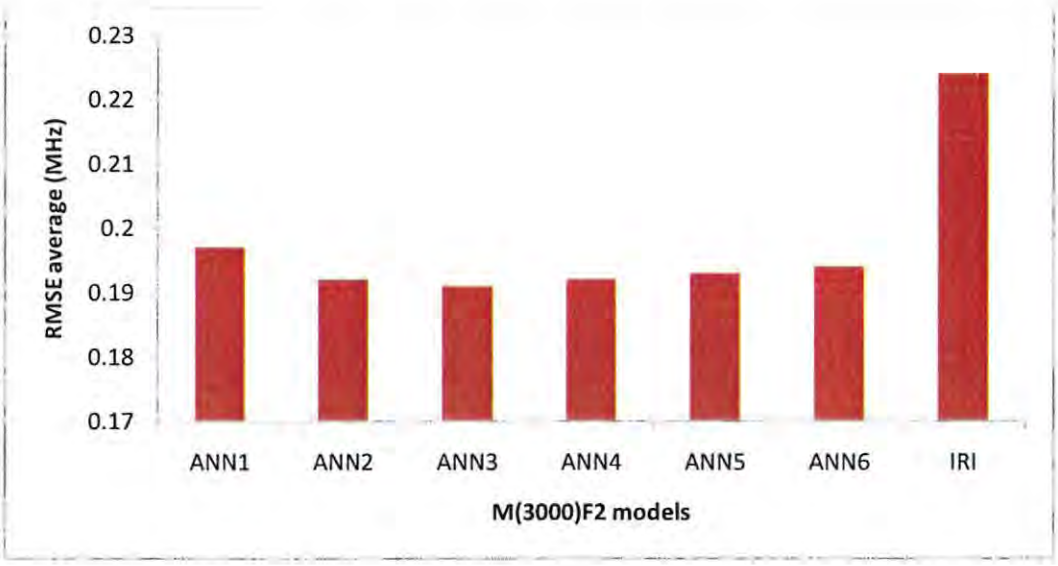

Figure 3.7: Graphical representation of average RMSE values between observed M(3000)F2 and modelled values by the ANN and IRI models for some selected stations around low and high solar activity period

Figure 3.7 indicates that ANN2, ANN3 and ANN4 show an improved performance over the rest of the networks (ANN1, ANN5 & ANN6). As a representation of solar cycle variation, ANN2 has both SF10.7 and SF81, ANN3 has both SF81 and P10.7, while ANN4 has only SF81 as an input parameter. It can be seen that there is some redundancy in both ANN2 and ANN3 in terms of the solar activity input parameter.

The results show that ANN4 is the most suitable for M(3000)F2 global modeling, and that the parameter SF81 is the most appropriate for representing the solar cycle variation in the network. The inclusion of this parameter is consistent with the IRI model which includes this parameter as an input variable.

3.5 Summary

This chapter presents a preliminary study of M(3000)F2 global modelling. The results of this initial investigation reveal the potential of the different neural networks trained in predicting the M(3000)F2 parameter. The performance of the networks in predicting M(3000)F2 outweighed the IRI version of the model at the stations indicated. The results of this preliminary study show that the network trained with the geophysical input parameters: day number (DNS and DNC), hour of the day (HS and HC), solar zenith angle (SCHI and CCHI), Modified dip latitude (Modip), 81-day running mean of daily F10.7 (SF81), ionospheric index based on ionosonde (SG12), ap index (A16), longitude (Long) and latitude (Lat) is the

optimum network which can be used successfully in modelling the M(3000)F2 parameter on a global scale. Thus, this architecture was used for the work discussed in the next chapter.

Chapter 4

M(3000)F2 Global Model

4.1 Introduction

The input space parameters used in ANN4, described in chapter 3 were used in the global modelling of the M(3000)F2 parameter. The work of Oyeyemi et al. (2007) employed day number (DNS and DNC), hour of the day (HS and HC), zenith angle (SCHI and CCHI), angle of meridian (MS and MC), magnetic inclination and declination (IS and DS), solar index (R12), magnetic index (A16), and geographic latitude (θ) as input space parameters for the M(3000)F2 global model.

For the purpose of this work, we have used DNS, DNC, HS, HC, SCHI, CCHI, Modip, SF81, SG12, A16, Long, and Lat. as input space parameters due to the reasons discussed in chapter 3 as well as the result obtained in the preliminary study.

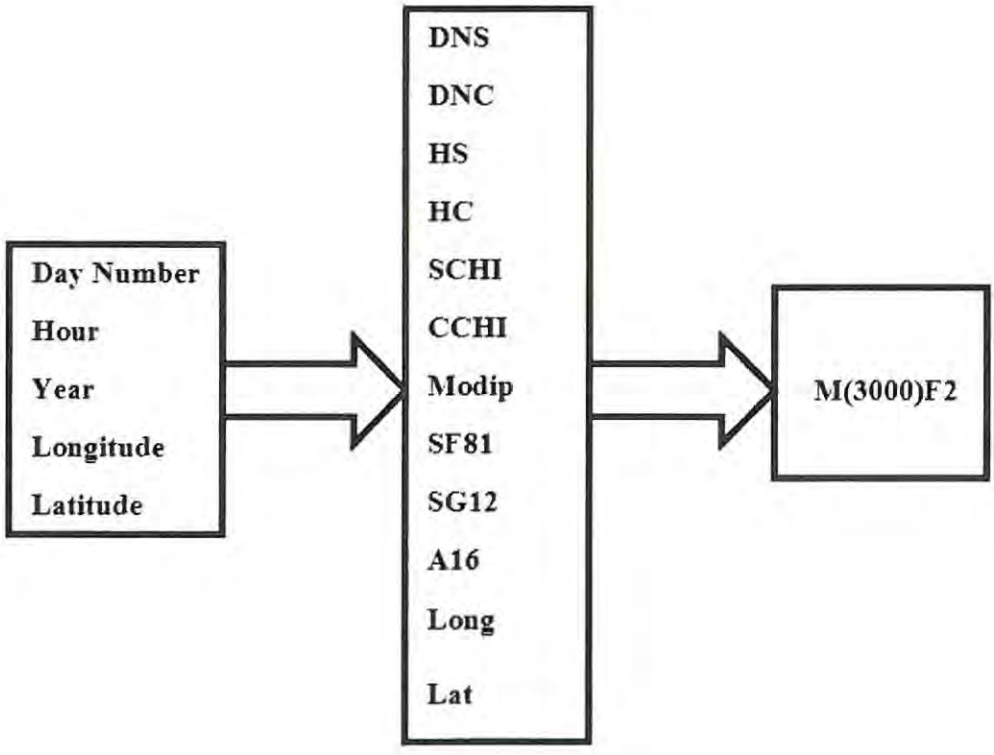

Figure 4.1: A block diagram of the inputs and outputs of the M(3000)F2 ANN

4.2 ANN Architecture, Training, Testing and Verification of the M(3000)F2 Global Model

Figure 4.1 is a block diagram of the ANN showing the input and output variables for the M(3000)F2 global model. Similar to the network architecture that was used in the preliminary stage, a feed-forward network architecture, performed in topological order, using randomized weights with a standard back-propagation algorithm was also used.

As earlier mentioned, archived hourly values of M(3000)F2 obtained from 135 ionospheric stations globally, spanning the period from 1976 to 2008 were available for this work. Some stations have data ranging from 1976 to 1986, while the majority of the stations provided data spanning the period 1987 to 2008. Data from 80 ionospheric stations were used for training, while the verification stations were selected from the remaining 55 stations. The training data ranges from the period of 1986 to 2008, the few stations with data covering 1976 to 1986 were included for verification. The training stations were selected in such a way that a good percentage of ionospheric stations in the various geographical regions (high, mid, and low-latitude) were adequately represented in the model. Table B.1 in Appendix B shows all the stations that were used for training while figure 4.2 is a global map of coordinates showing the training and verification stations. The majority of the stations were characterised by missing data. The problem of missing data at some stations was taken care of by the ANN because the technique does not require evenly distributed data points in the training process and thus, generating artificial data for the missing point is not necessary (see Oyeyemi 2005). Some stations did not have data for a complete solar cycle. Effort was made to ensure that stations, for which data were available for at least five years within a solar cycle, were used for training.

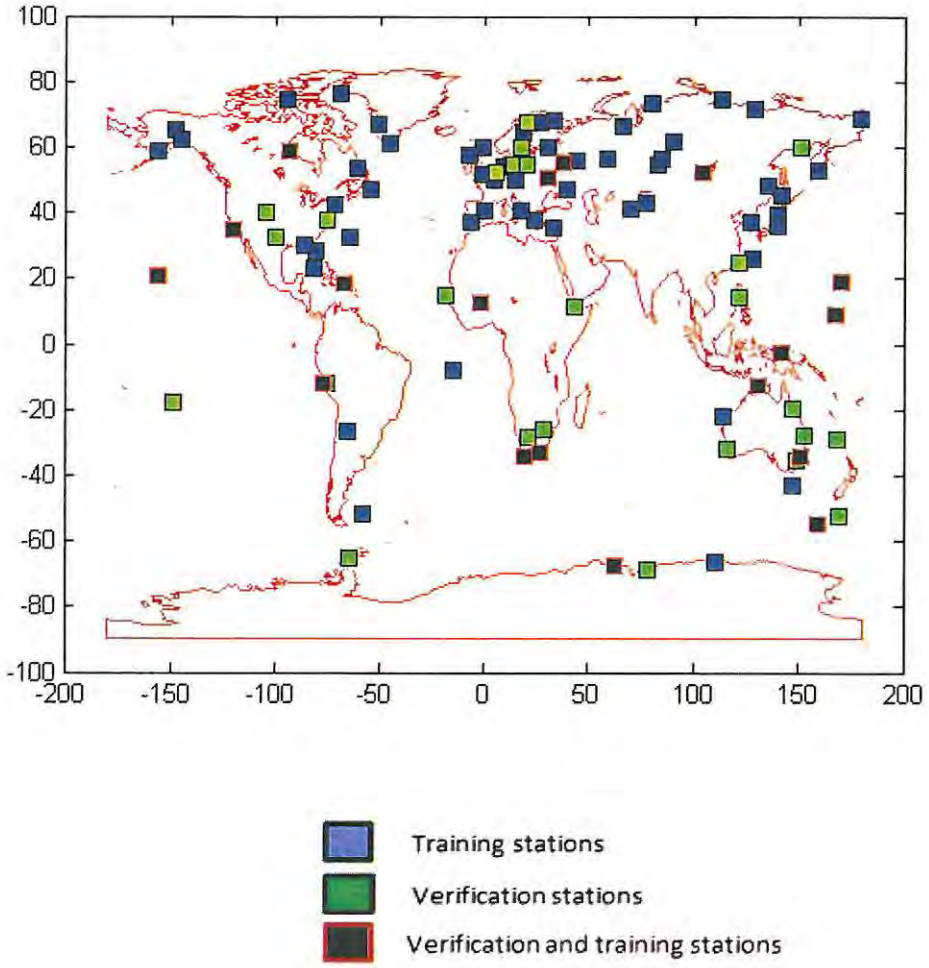

Figure 4.2: Global map of coordinates showing the training stations and the verification stations.

The same procedure discussed in Subsection 3.4.2 was applied in training the M(3000)F2-ANN global model. Based on previous work by some authors; considering the work done during the preliminary stage and the volume of data involved, the training was restricted to two and three hidden layer networks with nodes 35/30, 45/40, 55/50, 65/60, 75/70, 85/80, 35/30/25, 40/35/30, 45/40/35, 50/45/40, and 55/50/45.

The performance of these different network architectures was determined by evaluating their average RMSE using some specific stations, and applying equation 3.12. The network with lowest average RMSE was chosen as the best model for this work. Table 4.1 shows the RMSE values of the different network architectures trained with the specified number of hidden layers and nodes. Figure 4.3 is a graphical representation of the average RMSE values showing the performance of the different networks trained, and using the average RMSE values obtained for the IRI M(3000)F2 model as a standard.

Table 4.1: Comparison of the RMSE values ofthe different neural networks andthat of the IRI M(3000)F2 model.

Station	35/30	45/40	55/50	65/60	75/70	85/80	35/30/25	40/35/30	IRI	Year
Argentine	0.237	0.23	0.214	0.198	0.184	0.196	0.217	0.216	0.244	1987
Boulder	0.184	0.200	0.179	0.169	0.181	0.172	0.178	0.178	0.188	1987
Darwin	0.194	0.205	0.190	0.179	0.190	0.186	0.190	0.190	0.190	1987
Macquarie	0.201	0.202	0.189	0.159	0.163	0.169	0.189	0.187	0.176	1987
Moscow	0.144	0.146	0.146	0.142	0.152	0.145	0.146	0.146	0.158	1987
Mundaring	0.192	0.198	0.177	0.170	0.181	0.165	0.177	0.177	0.178	1987
Wallops	0.190	0.198	0.179	0.180	0.191	0.189	0.178	0.179	0.186	1987
Argentine	0.235	0.213	0.205	0.249	0.254	0.233	0.202	0.202	0.315	1992
Boulder	0.161	0.167	0.154	0.148	0.148	0.165	0.155	0.155	0.173	1991
Darwin	0.173	0.177	0.167	0.163	0.165	0.168	0.167	0.167	0.175	1991
Macquarie	0.163	0.160	0.161	0.156	0.151	0.161	0.161	0.161	0.174	1992
Moscow	0.241	0.231	0.216	0.211	0.224	0.217	0.216	0.216	0.255	1992
Mundaring	0.164	0.175	0.165	0.161	0.164	0.164	0.165	0.165	0.173	1991
Wallops	0.267	0.268	0.258	0.257	0.241	0.261	0.258	0.258	0.245	1991
$RMSE_{ave}$	0.196	0.198	0.186	0.182	0.185	0.185	0.186	0.186	0.202	

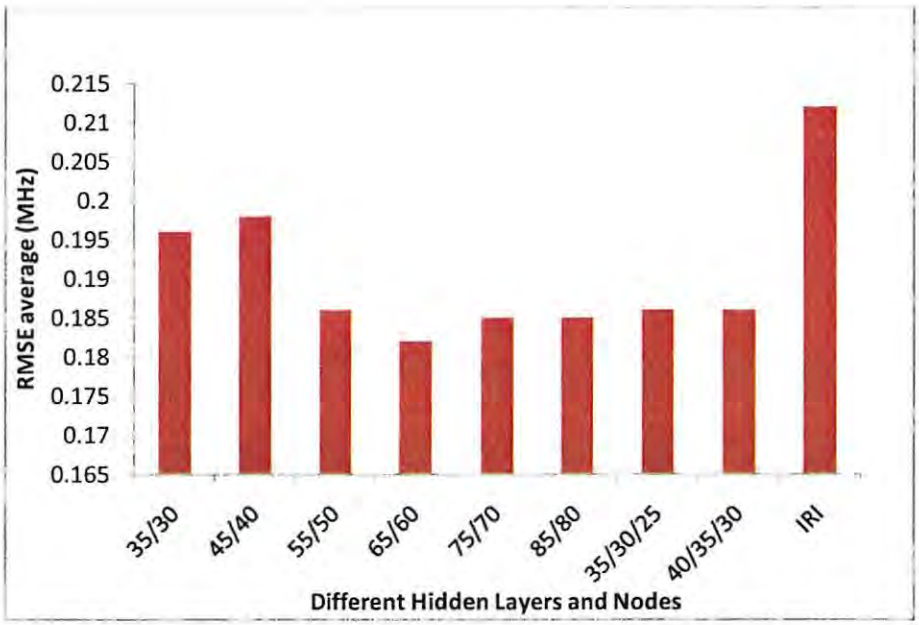

Figure 4.3: Graphical representation of the performance of the different neural network architectures.

Table 4.2: Verification stations for the ANNM(3000)F2 model

Station		Code	Longitude (°)	Latitude (°)
Argentine	T	AIJ6N	-64.30	-65.20
Boulder	T	BC840	-105.27	39.99
Brisbane		BR52P	152.90	-27.50
Campbell		CI65K	169.20	-52.50
Camden	T	CN53L	150.70	-34.00
Canberra		CB53N	149.00	-35.30
Chungli		CL424	121.20	24.90
Dakar		DKA14	-18.40	14.80
Darwin	T	DW41K	130.90	-12.40
Djibouti		DJ111	42.80	11.50
DyessAFB		DS932	-99.86	32.42
Grahamstown	T	GR13L	26.50	-33.30
Huancayo		HU91K	-75.30	-12.00
Irkutsk		IR352	104.00	52.50
Jicamarca		JI91J	-76.80	-12.00
Johannesburg		JO12O	28.10	-26.10
Kaliningrad		KL154	20.60	54.70
Kiruna		KI167	20.40	67.80
Louisvale		LV12P	21.20	-28.50
Macquariels	T	MQ55M	159.00	-54.50
Magadan		MG560	151.00	60.00
Manila		MN414	121.10	14.60
Moscow	T	MO155	37.30	55.50
Mundaring		MU43K	116.20	-32.00
Tahiti		TT71P	-149.30	-17.70
Townsville		TV51R	146.70	-19.30
Uppsala		UP158	17.60	59.80
Vanimo	T	VA50L	141.30	-2.70
Wallops		WP937	-75.47	37.94
Mawson	T	MW26P	62.90	-67.60
Churchhill	T	CH958	-94.20	58.80
Debilt		DT053	5.20	52.10
Norfolk		NI63	168.00	-29.00
Point Arguello		PA836	-120.53	34.77
Kiev	T	KV151	30.50	50.50
Maui	T	MA720	-156.46	20.76

4.3 Results and Discussion

To evaluate the effectiveness of the ANN model, daily hourly values of the ANN predicted M(3000)F2 were compared with observed values, and those predicted by the IRI 2007 M(3000)F2 model. The data from the verification stations listed in Table 4.2 were used to ascertain the performance of the model. The stations designated 'T' are part of the training stations.

Due to the difficulty in obtaining complete data sets for the same years in all the verification stations as a result of missing data, different years for which data were available were used for the validation of the ANN model. The computation of the RMSE was performed around low solar activity (referred to as LSA) (1977, 1978, 1987, 1988, 1997 and 2007), and high solar activity (referred to as HSA) (1981, 1991, 1992, 2000 and 2001) periods. The RMSE value between predicted and observed values of M(3000)F2 for each selected station was calculated as well as the average RMSE value over all the stations, using equations 3.13 and 3.12. To check the ability of the ANN model in the different geographical regions, care was taken to ensure that the various geographical regions (high, mid, and low latitudes) were adequately represented. The twenty six stations for which the RMSE values were evaluated within the specified periods are listed in Table 4.3.

Table 4.3: The RMSE values and percentage error difference in M(3000)F2 for ANN and IRI M(3000)F2 models

Stations Code	Long. (°)	Lat. (°)	RMSE (MHz):HSA				RMSE (MHz):LSA			
			ANN	IRI	%error	Year	ANN	IRI	%error	Year
Churchhill	-94.20	58.80	0.195	0.237	17.72	1991	0.172	0.197	12.69	1988
Darwin	130.90	-12.40	0.163	0.175	6.85	1991	0.179	0.189	5.29	1987
Grahamstown	26.50	-33.30	0.150	0.208	27.88	1992	0.236	0.269	12.27	1988
Macquarie	159.00	-54.50	0.156	0.174	10.34	1992	0.159	0.176	9.66	1987
Mawson	62.90	-67.60	0.247	0.302	18.21	1991	0.224	0.268	16.42	1987
Moscow	37.30	55.50	0.211	0.252	16.27	1992	0.144	0.157	8.28	1987
Vanimo	141.30	-2.70	0.190	0.197	3.55	1991	0.206	0.216	4.63	1987
Kiev	30.50	50.50	0.164	0.179	8.38	1991	0.151	0.174	13.23	1987
Maui	-156.50	20.76	0.206	0.228	9.65	1992	0.193	0.232	16.81	1988
Camden	150.70	-34.00	0.174	0.198	12.12	2001	0.300	0.310	3.23	2007
Argentine	-64.30	-65.20	0.249	0.315	20.95	1992	0.197	0.244	19.26	1987
Boulder	-105.30	39.99	0.148	0.154	3.90	1981	0.172	0.187	8.02	1977
Brisbane	152.90	27.50	0.140	0.170	17.65	1981	0.153	0.164	6.71	1977
Campbell	169.20	-52.50	0.162	0.210	22.86	1981	0.160	0.173	7.51	1977
Canberra	149.00	-35.30	0.143	0.174	17.82	1981	0.145	0.165	12.12	1977
Chung-Li	121.20	24.90	0.195	0.237	17.72	1991	0.210	0.261	19.54	1997
Davis	77.90	-68.60	0.210	0.259	18.92	1991	0.263	0.306	14.05	1987
Djibouti	42.80	11.50	0.152	0.157	3.18	1981	0.188	0.194	3.09	1977
Mundaring	116.20	-32.00	0.194	0.217	10.60	1981	0.169	0.176	4.00	1977
Grahamstown	26.50	-33.30	0.223	0.241	7.47	1981	0.227	0.276	17.75	1978
Huancayo	-75.30	-12.00	0.146	0.165	11.52	1981	0.182	0.190	4.21	1978
Kiruna	20.40	67.80	0.195	0.209	6.70	1992	0.183	0.198	7.58	1997
Magadan	151.00	60.00	0.169	0.185	8.65	1991	0.145	0.148	2.03	1977
Manila	121.10	14.60	0.189	0.210	10.00	1991	0.196	0.210	6.67	1988
Townsville	146.70	-19.30	0.148	0.165	10.30	1991	0.166	0.182	8.79	1987
Uppsala	17.60	59.80	0.149	0.168	11.31	2000	0.164	0.178	7.87	1997
$RMSE_{average}$			0.180	0.207	13.04		0.188	0.209	10.05	

To investigate the extent of the performance of the ANN model, percentage error differences between ANN and IRI models were evaluated using the relation:

$$\left(\frac{IRI_{RMSE} - ANN_{RMSE}}{IRI_{RMSE}}\right) \times 100\% \qquad 4.1$$

where ANN_{RMSE} and IRI_{RMSE} are the RMSE values derived from the predictions made with the ANN and the IRI models respectively. The results obtained for the percentage error are included in tables 4.3. The percentage error difference is a measure of improvement in the ANN over the IRI model.

The values obtained for RMSE in M(3000)F2 (shown in table 4.3) between the ANN and the IRI models reveal the effectiveness of the ANN model in predicting the M(3000)F2 parameter. Though there are some stations where the performance of the ANN model (based on percentage error difference) is not so strong, (e.g. Vanimo and Djibouti), this poor performance could be attributed to the paucity of data from those regions in the training database.

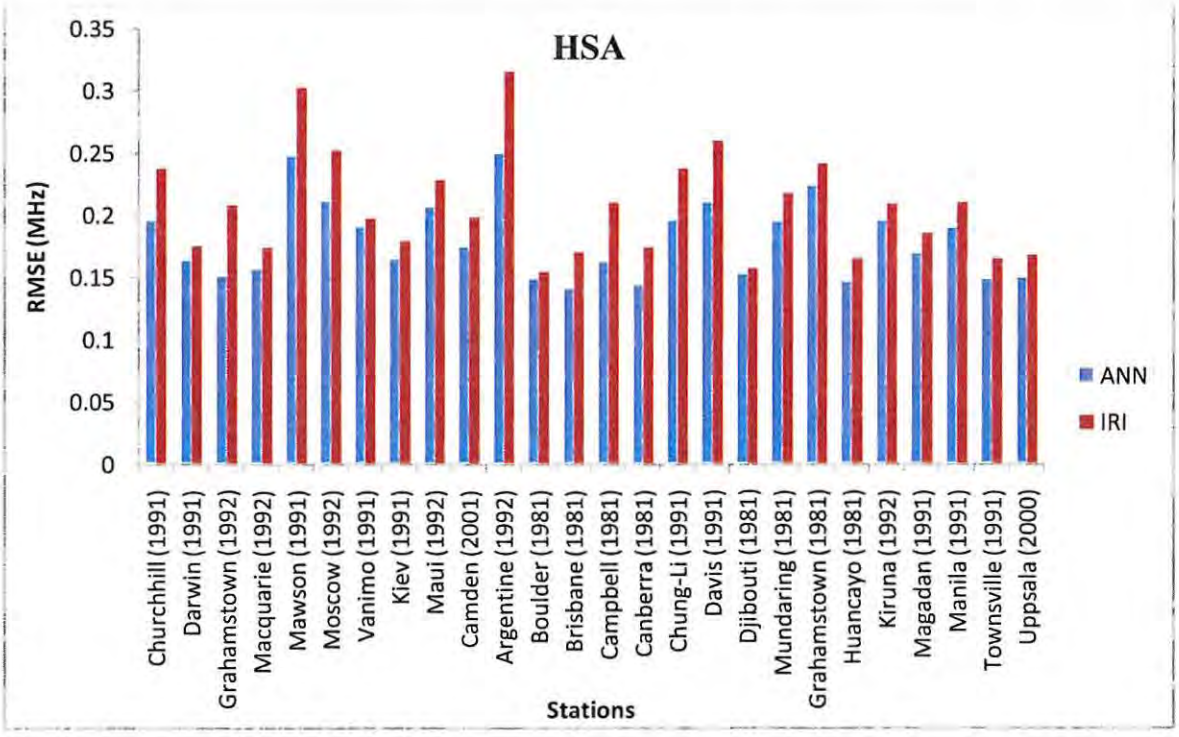

Figure 4.4: Graphical representation of the RMSE values between the observed and predicted values of the ANN and the IRI M(3000)F2 models at some verification stations around the HSA period.

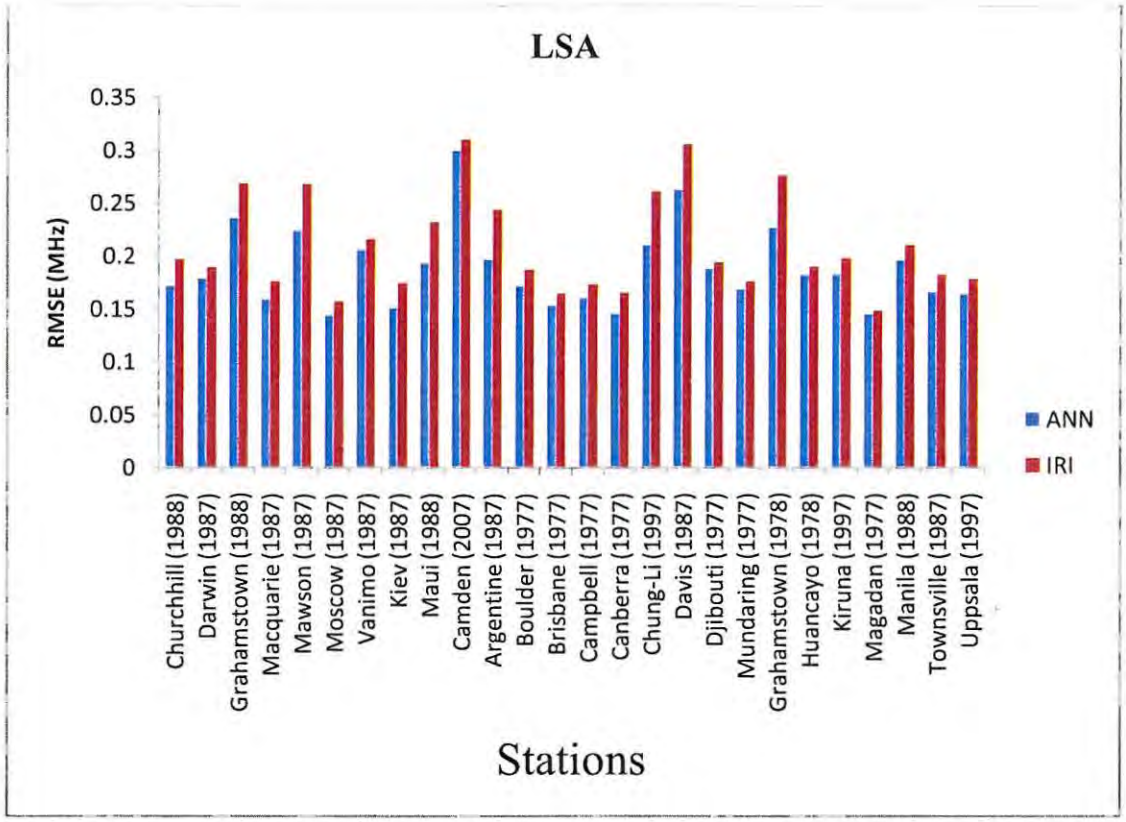

Figure 4.5: Graphical representation of the RMSE values between the observed and predicted values of the ANN and the IRI M(3000)F2 models at some verification stations around the LSA period.

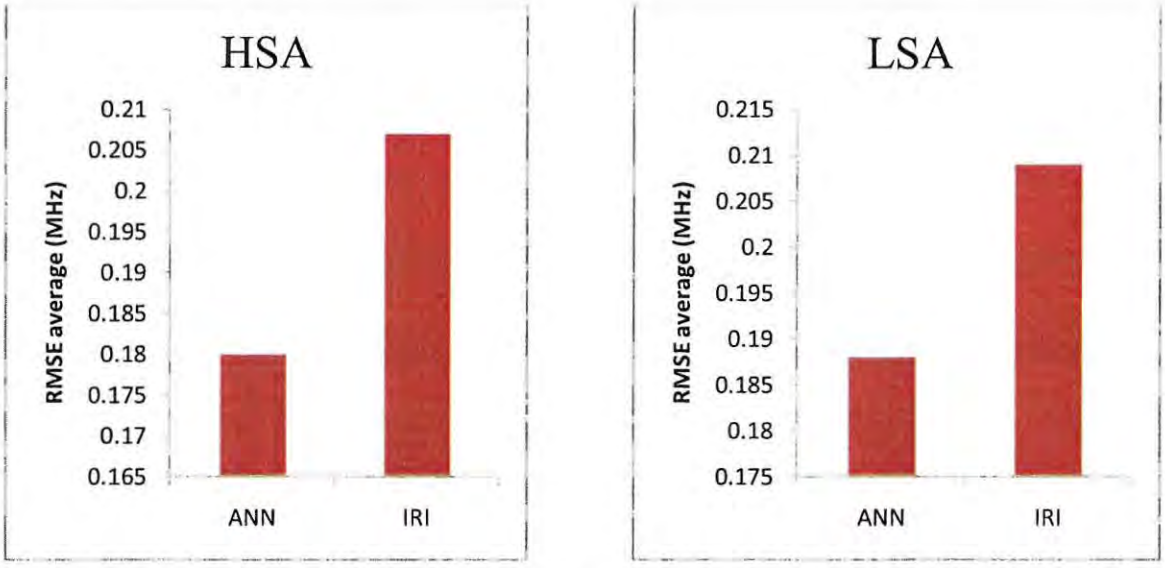

Figure 4.6: Graphical representation of the average RMSE values for predicted values of the ANN and the IRI models at some verification stations around the period of HSA and LSA respectively

Figures 4.4 and 4.5 are graphical representations of the RMSE values obtained around HSA and LSA periods respectively. The figures illustrate the improved performance of the

M(3000)F2 ANN model over the IRI version of the M(3000)F2 model in all the stations where the RMSE were evaluated during the years indicated.

The general performance of the ANN and the IRI model was determined using the average RMSE values. Figure 4.6 is a graphical illustration of the average RMSE values of the ANN and the IRI M(3000)F2 models for HSA and LSA periods. As can be observed from the figures, the margin between the average RMSE values obtained for the ANN and the IRI models is quite large. The average percentage improvement of the ANN model over the IRI version is 13.04% and 10.05% around HSA and LSA periods respectively.

The performance of the model was further investigated by evaluating the correlation coefficient between the observed values and the predicted values of the ANN and the IRI models. Correlation coefficient is a measure of how the strength and direction in the predicted values follows the trends in the observed values; in other words, it measures how well the predicted values of the model "fit" the measured data.

Table 4.4: Correlation coefficients of the ANN and IRI M(3000)F2 models around the LSA and HSA periods.

Stations	**Long (°)**	**Lat (°)**	**Correlation Coefficients HSA**			**Correlation Coefficients LSA**		
			ANN	**IRI**	**Year**	**ANN**	**IRI**	**Year**
Boulder	-105.27	39.99	0.79	0.72	1981	0.72	0.67	1977
Kiev	30.50	50.50	0.78	0.71	1991	0.78	0.75	1987
Campbell	169.20	-52.50	0.83	0.71	1981	0.75	0.66	1977
Canberra	149.00	-35.30	0.83	0.75	1981	0.76	0.70	1977
Chung-Li	121.20	24.90	0.65	0.59	1991	0.66	0.62	1997
Huancayo	-75.30	-12.00	0.92	0.91	1981	0.83	0.81	1977
Townsville	146.70	-19.30	0.75	0.72	1991	0.75	0.70	1987
Maui	-156.46	20.76	0.71	0.64	1992	0.65	0.53	1988
Moscow	37.30	55.50	0.72	0.67	1992	0.80	0.75	1987
Mawson	62.90	-67.60	0.65	0.48	1991	0.72	0.63	1987

The correlation coefficient between the observed and predicted values of the ANN and the IRI models were computed using equation 4.2.

$$r = \frac{N\sum xy - (\sum x)(\sum y)}{\sqrt{N(\sum x^2) - (\sum x)^2}\sqrt{N(\sum (y^2) - (\sum y)^2}} \qquad 4.2$$

where r is the correlation coefficient, N is the number of data points, and $x = M(3000)F2_{obs}$, $y = M(3000)F2_{pred}$ are the observed and predicted values of M(3000)F2 respectively.

The results obtained are tabulated in table 4.4. A careful inspection of the table shows that both models exhibit positive correlation with the observed data. However, the ANN model shows stronger correlation than the IRI version for both LSA and HSA periods.

Figures 4.7, 4.8 and 4.9 show the scatter plots of the observed and predicted values of the ANN and the IRI M(3000)F2 models for three stations (Brisbane, Debilt and Vanimo). The plots also show a stronger correlation coefficient for the ANN model than the IRI version. This result is a further proof of the effectiveness of the ANN model, and reaffirms the improved performance of ANN model.

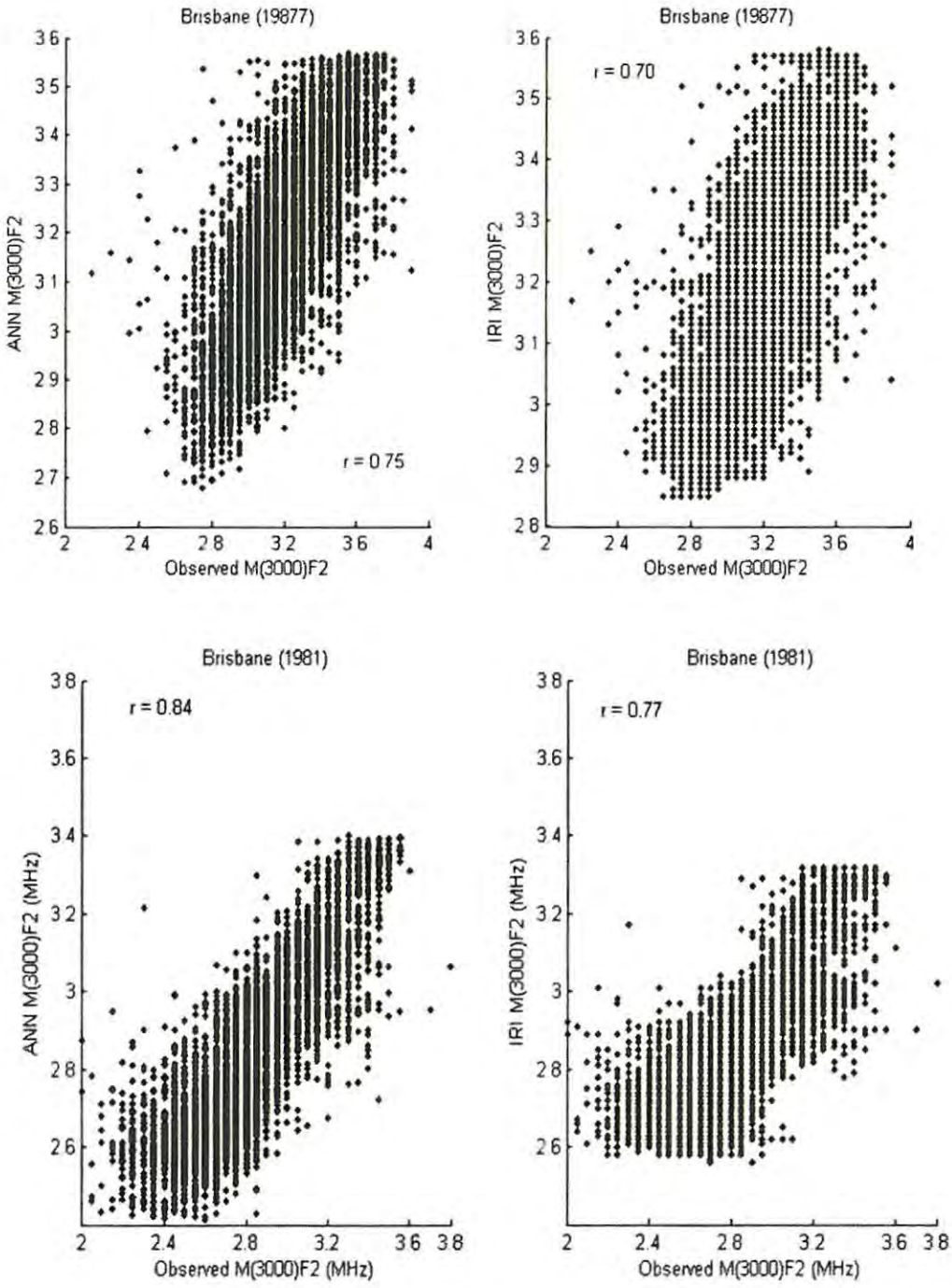

Figure 4.7: Scatter plots for observed and predicted values of ANN and IRI models at Brisbane around LSA and HSA periods respectively.

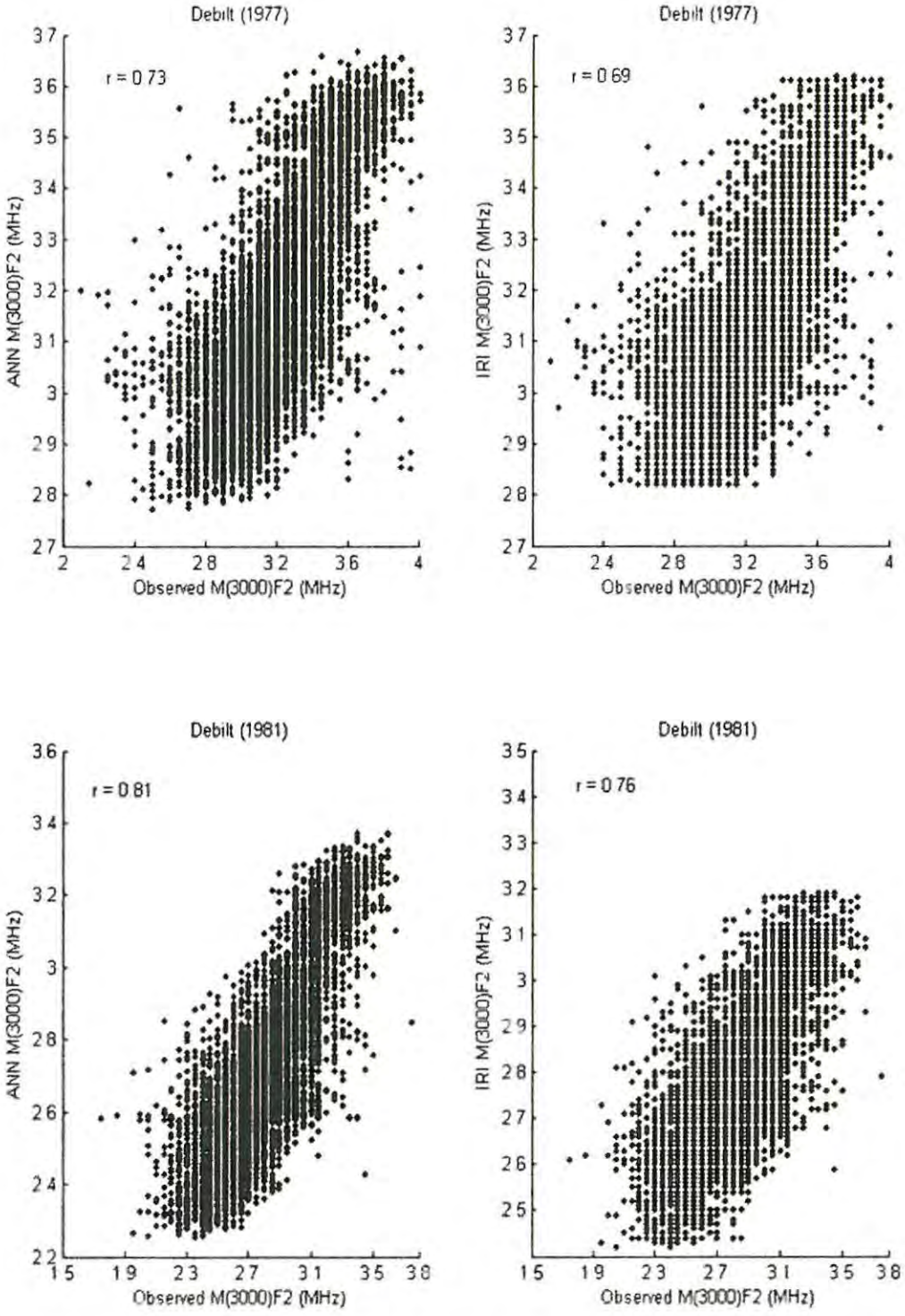

Figure 4.8: Scatter plots for observed and predicted values of ANN and IRI models at Debilt around LSA and HSA periods respectively.

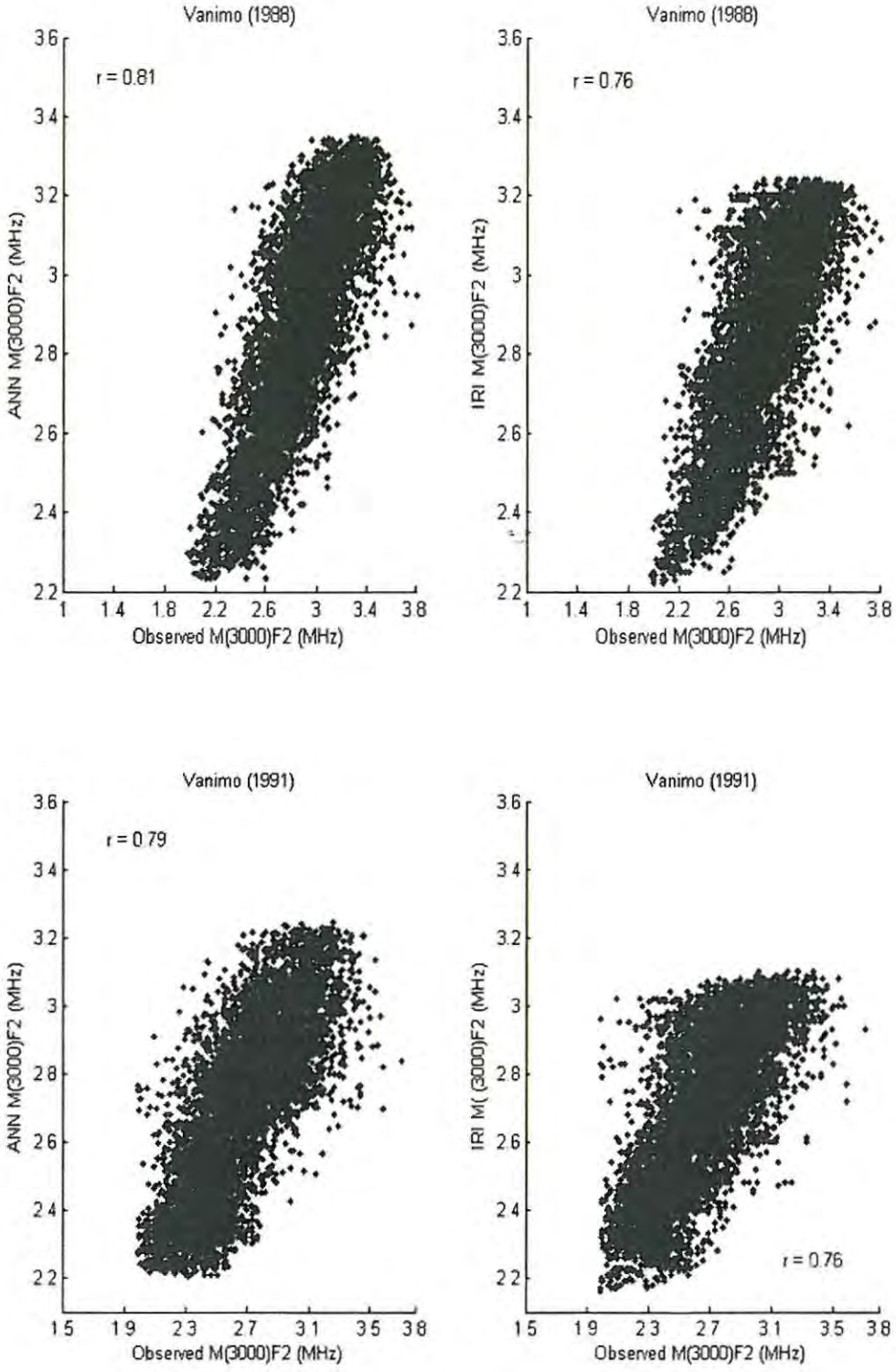

Figure 4.9: Scatter plots for observed and predicted values of ANN and IRI models at Vanimo around LSA and HSA periods respectively.

4.4 Diurnal and Seasonal Verification of ANN M(3000)F2

4.4.1 Diurnal Variation

Figures 4.10 to 4.13 show the diurnal variation of the M3000)F2 parameter. Both the ANN and IRI models successfully represent the diurnal structure of the M(3000)F2 values with some degrees of error, as can be observed from the plots. The diurnal shape is such that the plotted values begin at 00h00UT. The periods selected for the plots correspond to HSA and LSA periods. These periods were chosen in order to check the performance of the model during the periods of expected maximum and minimum electron density in the F2 region.

A close observation of the plots also shows an improved performance of the ANN model over the IRI version at some stations. This improvement of the ANN model over the IRI model is very obvious in Figure 4.11, where the IRI model over-predicts (e.g. Kalinigrad (day 181 and 182), Point-Arguello (day 220 and 221)) and under-predicts (e.g. Johannesburg (day 10 and 11, day 194 and 195), Wallops (day 10 and 11)) M(3000)F2 values. This trend is also noticeable in Figure 4.12.

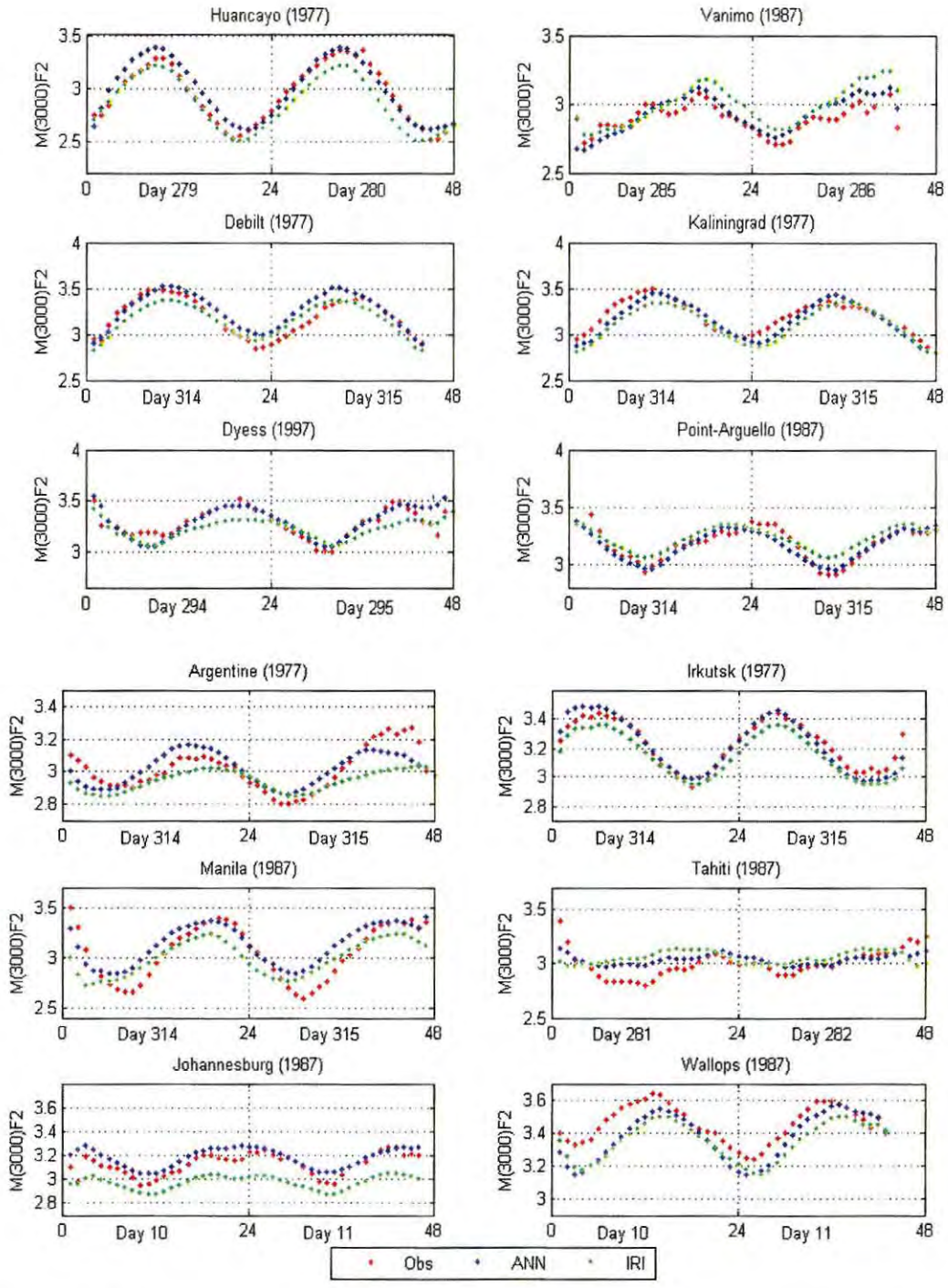

Figure 4.10: Comparison of the diurnal structure of M(3000)F2 values around the period of LSA predicted by ANN and IRI model with the observed values for two days beginning at 00h00UT.

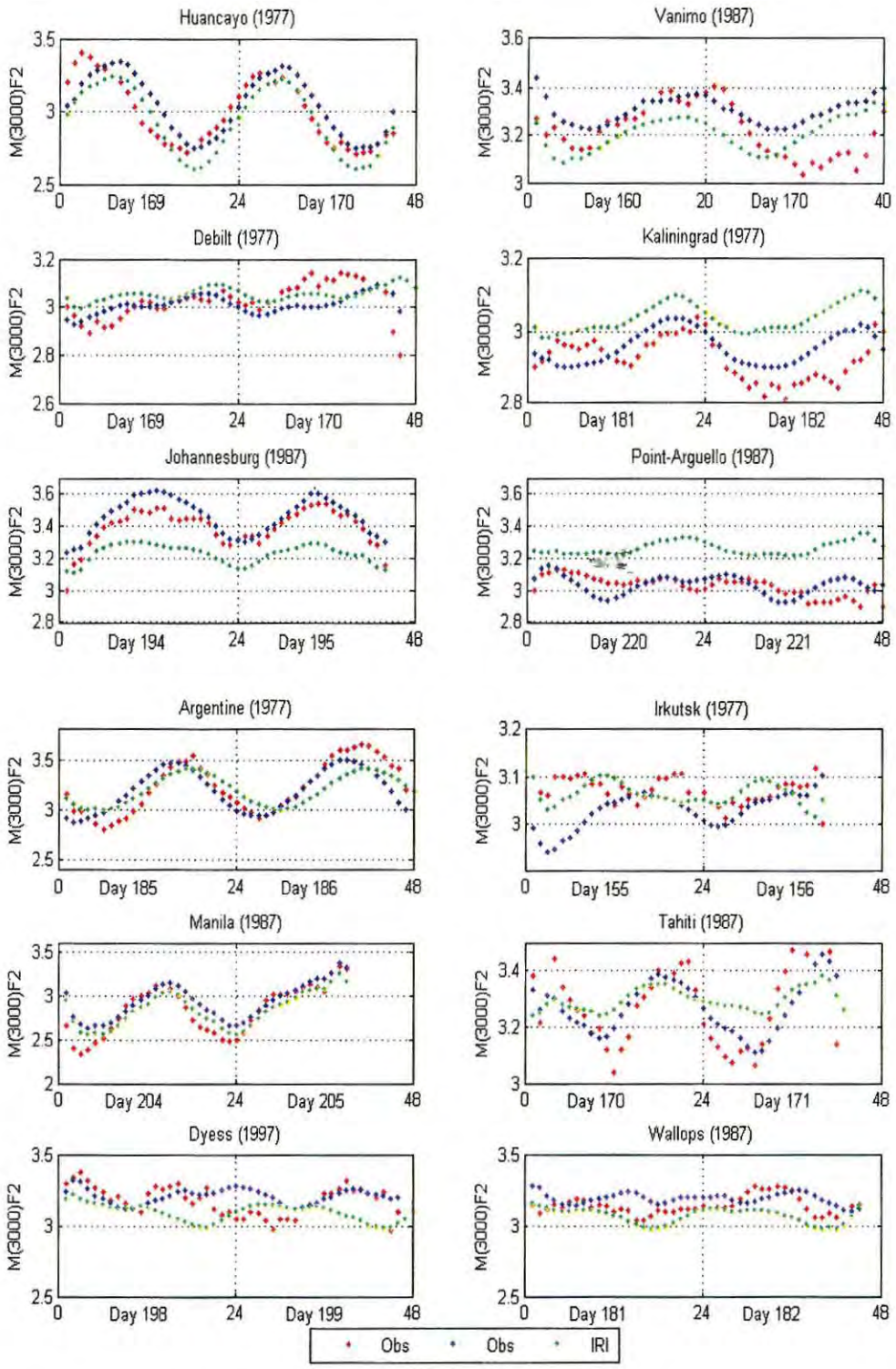

Figure 4.11: Comparison of the diurnal structure of M(3000)F2 values around the period of LSA predicted by ANN and IRI model with the observed values for two days beginning at 00h00UT.

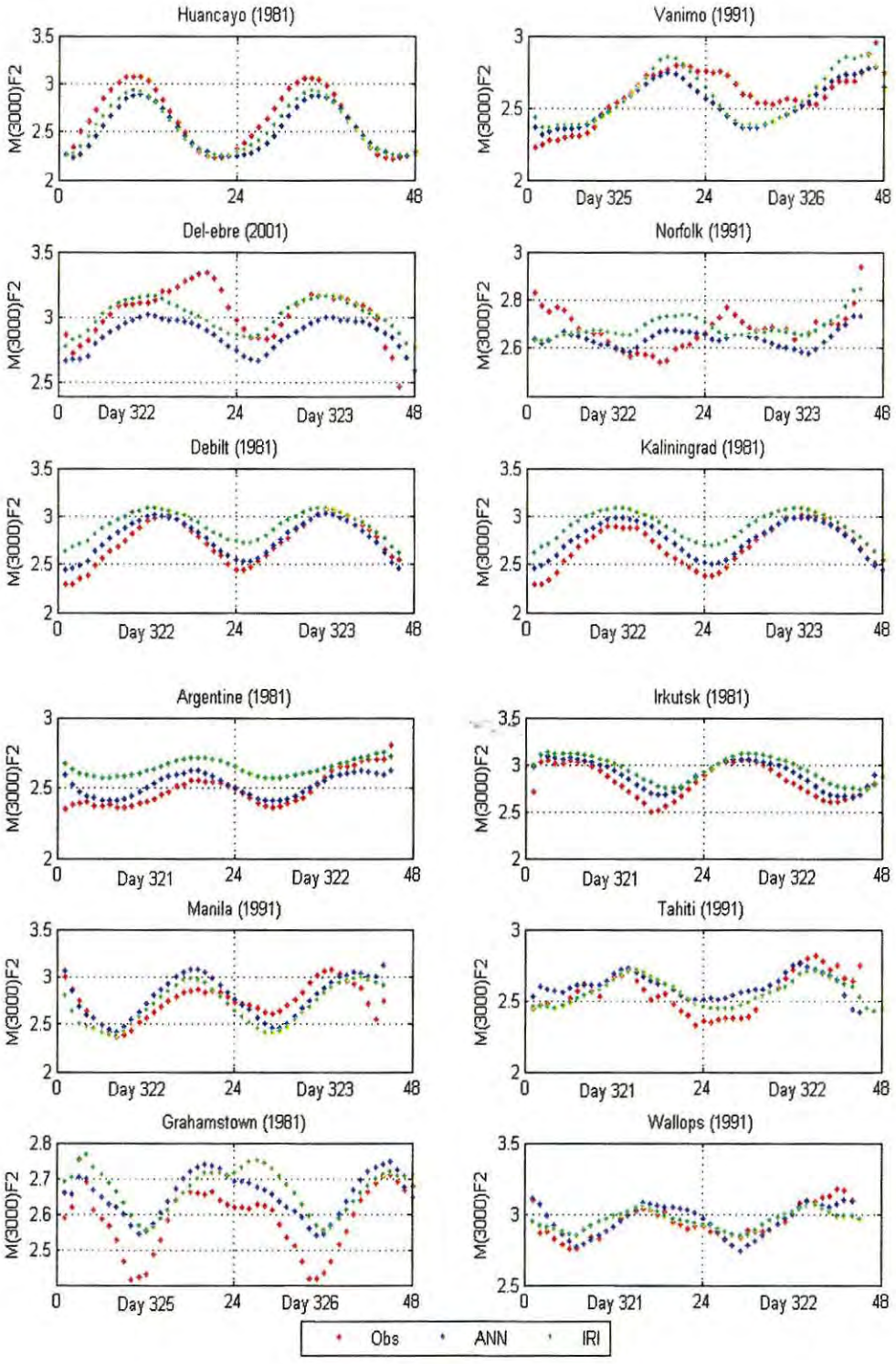

Figure 4.12: Comparison of the diurnal structure of M(3000)F2 values around the period of HSA predicted by ANN and IRI model with the observed values for two days beginning at 00h00UT.

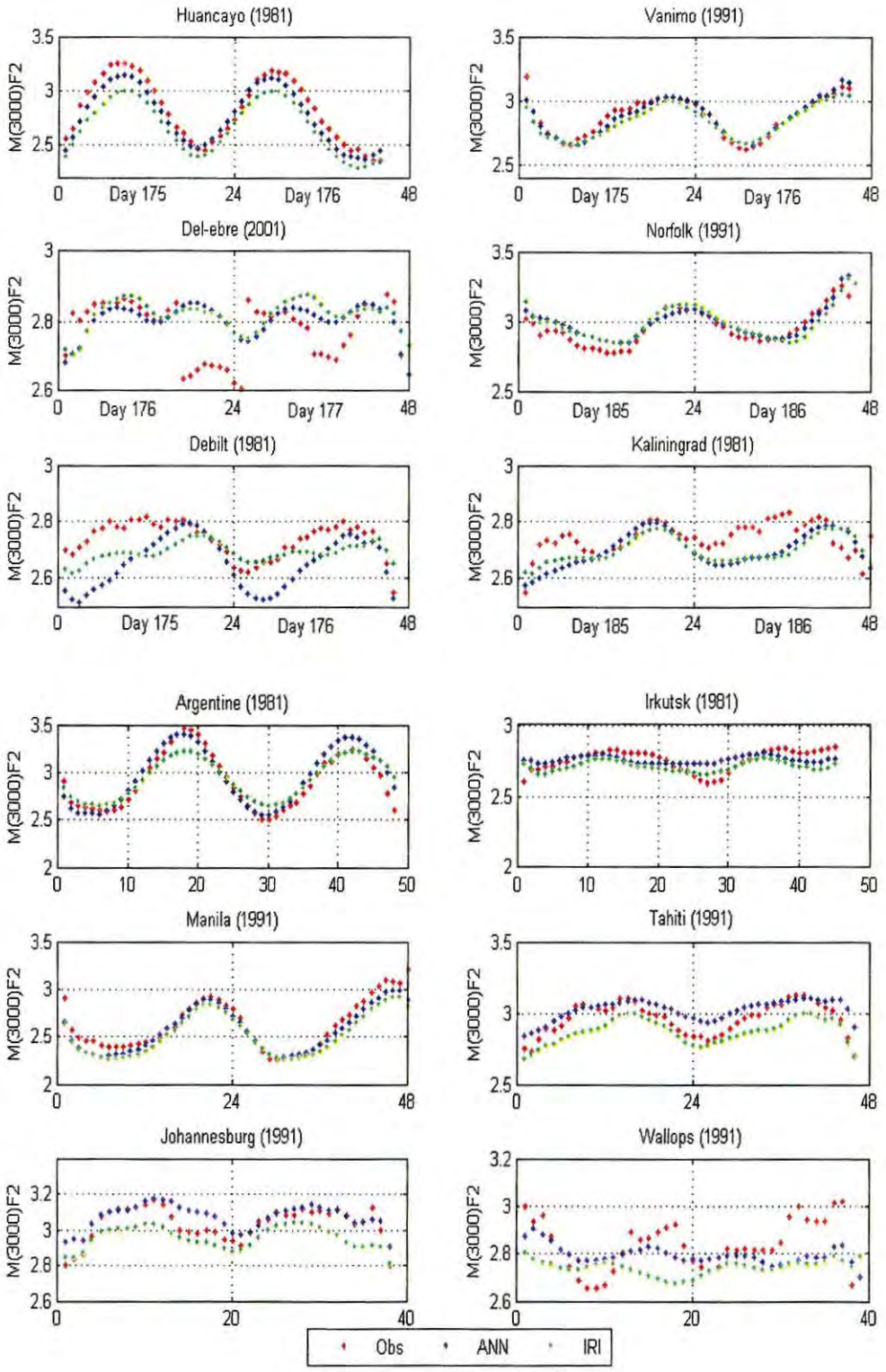

Figure 4.13: Comparison of the diurnal structure of M(3000)F2 values around the period of HSA predicted by ANN and IRI model with the observed values for two days beginning at 00h00UT.

From the figures, the diurnal variation pattern predicted by the ANN and the IRI M(3000)F2 models at some stations are almost the same. Therefore, model with the best performance cannot be easily inferred from the plots. As a result of this, the RMSE and percentage error difference were computed for a selected sample of such stations in the figures. The results are shown in Table 4.5.

Table 4.5: RMSE values and percentage error difference in M(3000)F2 between the ANN and the IRI-M(3000)F2 models at selected stations.

Station	**Long. (°)**	**Lat. (°)**	**RMSE (MHz)**		**% error**	**Day**	**Year**
			ANN	**IRI**			
Huancayo	-75.30	-12.00	0.204	0.209	2.39	279/280	1977
Manila	121.10	14.60	0.204	0.256	20.30	314/315	1987
Debilt	5.20	52.10	0.195	0.184	-5.98	314/315	1977
Irkutsk	104.00	52.50	0.126	0.143	11.89	314/315	1977
Dyess	-99.86	32.42	0.229	0.241	5.00	294/295	1997
Wallops	-75.47	37.94	0.209	0.180	-16.11	181/182	1987
Argentine	-64.30	-65.20	0.106	0.191	44.50	321/322	1981
Vanimo	141.30	-2.70	0.137	0.137	0.00	175/176	1991
Johannesburg	28.10	-26.10	0.171	0.197	13.20	198/199	1991
Norfolk	168.00	-29.00	0.129	0.131	1.53	175/176	1991
RMSEave			0.171	0.187	8.56		

The results presented in Table 4.5 are consistent with the performance of the ANN model over the IRI version. An average percentage error of 8.56% was determined indicating 8.56% improvement for the ANN model predictions over the IRI 2007 model.

The low-latitude region and equatorial ionosphere are known to be problematic for the IRI-M(3000)F2 model. The IRI 2007 model's inability to reproduce the diurnal structure adequately, particularly the post-sunset values of the M(3000)F2, have been reported (see Obrou et al., 2003; Adeniyi et al., 2003; Zhang et al., 2004 and 2007). To check the ability of the ANN model in addressing this inadequacy, particular periods and stations were chosen.

The equator is tilted towards the overhead sun twice a year; giving rise to equal day and night (equinox). The high variability of the ionospheric electron density especially in the equatorial and the low latitude regions during these periods have been reported (see Bailey et al., 2000 and Liu et al., 2010). As a result of this, the ability of the ANN and the IRI models to predict the M(3000)F2 values at equinox was investigated. Equinox occurs every September 21 (southern hemisphere) and March 21 (northern hemisphere); hence day 80 and 264 (depending on the geographical location of the station) were chosen to correspond to the

equinox days. Eight stations within the low latitude region were used. Figure 4.14 is a comparison of the diurnal variation of the M(3000)F2 values as predicted by the ANN and the IRI models with respect to the observed values during the periods of LSA and HSA respectively. From figure 4.14, the ANN model represents the diurnal variation of the M(3000)F2 values more accurately than the IRI model at most of the stations. The inability of the IRI model to reproduce the post-sunset (18:00 to 20:00) values of the M(3000)F2 is also obvious from these plots at some stations, as earlier pointed out by Obrou et al. (2003), Adeniyi et al. (2003), and Zhang et al. (2004 and 2007). As can be observed in the graphs, there are also cases of over-prediction and under-prediction of the M(3000)F2 values (Townsville (1991), Manila (1988), Ascension (2002), Jicamarca (2007) & Maui) by the IRI M(3000)F2 model.

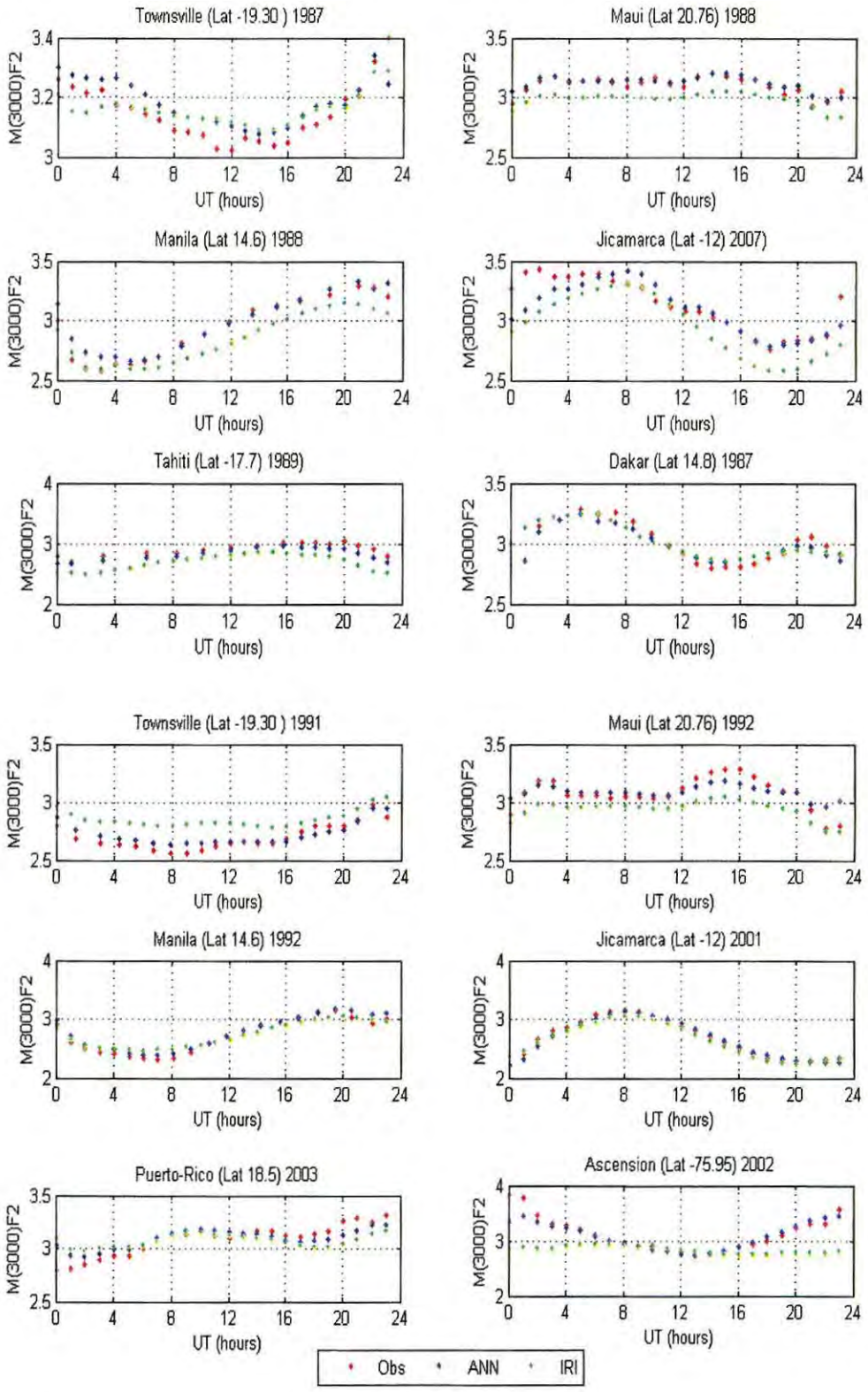

Figure 4.14: Comparisons of M(3000)F2 values as predicted by the ANN and IRI models with respect to observed values at equinox.

A further investigation of the performance of the ANN model in the low latitude region was carried out for two stations (Ouagadougou (lat. 12.4°) and (Jicamarca lat. -12°)), representing the northern and the southern hemispheres. This was done to check how well the ANN model can predict the post-sunset values of the M(3000)F2. Similar studies were performed by Adeniyi et al. (2003) and Obrou et al. (2003), in which they found that the IRI M(3000)F2 model was unable to reproduce the post-sunset values of M(3000)F2 in the low-latitude region adequately. These previous studies were performed over two stations (Ouagadougou (lat 12.4) and Korhogo (lat. 9.3)).

Figure 4.15 is a plot of the monthly median hourly values of the observed M(3000)F2 as well as the values predicted by the ANN and the IRI models for the months of January, April, July and October, corresponding to the four seasons in year 1988 and 2007. There is a better agreement between the observed and the ANN values compared to the IRI values. In other words, the ANN values closely follow the observed values more accurately than the IRI values, e.g. values at 12h00, 13h00 and 18h00 were predicted with minimal error by the ANN model compared to the IRI version. The ANN model provides a more accurate prediction for the post-sunset (18h00 to 20h00) values of M(3000)F2 than the IRI version. This is an important result which addresses the inadequacy of the M(3000)F2 IRI model which was pointed out by Adeniyi et al. (2003) for Ouagadougou station in the low latitude region.

The general performance of the ANN model in the low-latitude region demonstrates its capability in describing the M(3000)F2 parameter in the low-latitude area and the equatorial ionosphere with minimal error on a global scale.

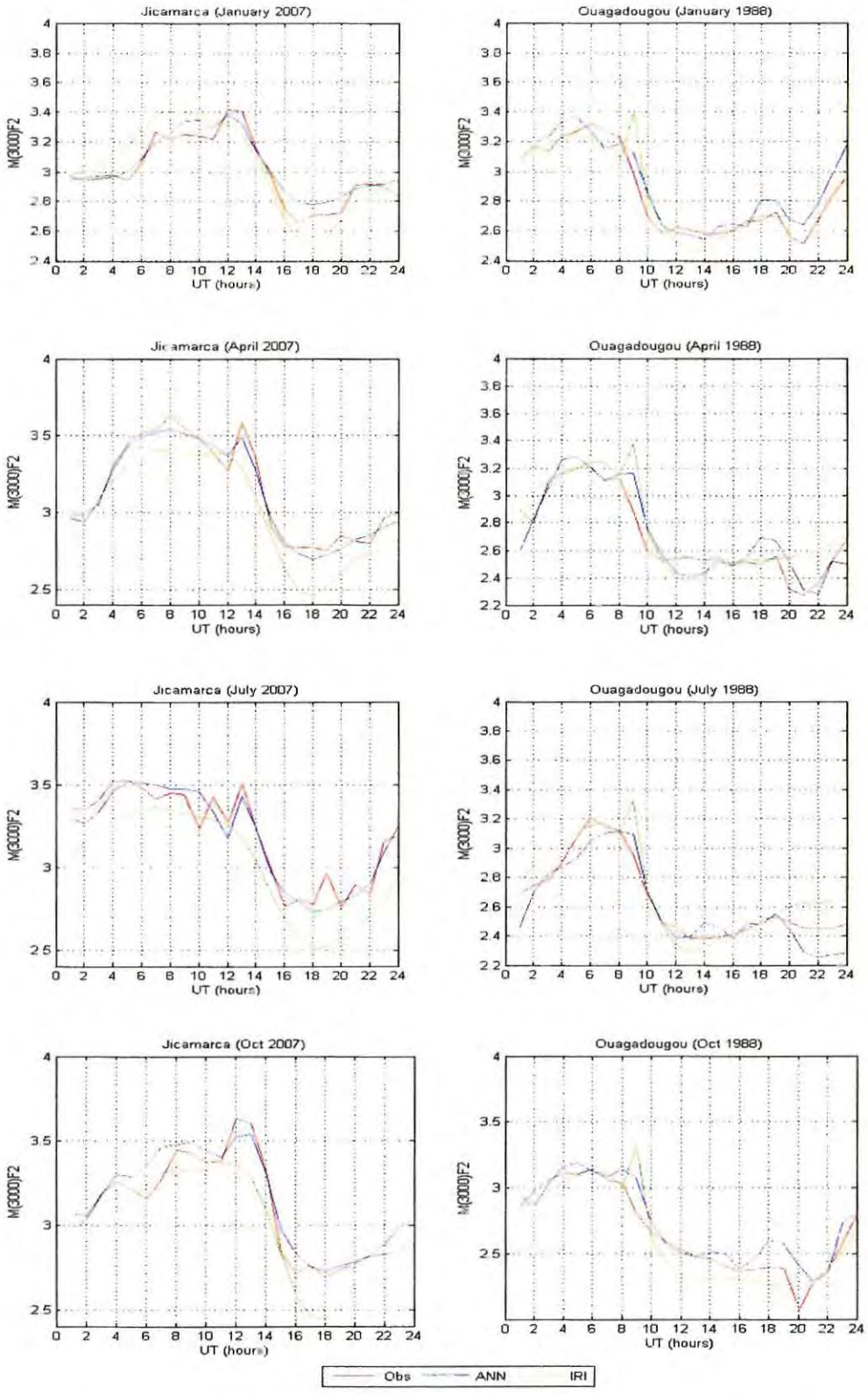

Figure 4.15: Comparisons of the monthly median hourly values of observed and predicted values of M(3000)F2 for Jicamarca and Ouagadougou.

4.4.2 Seasonal Variation

The seasonal variation patterns of M(3000)F2 at 00h00UT, 06h00UT, 12h00UT and 18h00UT, corresponding to midnight, sunrise, midday and sunset are illustrated in Figures 4.16 to 4.23. These time periods were chosen due to the variability of the M(3000)F2 parameter during these periods, to verify how well the model can reproduce the seasonal variation pattern of M(3000)F2, across the various geographical regions. The comparison of the seasonal variation of the ANN and the IRI predicted values with respect to the observed values was performed for twelve verification stations. This was done around the period of LSA (1977, 1987, & 1988) and HSA (1981, 1991, & 1992) based on the availability of data.

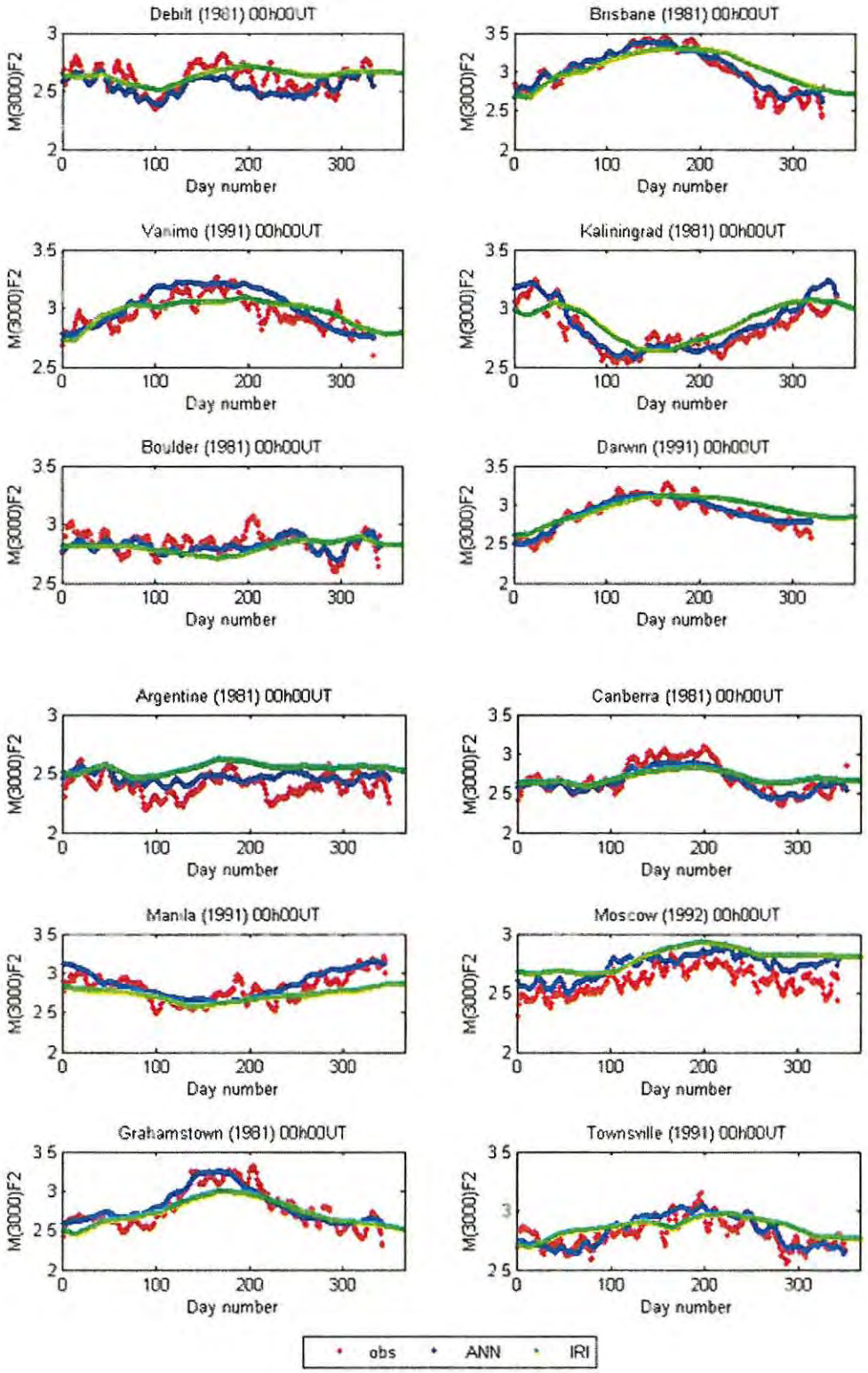

Figure 4.16: Comparison of seasonal variations of M(3000)F2 values predicted by the ANN and the IRI models with respect to the observed values around HSA at 00h00UT.

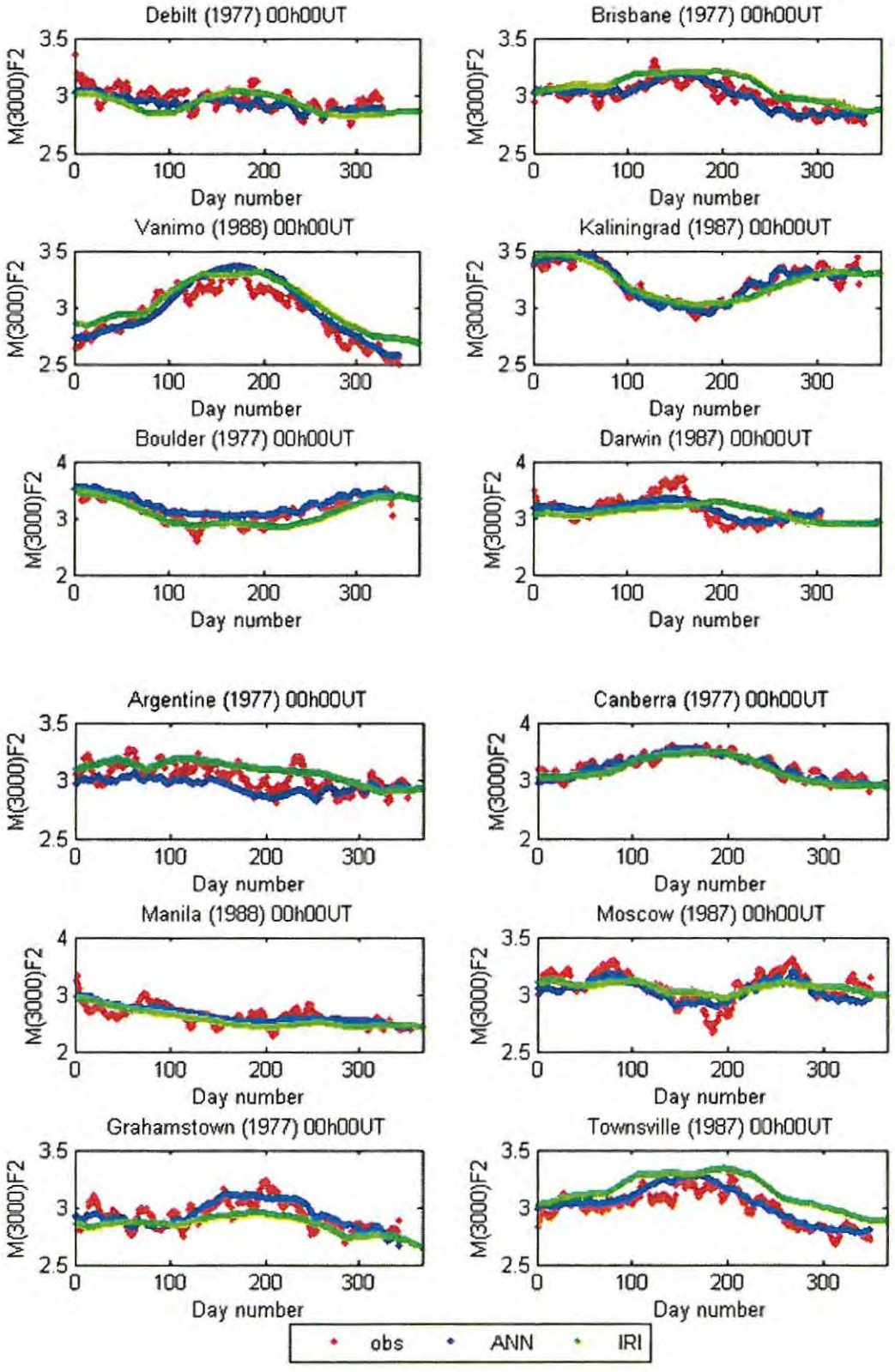

Figure 4.17: Comparison of seasonal variations of M(3000)F2 values predicted by the ANN and the IRI models with respect to the observed values around LSA at 00h00UT.

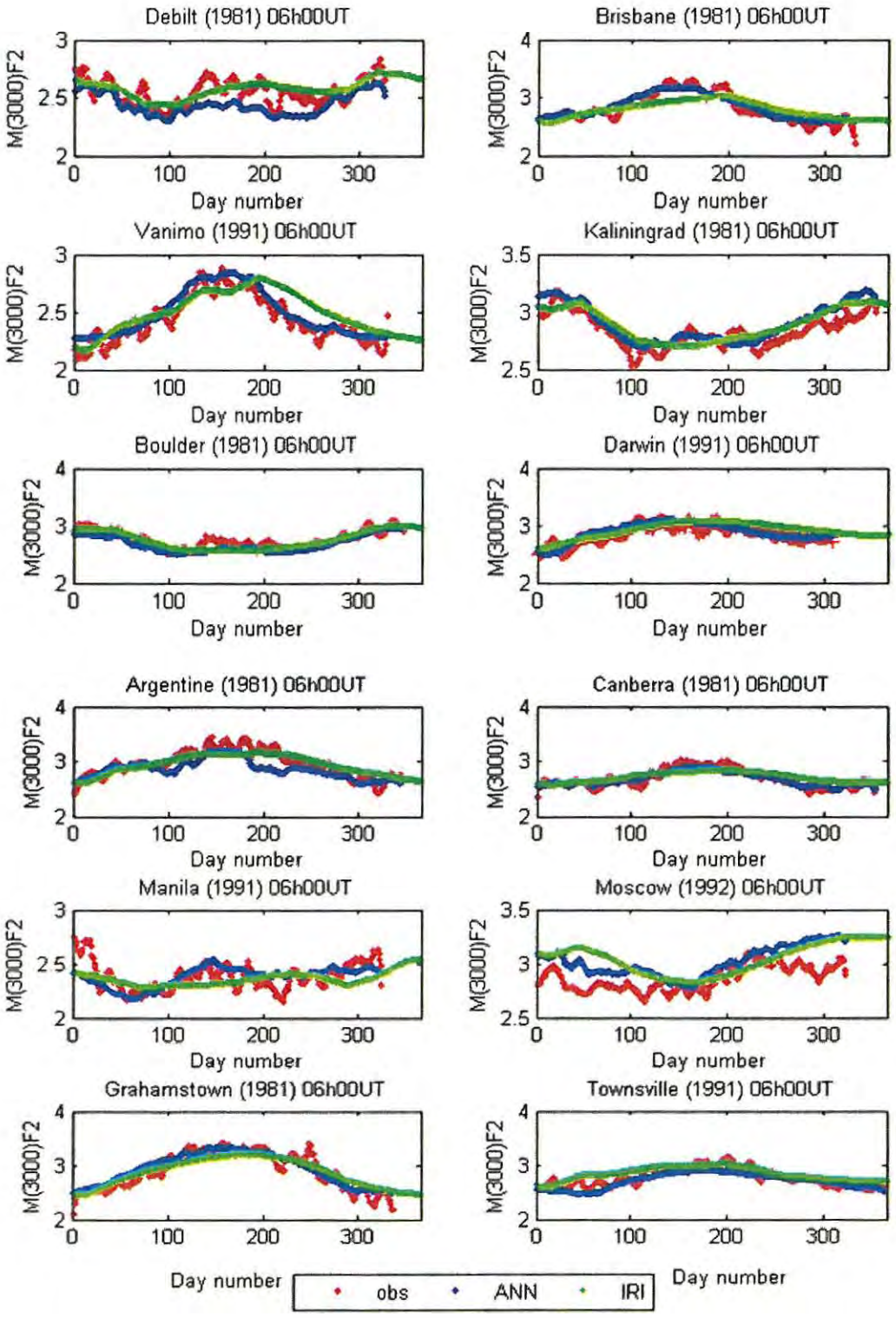

Figure 4.18: Comparison of seasonal variations of M(3000)F2 values predicted by the ANN and the IRI models with respect to the observed values around HSA at 06h00UT.

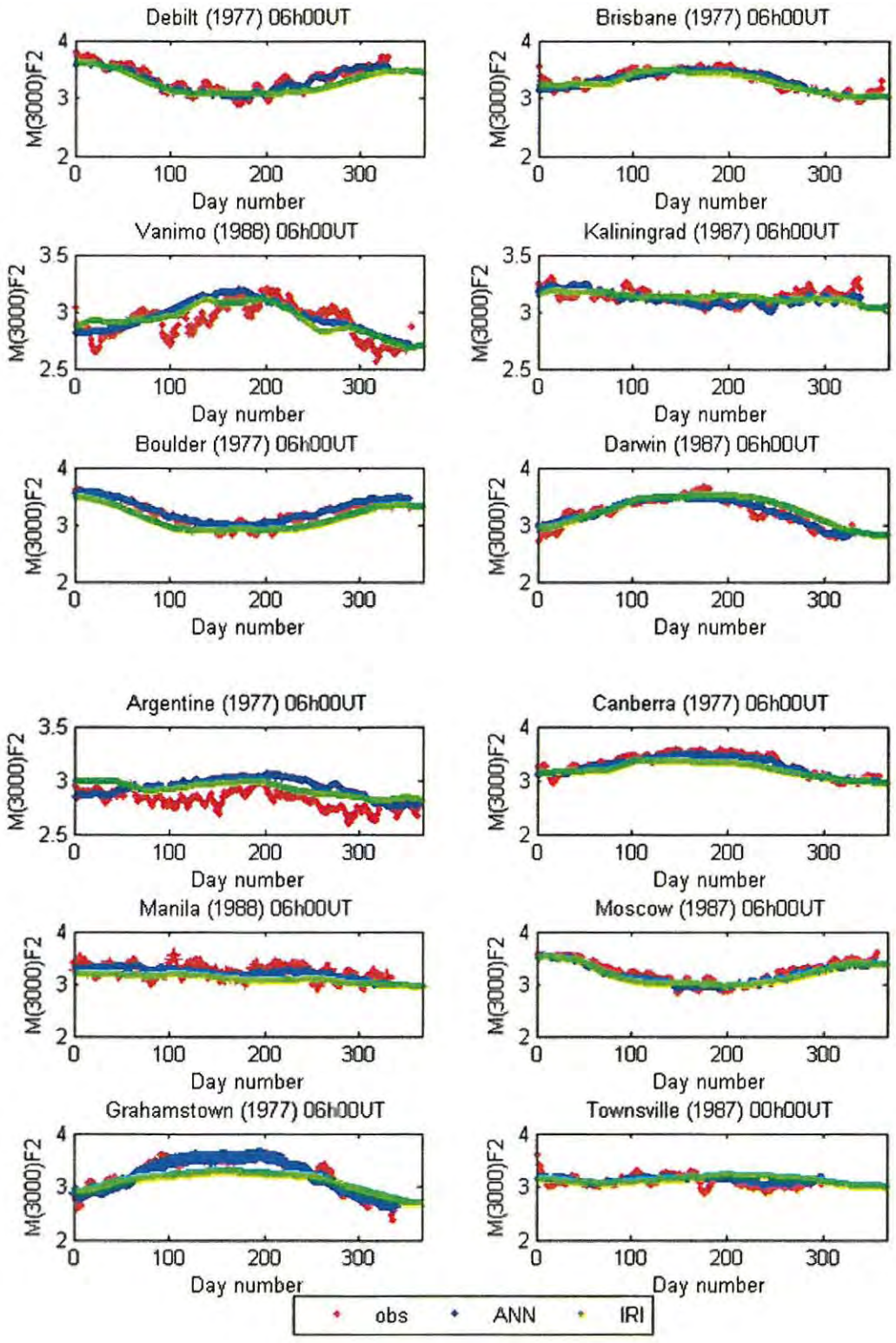

Figure 4.19: Comparison of seasonal variations of M(3000)F2 values predicted by the ANN and the IRI models with respect to the observed values around LSA at 06h00UT.

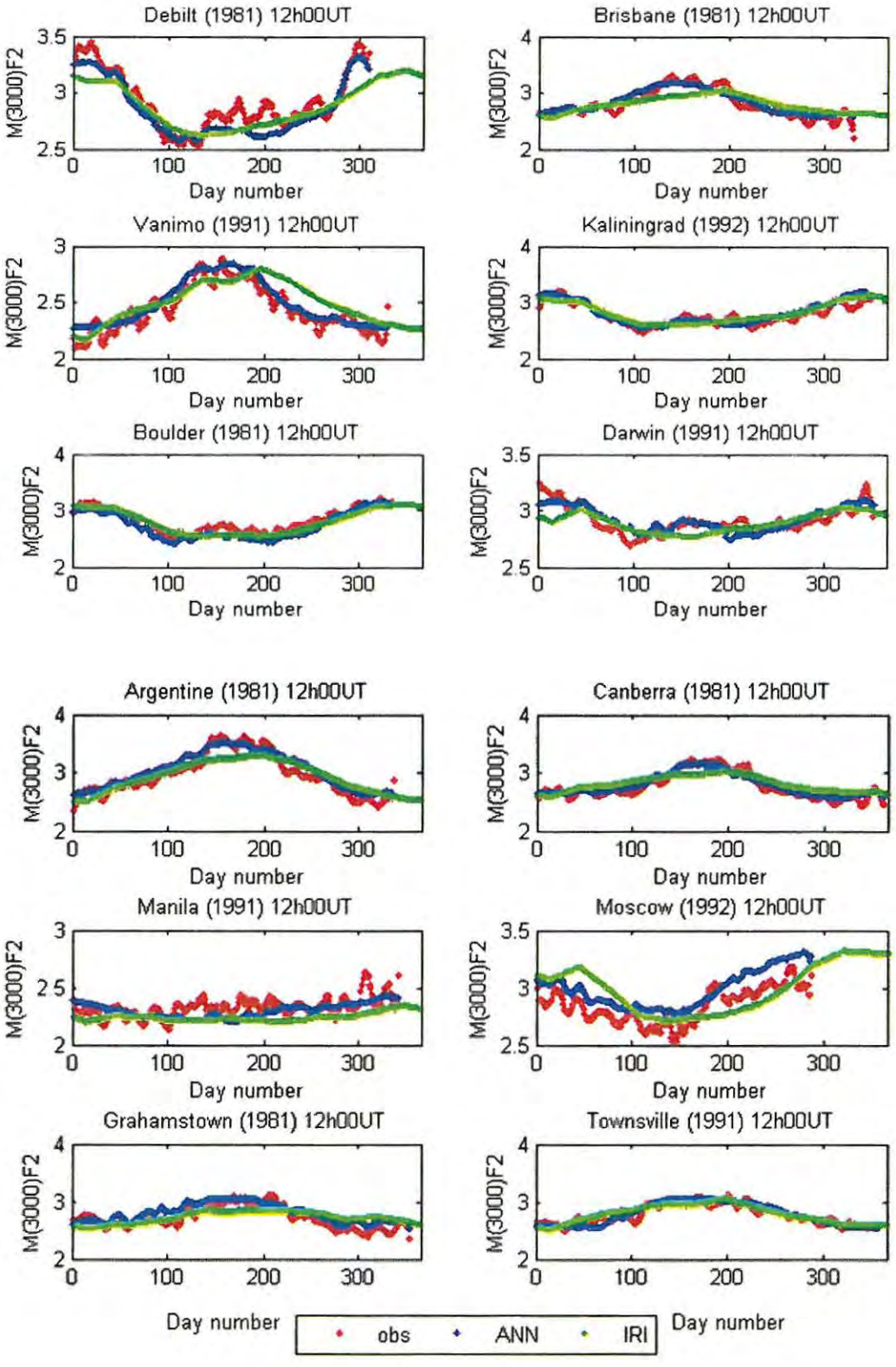

Figure 4.20: Comparison of seasonal variations of M(3000)F2 values predicted by the ANN and the IRI models with respect to the observed values around HSA at 12h00UT.

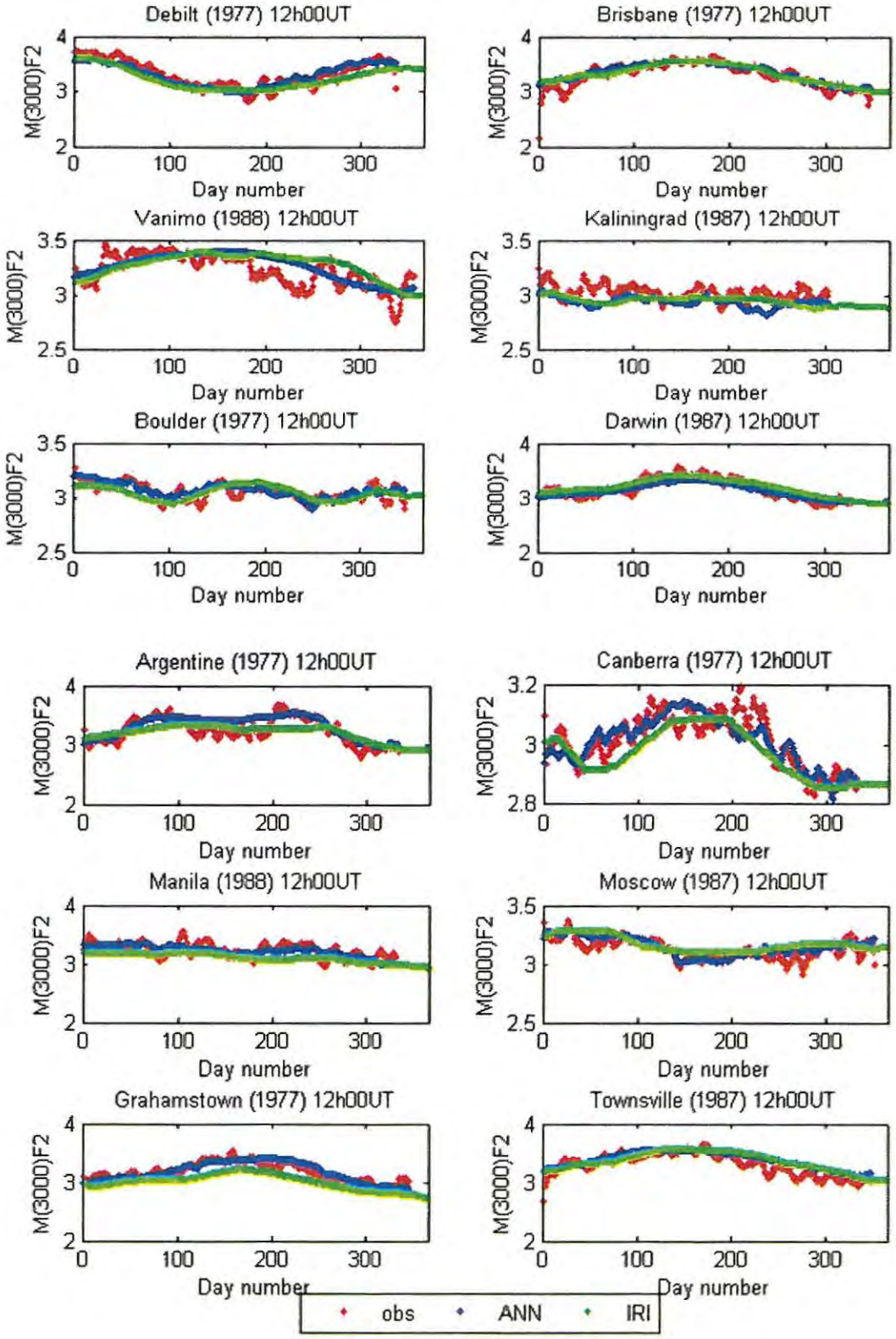

Figure 4.21: Comparison of seasonal variations of M(3000)F2 values predicted by the ANN and the IRI models with respect to the observed values around LSA at 12h00UT.

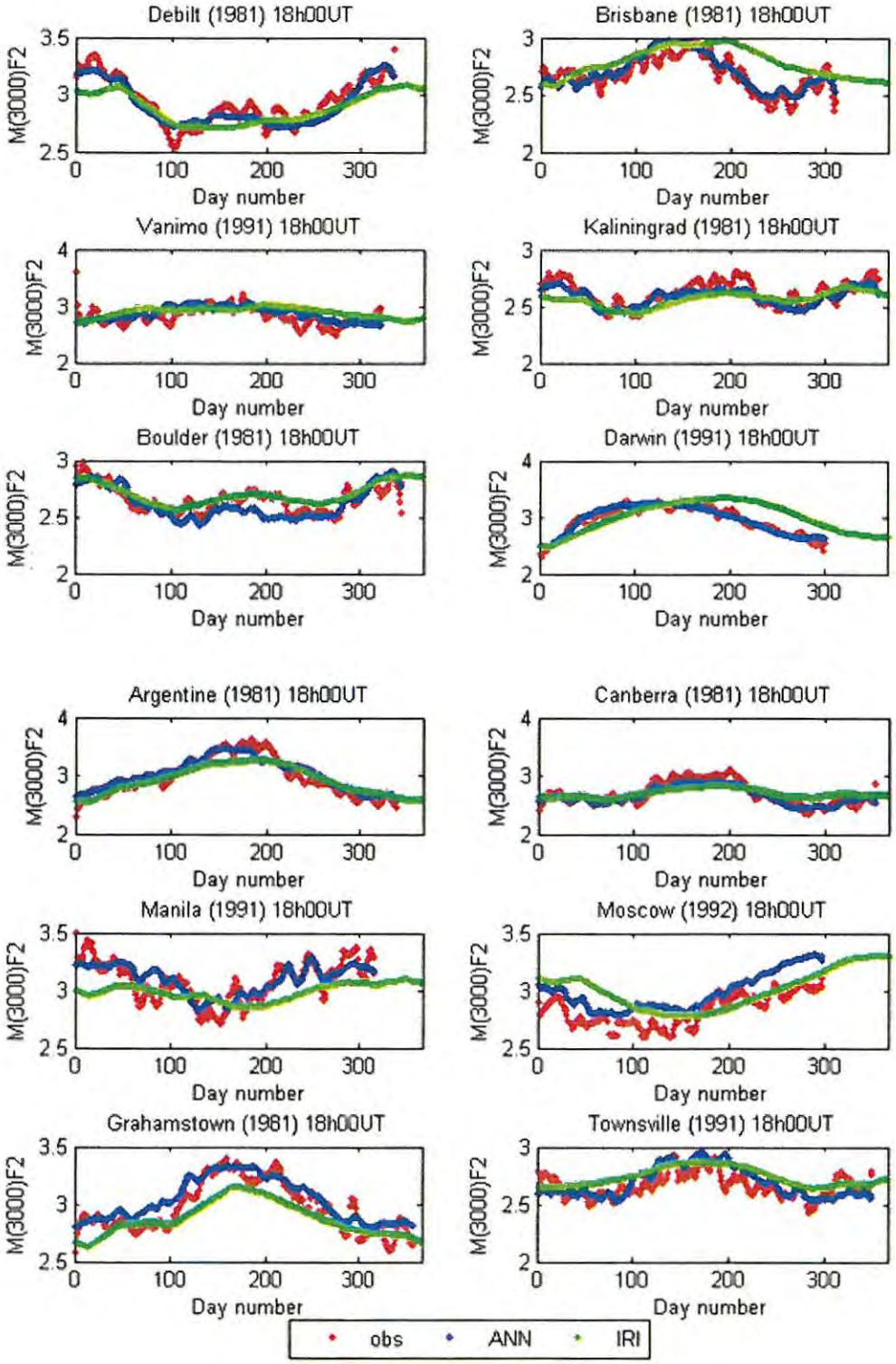

Figure 4.22: Comparison of seasonal variations of M(3000)F2 values predicted by the ANN and the IRI models with respect to observed values around HSA at 18h00UT.

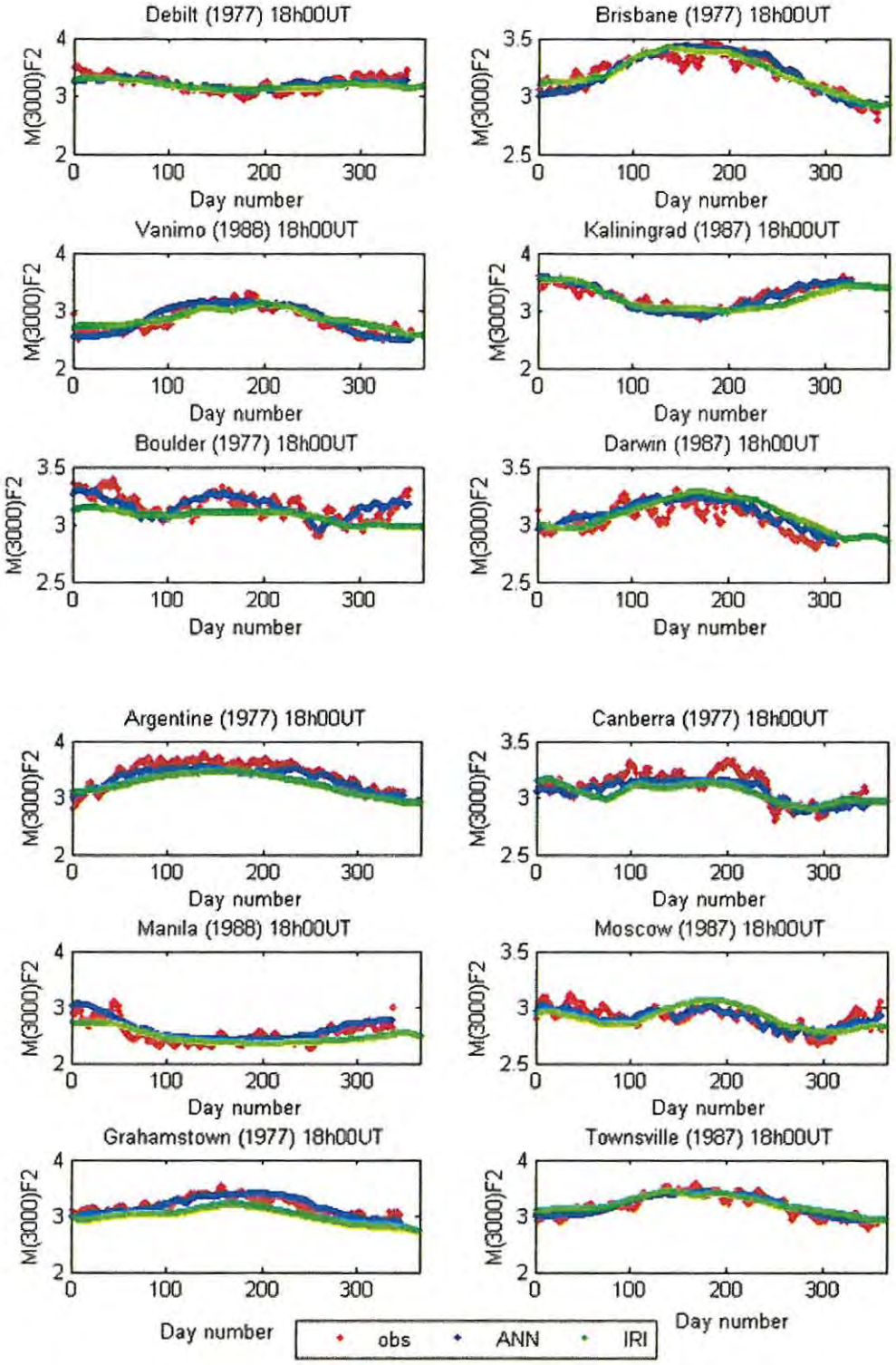

Figure 4.23: Comparison of seasonal variations of M(3000)F2 values predicted by the ANN and the IRI models with respect to the observed values around LSA at 18h00UT.

As can be observed in the figures 4.16 to 4.23, the seasonal variation pattern predicted by the ANN and the IRI M(3000)F2 models are similar. Therefore, the model with better performance cannot be easily deduced from the figures. To determine which of the models is more effective in this regard, the RMSE and the percentage error improvement were evaluated for selected stations. Table 4.6 shows the values of the percentage error and the RMSE obtained for the ANN and IRI M(3000)F2 models. The values indicate that the ANN model is more effective than the IRI version. In those cases where the percentage error has a negative value the IRI model has predicted M(3000)F2 more accurately that the ANN model. However, on the average, the ANN model performs5.68% better than the IRI version when looking at the seasonal variation.

Table 4.6: RMSE values and percentage error difference in M(3000)F2 between the ANN and the IRI-M(3000)F2 models for selected stations.

Station	**Long. (°)**	**Lat (°)**	**RMSE (MHz)**		**% error**	**Year**
			ANN	**IRI**		
Boulder	-105.27	39.99	0.138	0.172	19.77	1981
Brisbane	152.90	-27.50	0.132	0.131	-0.76	1977
Grahamstown	26.50	-33.30	0.170	0.171	0.58	1981
Manila	121.10	14.60	0.243	0.222	-9.46	1988
Darwin	130.90	-12.40	0.155	0.173	10.4	1991
Townsville	146.70	-19.30	0.154	0.194	20.62	1991
Moscow	37.30	55.50	0.158	0.164	3.66	1987
Kaliningrad	20.60	54.70	0.141	0.154	8.44	1981
Debilt	5.20	52.10	0.204	0.203	-0.49	1977
RMSEaverage			0.166	0.176	5.68	

4.5 Comparison of the ANN Model and the Oyeyemi et al. (2007) Model

The comparison of the ANN model and the model of Oyeyemi et al. (2007) (referred to as NNO) is presented here. The performance of the ANN model over the IRI model has been established in sections 4.3 and 4.4. The NNO version of M(3000)F2 also showed a remarkable performance over the IRI version (see Oyeyemi et al., 2007), except for the equatorial region which was under-represented. The aim of this research is to build on the work of Oyeyemi et al. (2007) and produce an improved updated M(3000)F2 model. Therefore, it was necessary to undertake a validation of the new ANN model compared to the NNO model, and to quantify the improvement.

A comparison with the RMSE values for NNO obtained by Oyeyemi et al., (2007) was performed. The percentage improvement was evaluated using the relation:

$$\left(\frac{NNO\_RMSE - ANN\_RMSE}{NNO\_RMSE}\right)\times 100\% \qquad 4.3$$

where NNO_RMSE and ANN_RMSE are the RMSE values for the NNO and the ANN models respectively. The percentage difference and the RMSE values are presented in Table 4.7. The evaluation of the RMSE and the percentage improvement was performed around HSA (1991, 1992 & 1999) and LSA (1987, 1988 & 1997) accordingly.

Table 4.7: The RMSE values and the percentage error difference in M(3000)F2 between the ANN and the NNO models around HSA and LSA period respectively.

Stations	**Long. (°)**	**Lat.(°)**	**RMSE (MHz): HSA**				**RMSE (MHz): LSA**			
			ANN	**NNO**	**%error**	**Year**	**ANN**	**NNO**	**%error**	**Year**
Argentine	-64.30	-65.20	0.249	0.310	19.68	1992	0.198	0.226	12.39	1987
Boulder	-105.30	40.00	0.148	0.150	1.33	1991	0.169	0.163	-3.68	1987
Grahamstown	26.50	-33.30	0.150	0.175	14.29	1992	0.236	0.237	0.42	1988
Macquarie	159.00	-54.50	0.156	0.158	1.27	1992	0.159	0.165	3.64	1987
Moscow	37.30	55.50	0.211	0.230	8.26	1992	0.144	0.145	0.69	1987
Mundaring	116.20	-32.00	0.161	0.164	1.83	1991	0.170	0.175	2.86	1987
Uppsala	17.60	59.80	0.150	0.165	9.09	1999	0.164	0.185	11.35	1997
Wallops	-75.47	37.94	0.257	0.241	-6.64	1991	0.180	0.176	-2.27	1987
Magadan	151.00	60.00	0.169	0.181	6.63	1991	0.151	0.167	9.58	1987
$RMSE_{average}$			0.183	0.197	7.11		0.175	0.182	3.85	

Table 4.7 shows that the ANN model has lower RMSE values compared to the NNO model. There are some stations where the NNO model performs better than the ANN model, but the percentage is not significant enough to outweigh the performance of the ANN model. Observe that some values of the percentage error difference are "negative" which indicate that the ANN model does not predict well for those stations during the specified period of solar activity, compared to the NNO model. However, the average RMSE value and its percentage error values portray the general performance of the ANN model over the NNO version. The average percentage improvement of the ANN model over NNO version is 7.11% and 3.85% for HSA and LSA periods respectively.

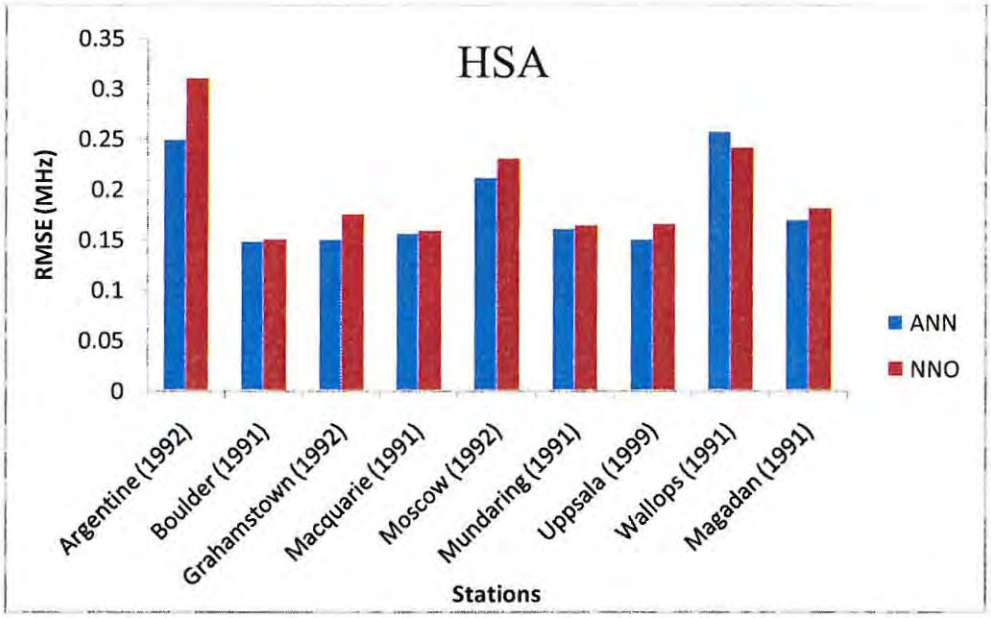

Figure 4.24: Graphical representation of RMSE values between the observed M(3000)F2 values and the predicted values of the ANN and the NNO models around the period of HSA.

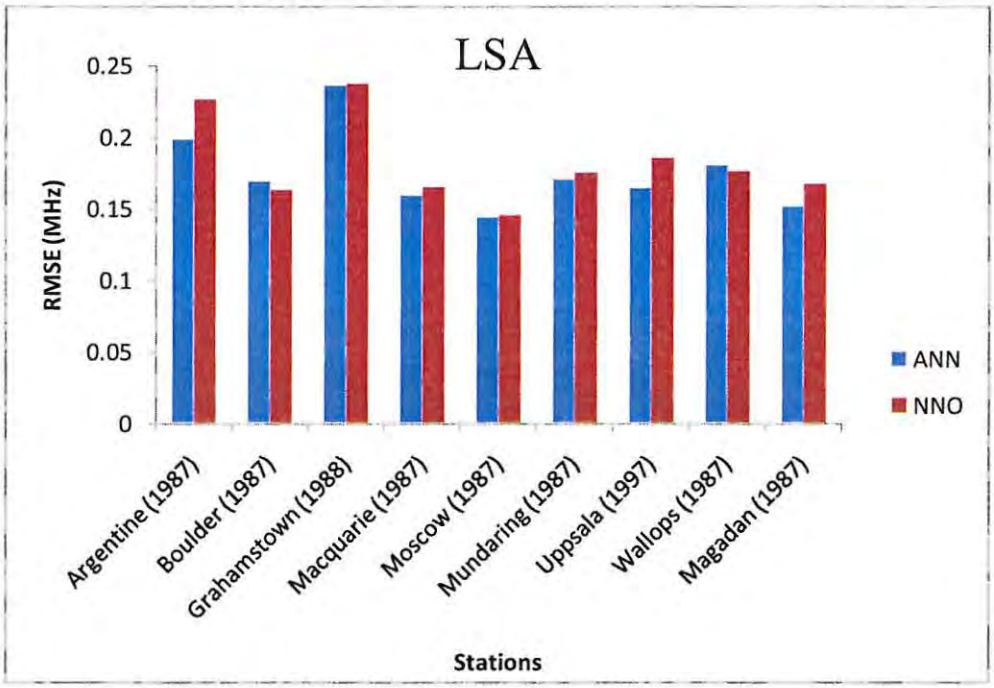

Figure 4.25: Graphical representation of RMSE values between the observed M(3000)F2 values and the predicted values of the ANN and the NNO models around the period of LSA.

Figures 4.24 and 4.25 are graphical representations of the RMSE values obtained from the NNO and the ANN models around the period of HSA and LSA periods respectively. As can be observed from the figures, the ANN model shows significant improvement over the NNO model at the majority of the stations specified. Figure 4.26 is a graphical representation of the average RMSE values obtained for both the NNO and the ANN models around HSA and LSA periods.

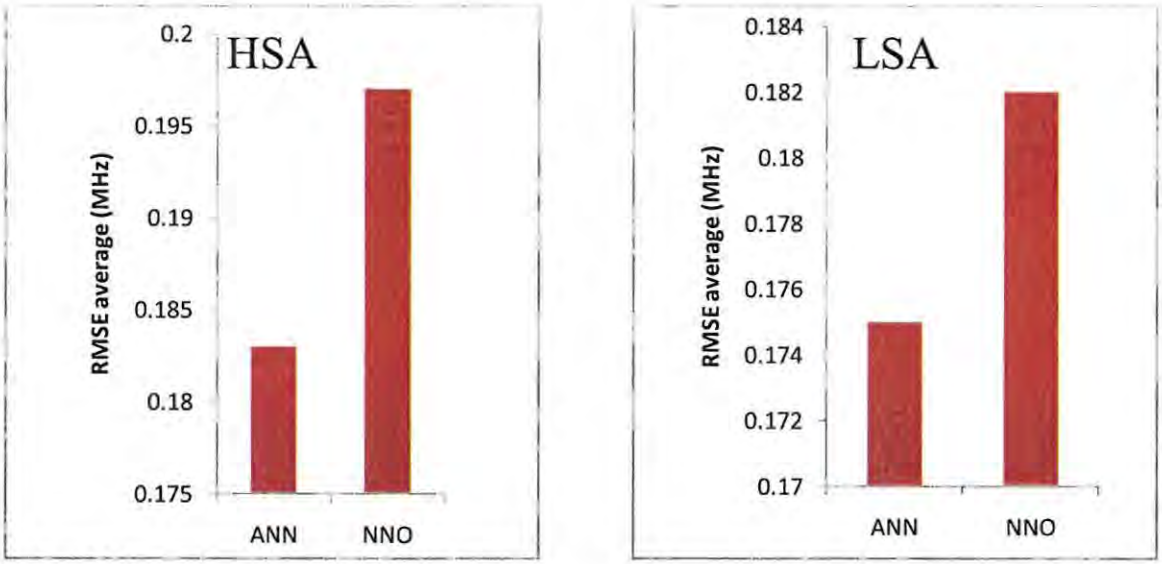

Figure 4.26: Graphical representation of the average RMSE values of the predicted values of the ANN and the NNO models at some verification stations around the period of HSA and LSA respectively.

The average percentage error difference between the ANN and the NNO models are 3.85% and 7.11% for HSA and LSA periods respectively. The ANN model has smaller average RMSE value (0.183 and 0.175) compared to the NNO version (0.197 and 0.182) around the HSA and LSA periods. This is a clear indication of the overall general performance of the ANN model over the NNO version. Hence, the ANN model is an improvement on the NNO model and the IRI version in general.

4.6 Conclusion

The input space variable established for modeling the M(3000)F2 parameter in Chapter 3 was applied for the global modeling of the M(3000)F2 variable in this chapter. Different neural network architectures were trained, and the architecture with the least RMSE was chosen as the network for the M(3000)F2 global model.

A comparison of the ANN and the IRI models based on the RMSE evaluation shows that the ANN model is better at predicting the M(3000)F2 parameter than the IRI M(3000)F2 model. The correlation coefficients reaffirmed the results of the RMSE evaluation.

The diurnal and seasonal variations of the M(3000)F2 predicted by the ANN and the IRI M(3000)F2 models were also compared with respect to the observed values. The results also indicate an improved performance of the ANN model over the IRI model.

The ability of the ANN model to predict the diurnal pattern as well as the post-sunset values of the M(3000)F2 parameter in the low latitude region was also investigated. The ANN model was found to predict more accurately the diurnal structure as well as the post-sunset values of the M(3000)F2 values in the low latitude region than the IRI version. This is an important result, as previous studies showed the inability of the IRI model in reproducing the post-sunset variability of the M(3000)F2 parameter (Adeniyi et al., 2003; Obrou et al., 2003).

The ANN model was also found to be an improvement on the NNO model based on the evaluation of the RMSE and the average RMSE. Although the percentage improvement shown was not very significant, it should be noted that there is an improvement in the input space that provides for a better integration into the IRI model. The results obtained in this chapter demonstrate the ability of the ANN model to better predict both spatially and temporally, the M(3000)F2 parameter than the IRI version on a global scale, and is an improved version of the earlier developed model (Oyeyemi et al., 2007).

Chapter 5

Conclusion

5.1 Introduction

This study utilised the ANN technique to update and improve on the existing neural network-based global empirical model for the M(3000)F2 ionospheric parameter, using the relevant extended geophysical input space variables. The original model was developed by Oyeyemi et al. (2007). Although the technique has been applied successfully by some authors for single station and global modelling of the M(3000)F2 parameter (Xenos, 2002; McKinnell and Oyeyemi, 2010), this work is another version of the neural network based model which aimed at addressing the inadequacies of the existing NNO model and the IRI M(3000)F2 model.

5.2 Summary

The archived database of daily hourly values of the M(3000)F2 parameter recorded by the global network of ground ionosondes worldwide was used in this study. Data from 80 ionospheric stations spanning the period from 1986 to 2008 and covering all periods of both low and high activity were used for training the network for the M(3000)F2 global model.

As a result of the numerous geophysical parameters which are known to influence the M(3000)F2 parameter, a preliminary study was carried out to investigate the parameters that would be most appropriate for M(3000)F2 global modelling. Data from 20 ionospheric stations across the various geographical regions were used for training six different neural networks. A comparison of the different neural networks with respect to the M(3000)F2 IRI-2007 version was carried out. The result revealed the varying potential of the different neural networks trained in predicting the M(3000)F2 parameter. The major finding of this study was that the optimum input space to this model should consist of the following: day number (DNS and DNC), hour of the day (HS and HC), solar zenith angle (SCHI and CCHI), Modified dip latitude (Modip), 81-day running mean of daily F10.7 (SF81), global ionospheric index based on ionosonde (SG12), ap index (A16), longitude (Long) and latitude (Lat). This finding was based on the root mean square error (RMSE) evaluation for each of the networks.

The established input variables were used to train the global M(3000)F2 model as presented in Chapter 4. A comparison of the RMSE values and correlation coefficients obtained for the ANN model and the M(3000)F2 IRI-2007 model was carried out. The ANN model shows an improved performance over the IRI version, with percentage improvement of 13.04% and

10.05% around HSA and LSA periods respectively. The diurnal and seasonal variation of the M(3000)F2 values predicted by the ANN model and the IRI version were compared with respect to the observed values. Both models reproduced the expected diurnal and seasonal structure of the M(3000)F2 parameter. However, the ANN-predicted values show a better representation of the diurnal and seasonal pattern of M(3000)F2 values compared to the IRI-M(3000)F2 model.

The ability of the ANN model to reproduce the diurnal structure as well as the post-sunset values of M(3000)F2 in the low latitude region was also investigated. The result of this investigation shows that the ANN model has more potential in reproducing the diurnal structure as well as the post-sunset values of the M(3000)F2 in the low latitude region than the IRI version. This is a remarkable result which addresses the limitations of the IRI M(3000)F2 model earlier pointed out by Obrou et al. (2003), Adeniyi et al. (2003), Zhang et al. (2004 and 2007).

The values of M(3000)F2 predicted by the NNO and the ANN models were also compared based on their RMSE values. The ANN model was also found to show an improvement on the NNO model. Although the percentage improvement is not significant, the input parameters used in the ANN model are more adaptable for incorporation into the IRI model than the input parameters used in the NNO model, and thus reduce complexity in the IRI model. Again, the improved representation of the low-latitude region in the ANN model is also a significant improvement of the ANN model on the NNO model.

The satisfactory results presented in this work, shows significant improvement over the NNO model and the IRI M(3000)F2 model, and therefore, demonstrates the potential of the ANN model in predicting M(3000)F2 values both spatially and temporally on a global scale.

5.3 Recommendations

This study provides a satisfactory model for predicting the M(3000)F2 values globally. However, there is room for improving the global modelling of this parameter. The major limitation of this work is the uneven distribution of ionosonde stations globally. In some areas where ionosonde stations are available, the data from such stations are characterised with missing data points. Habarulema (2010) pointed out, that in order to develop a global and fully representative ionospheric model continuously available ionospheric data is necessary.

In spite of the paucity of data for some geographical regions (e.g. the low-latitude region), the result of the analysis of the ANN predicted values presented in this work shows that the ANN

model is capable of predicting the M(3000)F2 values at any geographical region at any given time.

To enhance the performance of the ANN-based M(3000)F2 model, efforts should be made to increase the number of ionospheric stations especially in the African region, as this will enhance the development of a global and fully representative M(3000)F2 model. Future work should include the periodic update of this model as more data becomes available, and more extensive investigations on the ability of the model to reproduce M(3000)F2 values under all conditions.

The result presented in this study shows that the ANN model is capable of replacing the IRI M(3000)F2 model, hence, it should be incorporated into the IRI model for the M(3000)F2 parameter.

REFERENCES

Adeniyi, J.O., Bilitza, D., Radicella, S.M., and Willoughby, A.A.: Equatorial F2-peak parameters in the IRI model. Advances in Space Research, 31, 507-512, 2003.

Bailey, G.J., Su, Y.Z. and Oyama, K.I.: Yearly variations in the low latitude topside ionosphere. Annales Geophysicae, 18, 789-798, 2000.

Berry, M.J.A. and Linoff, G.: Data mining techniques for marketing, sales, and customer support. New York: John Wiley & Sons, 1997.

Bilitza, D., Sheikh, N.N. and Eyfrig, R.: A global model for the height of the F-2peak using M3000 values from the CCIR numerical maps. Telecommunications Journal, 46, 549-553, 1979.

Bilitza, D.: International Reference Ionosphere 1990. Report 90-22, Greenbelt, MD: National Science Data Center, 1990.

Bilitza, D., Bhardwaj S., Koblinsky C.: Improved IRI predictions for the GEOSAT time period. Advances in Space Research, 20, 1755-1760, 1997.

Bilitza, D.: The importance of EUV indices for the International Reference Ionosphere, Physics and Chemistry of the Earth(c). 25, 515-521, 2000.

Bilitza, D.: International Reference Ionosphere 2000. Radio Science, 36, 261 – 275, 2001.

Bilitza, D.: Ionospheric models for radio propagations studies. In Review of radio Science 1999-2002, Piscataway NJ: IEEE Press, 2002, 625-679.

Bilitza, D.: The International Reference Ionosphere-climatological standard for the ionosphere. In characterising the ionosphere proceedings RTO-MP-IST-056, Neuilly-sur-Seine, France: RTO, 2006, 32-1 – 32-12.

Bilitza, D. and Reinisch, B.W.: International Reference Ionosphere 2007: improvements and new parameters. Advances in Space Research, 42, 599-609, 2007.

Bonnet, R. and Woltjer, L.: Surviving 1,000 centuries: can we do it?, Chichester: Praxis Publishing, 2008.

Bradley, P. A. and Dick, M. I.: Use of ground-based and satellite data for an improved procedure for testing the accuracy of ionospheric maps, Technical report, Chilton: Rutherford Appleton Laboratory, 1997.

Bradley, P.A.: PRIME, prediction and retrospective ionospheric modelling over Europe; final reports to project COST238. Chilton: Rutherford Appleton Laboratory, 1999.

Bradley, P.A. and Dudeney, J.R.: A simple model of the vertical distribution of electron concentration in the ionosphere. Journal of Atmospheric and Terrestrial Physics.35, 2131-2146, 1973.

CCIR, Comite Consultatif International des Radiocommunications. Reports 340, 340-2 and later supplements, Geneva, 1967.

Duncan, R.A.: F-regions seasonal and magnetic-storm behaviour. Journal of Atmospheric and Terrestrial Physics, 31, 59-70, 1969.

Enquist, M. and Ghirlanda, S.: Neural networks and animal behaviour. New Jersey: Princeton University Press, 2005.

Fausett, L.: Fundamentals of neural networks; architectures, algorithms and applications. Eaglewood Cliffs NJ: Prentice-Hall, 1994.

Forbes, J.M., Scott, E.P. and Xiaoli Z.: Variability of the ionosphere. Journal of Atmospheric and Solar-Terrestrial Physics, 62, 685-693, 2000.

Fox, M.W. and McNamara, L.F.: Improved world-wide maps of monthly median of foF2. Journal of Atmospheric and Terrestrial Physics, 50, 1077-1086, 1988.

Fuller-Rowell, T.J., Araujo-Pradere E. and Codrescu M.V.: An empirical ionospheric storm-time correction model. Advances in Space Research, 25, 139-146, 2000.

Geman, S., Bienenstock, E. and Doursat, R.: Neural networks and the bias/variance dilemma. Neural Computation, 4, 1-58, 1992.

Habarulema, J.B.: A contribution to TEC modelling over Southern Africa using GPS data. PhD thesis, Rhodes University, Grahamstown, South Africa, 2010.

Habarulema, J.B., McKinnell, L.A., Opperman, B.D.L.: Regional GPS TEC modelling; attempted spatial and temporal extrapolation of TEC using neural networks. Journal of Geophysical Research, 116, A04314, 2011.

Habarulema, J.B. and McKinnell, L.A.: Investigating the performance of neural network backpropagation algorithms for TEC estimations using South African GPS data. Annales Geophysicae, 30, 857–866, 2012.

Hargreaves, J.K.: The upper atmospheric and solar-terrestrial relations: an introduction to the aerospace environment. New York: Van Nostrand Reinhold Company, 1979.

Haykin, S.: Neural networks: A comprehensive foundation. New York: Macmillan, 1994.

Hunsucker, R.D. and Hargreaves, J.K.: The high-latitude ionosphere and its effects on radio propagation. Cambridge: Cambridge University Press, 2003.

Jones, W.B. and Gallet R.M.: The representation of diurnal and geographic variations of ionospheric data by numerical methods. Telecommunications Journal, 29,129-149, 1962.

Jones, W.B. and Gallet R.M.: The representation of diurnal and geographic variations of ionospheric data by numerical methods. Telecommunications Journal, 32, 18-28, 1965.

King, J.W. and Smith P.A.: The seasonal anomaly in the behaviour of the F2-layer critical frequency. Journal of Atmospheric and Terrestrial Physics, 30, 1707-1713, 1968.

Lamming, X. and Cander, L.R.: Monthly median foF2 modelling COST 251 area by neural networks. Physics and Chemistry of the Earth (c).24, 349-354, 1999.

Leandro, R. F. and Santos, M. C.: A neural network approach for regional vertical total electron content modelling. Studia Geophysicaet Geodaetica, 51, 279–292, 2007.

Liu, J.Y., Chen, Y.I. and Lin, J.S.: Statistical investigation of the saturation effect in the ionospheric foF2 versus sunspot, solar radio noise, and solar EUV radiation. Journal of Geophysical Research, 108, A21067, 2003.

Liu, L., He, M., Yue, X., Ning, B. and Wan, W.: Ionosphere around equinoxes during low activity. Journal of Geophysical Research; 115, A09307, 2010.

Liu, L., Wan, W. and Ning B.: Statistical modelling of ionospheric foF2 over Wuhan. Radio Science, 39, RS2013, 2004.

Liu, C., Zhang, M. L., Wan, W., Liu, L., and B. Ning.: Modelling M(3000)F2 based on empirical and orthogonal function analysis method. Radio Science, 43, RS1003, 2008.

Lundstedt, H., Gleisner, and Wintoft, P.: Operational forecasts of the geomagnetic Dst index. Geophysical Research Letters, 29, 2181, 2002.

McKinnell L.A.: A new empirical model for the peak ionospheric electron density using neural networks. MSc thesis, Rhodes University, Grahamstown, South Africa, 1996.

Mckinnell, L. A., and Poole, A.W.V.: Neural network-based ionospheric modelling over the South Africa region, South African Journal of Science, 100, 519-523, 2004.

Mckinnell, L. A. and Poole, A.W.V.: The development of a neural network based short term foF2 forecast program. Physics and Chemistry of the Earth, 25, 287-290, 2000.

McKinnell, L.A. and Oyeyemi, E.O: Equatorial predictions from a new neural network based global foF2 model. Advances in Space Research, 46, 1016-1023, 2010.

McNamara, L. F.: The Ionosphere: communications, surveillance, and direction finding. Malabar FL: Krieger, 1991.

McNamara, L.F.: Radio amateurs guide to the ionosphere. Malabar FL: Krieger, 1994.

Obrou, O.K., Bilitza, D., Adeniyi J.O., Radicella S.M.: Equatorial F2-layer peak height and correlation with vertical ion drift and M(3000)F2. Advances in Space Research, 31, 513520, 2003.

Oyeyemi, E.O.: A global ionospheric F2 region peak electron density model using neural networks and extended geophysically relevant inputs, PhD thesis, Rhodes University, Grahamstown, South Africa, 2005.

Oyeyemi, E.O., McKinnell, L. A., and A. Poole, A.W.V.: Neural network based prediction techniques for global modelling of M(3000)F2 ionosheric parameter. Advances in Space Research, 39, 643-650, 2007.

Piggott, W.R. and Rawer, K.: U.R.S.I. handbook of ionogram interpretation and reduction, Report number UAG 23, (2nd edition). Boulder, CO: World Data Centre A, NOAA, 1972.

Piggott, W.R. and Rawer, K.: Revision of chapters 1-4 of the U.R.SI. handbook on ionogram interpretation and reduction, Report number UAGA 23. Boulder, CO: World Data Centre A, NOAA, 1978.

Poole, A.W.V. and McKinnell, L.A.: On the predictability of foF2 using neural networks. Radio Science, 35, 225-234, 2000.

Rawer, K. (ed): Encyclopedia of Physics, Geophysics III, part VII. Berlin: Springer-Verlag, 387-391, 1984.

Richards, P.G.: Seasonal and solar cycle variations of the ionospheric peak electron density: comparison of measured and models. Journal of Geophysics Research, 106, A712803-12819, 2001.

Rishbeth, H., Setty, C.S.G.K.: The F-layer at sunrise, Journal of Atmospheric and Terrestrial Physics, 20, 263-276, 1961.

Rishbeth, H.: The effect of winds on the ionospheric F2-peak. Journal of Atmospheric and Terrestrial Physics, 29, 225-238, 1967.

Rishbeth, H. and Garriott, O.K.: Introduction to ionospheric physics. New York: Academic press, 1969.

Rishbeth, H. and Mendillo, M.: Patterns of F2-layer variability. Journal of Atmospheric and Solar-TerrestrialPhysics, 63, 1661-1680, 2001.

Rishbeth, H.: How the thermospheric composition affects the ionospheric F2-layer. Journal of Atmospheric and Solar-Terrestrial Physics, 60, 1385-1402, 1998.

Rojas, R.: Neural networks – A systematic introduction. Berlin: Springer-Verlag, 1996

Rush, C.M., Pokempner, M., Anderson, D.N., Stewart, F.G. and Perry, J.: Improving ionospheric maps using theoretically derived values of foF2. Radio Science, 28, 95-107, 1983.

Rush, C.M., Pokempner, M., Anderson, D.N. and Stewart, F.G.: Perry J.: Maps of foF2 derived from observations and theoretical data. Radio Science, 19, 1083-1097, 1984.

Rush, C.M., Fox, M., Bilitza, D., Davies, K., McNamara, L., Stewart, F. and PoKempner, M.: Ionospheric mapping: an update of foF2 coefficients. Telecommunications Journal, 56, 179-182, 1989.

Sethi, N.K., Goel, M.K. and Mahajan, K.K.: Solar cycle variations of foF2 from IGY to 1990. Annales Geophysicae, 20, 1677-1685, 2002.

Sibanda, P.: Challenges in topside ionospheric modelling over South Africa. PhD thesis, Rhodes University, Grahamstown, South Africa, 2010.

SNNS, Stuttgart Neural Network Simulator user manual, version 4.2.Stuttgart: University of Stuttgart, Institute for Parallel and Distributed High Performance Systems, 1995a.

SNNS, Stuttgart Neural Network Simulator. Website: http://wwwra.informatik.uni-tuebingen.de/SNNS/, 1995b.

Space Physics Interactive Data Resource (SPIDR) website: http://spidr.ngdc.noaa.gov/spidr/, October 2011.

Tulunay E, Özkaptan C., Tulunay Y.: Temporal and spatial forecasting of the foF2 values up to twenty four hours in advance. Physics and Chemistry of the Earth(c).25, 281-285, 2000.

Vandegriff, J., Wagstaff, K., Ho, G., and Plauger, J.: Forecasting space weather: predicting interplanetary shocks using neural networks. Advances in Space Research, 36, 2323–2327, 2005.

Werbos, P.J.: Beyond regression: new tools for prediction and analysis in the behavioural sciences, PhD thesis, Harvard University, 1974.

Wells, R.: Synaptic weight modulation and adaptation: a technical strategy brief for the neurofuzzy soft computing program, May 15, 2003.

Williscroft L.A., A.W.V. Poole.: Neural networks, foF2, sunspot and magnetic activity. Geophysical Research Letters, 23, 3659-3662, 1996.

Wintoft, P. and Cander L.R.: Short-term prediction of foF2 using time delay neural networks. Physics and Chemistry of the Earth (c). 24, 343-347, 1999.

Wright, J.W.: The F-region seasonal anomaly. Journal of Geophysics Research, 68, 4379-4381, 1963.

Xenos, T. D.: Neural-network-based prediction techniques for single station modelling and regional mapping of the foF2 and M(3000)F2 ionospheric characteristics. Nonlinear Process in Geophysics, 9, 477-486, 2002.

Yilmaz, A., Akdogan, K. E., and Gurun, M.: Regional TEC mapping using neural networks, Radio Science, 44, RS3007, 2009.

Zell, A., Mamier, G., Vogt, M., Mache, N., Hubner, R., Doring, S., Herrmann, K.-U., Soyez, T., Schmalzl, M., Sommer, T., Hatzigeorgiou, A., Posselt, D., Schreiner, T., Kett, B., Clemente, G.,Wieland, J., and Gatter, J.: Stuttgart neural network simulator (SNNS),

user manual, version 4.2, Universities of Stuttgart and Tubingen, and the European Particle Research Lab, CERN, Geneva, 1998.

Zhang, M.L., Shi, J.K., Wang, X., Wu, S.Z. and Zhang, S.R.: Comparative study of ionospheric characteristic parameters obtained by DPS-4 digisonde with IRI2000 for low-latitude station in China. Advances in Space Research, 33, 869-873, 2004.

Zhang, M.L., Shi, J.K., Wang, X., Shang, S.P. and Wu, S.Z.: Ionospheric behaviour of the F2 peak parameters foF2 and hmF2 at Hainan and comparisons with IRI Model predictions. Advances in Space Research, 39, 661-667, 2007.

Zhang, M.L., Liu, C., Wan, W., Liu, L. and Ning, B.: Evaluation of global modelling of M(3000)F2 and hmF2 based on alternative empirical orthogonal function expansions. Advances in Space Research, 46, 2010.

APPENDIX A

GLOBAL IONOSPHERIC STATIONS

Table A. 1:Ionospheric Stations where data was available for M(3000)F2 global modelling.

Station	Code	Long(°)	Lat (°)
Akita	AK539	140.1	39.7
AlmaAta	AA343	76.9	43.2
Amderma	AM269	61.4	69.5
Anyang	AN438	126.9	37.4
Argentia	AFJ49	-54	47.3
Argentine	AIJ6N	-64.3	-65.2
Arkhangelsk	AZ163	40.5	64.6
Ascension	AS00Q	-14.4	-7.95
Ashkhabad	AS237	58.3	37.9
Athens	AT138	23.6	38
Bekescsaba	BH148	21.2	46.7
Bermuda	BJJ32	-64.7	32.4
Bombay	BM219	72.8	19
Boulder	BC840	-105.27	39.99
Brisbane	BR52P	152.9	-27.5
Bundoora	BV53Q	144.6	-37.3
Campbell	CI65K	169.2	-52.5
Camden	CN53L	150.7	-34
Canberra	CB53N	149	-35.3
CapeKennedy	CC929	-80.6	28.4
CapeSchmidt	CE669	179.5	68.8
Capetown	CT13M	18.3	-34.1
Casey	CW46O	110.5	-66.3
Chilton	RL052	-1.3	51.6
Chungli	CL424	121.2	24.9
Churchhill	CH958	-94.2	58.8
College	CO764	-147.99	64.92
Concepcion	CPJ30	-73	-36.6
Dakar	DKA14	-18.4	14.8
Darwin	DW41K	130.9	-12.4
Davis	DV36Q	77.9	-68.6
Debilt	DT053	5.2	52.1
Delebre	EB040	0.3	40.4
Delhi	DH328	77.2	28.6
Dikson	DI373	80.4	73.5
Djibouti	DJ111	42.8	11.5
Dourbes	DB049	4.6	50.1
DyessAFB	DS932	-99.86	32.42
EglinAFB	EG931	-86.7	30.4
ElArenosillo	EA036	-6.7	37.1
Fairford	FF051	-1.8	51.7

Stattion	Code	Long(°)	Lat(°)
Gibilmanna	GM037	14	37.6
Goosebay	GSJ53	-60.46	53.32
Gorky	GK156	44.3	56.1
Grahamstown	GR13L	26.5	-33.3
Halleybay	HBA7N	-26.6	-75.5
HanscomAfb	HAJ43	-71.5	42.6
Havana	HQ924	-82.1	23
Hermanus	HE13N	19.22	-34.42
Hobart	HO54K	147.2	-42.9
Huancayo	HU91K	-75.3	-12
Irkutsk	IR352	104	52.5
Jicamarca	JI91J	-76.8	-12
Johannesburg	JO12O	28.1	-26.1
JuliusruhRugen	JR055	13.4	54.6
Kaliningrad	KL154	20.6	54.7
Karaganda	KR250	73.1	49.8
Kerguelen	KG24R	70.3	-49.4
Khabarovsk	KB548	135.1	48.5
Kheysals	BT280	58	80.6
Kiev	KV151	30.5	50.5
KingSalmon	KS759	-156.6	58.7
Kiruna	KI167	20.4	67.8
Kodaikana	KO310	77.5	10.2
Kokubunji	TO535	139.5	35.7
Kwajalein	KJ609	167.2	9
LaReunion	LR22J	55.9	-21.1
Lannion	LN047	-3.3	48.5
Learmonth	LM42B	114	-21.9
Lindau	LI050	10.1	51.6
Leningrad	LD160	30.7	60
Lerwick	LE061	-1.2	60.1
Lisbonne	LE038	-9.3	38.4
Loparskaya	MM168	33	68
Louisvale	LV12P	21.2	-28.5
Lycksele	LY164	18.8	64.6
Macquariels	MQ55M	159	-54.5
Magadan	MG560	151	60
Manila	MN414	121.1	14.6
Maui	MA720	-156.46	20.76
Mawson	MW26P	62.9	-67.6
MillstoneHill	MHJ45	-71.5	42.61

Station	Code	Long(°)	Lat(°)
Fortaleza	FZA0M	-38.8	-3.7
Gakona	GA762	-145.16	62.41
Narssarssuaq	NQJ61	-45.44	61.16
Nicosia	NC136	33.2	35.1
NiueIsland	ND61R	169.9	19.1
NorfolkIs	NI63_	168	-29
Norilsk	NO369	88.1	69.4
Novokazalinsk	NK246	62.1	45.5
Novosibirsk	NS355	83.2	54.6
Nurmijarvi	NU159	24.6	60.5
Okinawa	OK426	127.8	26.3
Osan	SN437	127.1	37.2
Ottawa	OT945	-75.9	45.4
Ouagadougou	OU012	-1.5	12.4
Petropavlovsk	PK553	158.7	53
Podkamennaya	TZ362	90	61.6
PointArguello	PA836	-120.53	34.77
Poitiers	PT046	0.3	46.6
PortStanley	PSJ5J	-57.8	-51.7
Preobrazheniya	PZ374	113	74.7
Pruhonice	PQ052	14.6	50
PuertoRico	PRJ18	-67.2	18.5
ResoluteBay	RB974	-94.9	74.7
Rome	RO041	12.5	41.8
Rostov	RV149	39.7	47.2
Salekhard	SD266	66.5	66.5
Salisbury	SR53M	138.6	-34.7
SanVito	VT139	17.9	40.7
ScottBase	SQ67Q	166.8	-77.9
Slough	SL051	-0.6	51.5
Sodankyla	SO166	26.6	67.4
Sondrestrom	SMJ67	-50.94	66.99
SouthUist	UI057	-7.3	57.4
StPeterording	PE054	9.3	54
Sverdlovsk	SV256	58.6	56.4
Tahiti	TT71P	-149.3	-17.7
Tashkent	TQ241	69.6	41.3
Terreadelie	THJ77	-68.7	76.4
TiksiBay	TX471	128.9	71.6
Tomsk	TK356	84.9	56.5
Tortosa	EB040	0.3	40.4
Townsville	TV51R	146.7	-19.3
Tromso	TR169	19	69.7
Tucuman	TUJ2O	-65.4	-26.9
Uppsala	UP158	17.6	59.8

Station	Code	Long(°)	Lat(°)
Moscow	MO155	37.3	55.5
Mundaring	MU43K	116.2	-32
Vanimo	VA50L	141.3	-2.7
Wakkanai	WK545	141.7	45.4
Wallops	WP937	-75.47	37.94
Wellen	WE667	-169.8	66.6
Yakutsk	YA462	129.6	62
Zhongshan	ZS36R	76.2	-69.2

APPENDIX B

Table B. 1: Training database for ANN M(3000)F2 Global Model

Station	Code	Long(°)	Lat(°)
AlmaAta	AA343	76.9	43.2
Argentia	AFJ49	-54	47.3
Ascension	AS00Q	-14.4	-7.95
Athens	AT138	23.6	38
Bermuda	BJJ32	-64.7	32.4
Argentine	AIJ6N	-64.3	-65.2
Camden	CN53L	150.7	-34
CapeKennedy	CC929	-80.6	28.4
CapeSchmidt	CE669	179.5	68.8
Casey	CW46O	110.5	-66.3
Chilton	RL052	-1.3	51.6
College	CO764	-147.99	64.924
Akita	AK539	140.1	39.7
Churchhill	CH958	-94.2	58.8
Darwin	DW41K	130.9	-12.4
Delebre	EB040	0.3	40.4
Brisbane	BR52P	152.9	-27.5
Dikson	DI373	80.4	73.5
Dourbes	DB049	4.6	50.1
EglinAFB	EG931	-86.7	30.4
ElArenosillo	EA036	-6.7	37.1
Gakona	GA762	-145.16	62.4072
Anyang	AN438	126.9	37.4
Goosebay	GSJ53	-60.46	53.3162
Gorky	GK156	44.3	56.1
Grahamstown	GR13L	26.5	-33.3
Havana	HQ924	-82.1	23
Hobart	HO54K	147.2	-42.9
Huancayo	HU91K	-75.3	-12
Irkutsk	IR352	104	52.5
Khabarovsk	KB548	135.1	48.5
Kiev	KV151	30.5	50.5
KingSalmon	KS759	-156.6	58.7
Kokubunji	TO535	139.5	35.7
Kwajalein	KJ609	167.2	9
Johannesburg	JO120	28.1	-26.1
Learmonth	LM42B	114	-21.9
Leningrad	LD160	30.7	60
Lerwick	LE061	-1.2	60.1
Loparskaya	MM168	33	68
Louisvale	LV12P	21.2	-28.5

Station	Code	Long(°)	Lat(°)
MacquarieIs	MQ55M	159	-54.5
Magadan	MG560	151	60
Maui	MA720	-156.46	20.7644
Mawson	MW26P	62.9	-67.6
MillstoneHill	MHJ45	-71.5	42.6107
Moscow	MO155	37.3	55.5
Mundaring	MU43K	116.2	-32
Narssarssuaq	NQJ61	-45.44	61.1621
NiueIsland	ND61R	169.9	19.1
Nicosia	NC136	33.2	35.1
Novosibirsk	NS355	83.2	54.6
Okinawa	OK426	127.8	26.3
Osan	SN437	127.1	37.2
Podkamennaya	TZ362	90	61.6
Petropavlovsk	PK553	158.7	53
PortStanley	PSJ5J	-57.8	-51.7
Preobrazheniya	PZ374	113	74.7
PuertoRico	PRJ18	-67.2	18.5
ResoluteBay	RB974	-94.9	74.7
Rostov	RV149	39.7	47.2
Salekhard	SD266	66.5	66.5
Slough	SL051	-0.6	51.5
SanVito	VT139	17.9	40.7
Slough	SL051	-0.6	51.5
Sodankyla	SO166	26.6	67.4
Sondrestrom	SMJ67	-50.94	66.9856
SouthUist	UI057	-7.3	57.4
StPeterording	PE054	9.3	54
Sverdlovsk	SV256	58.6	56.4
Tashkent	TQ241	69.6	41.3
Terreadelie	THJ77	-68.7	76.4
TiksiBay	TX471	128.9	71.6
Tomsk	TK356	84.9	56.5
Tortosa	EB040	0.3	40.4
Dakar	DKA14	-18.4	14.8
Tucuman	TUJ2O	-65.4	-26.9
Vanimo	VA50L	141.3	-2.7
Wakkanai	WK545	141.7	45.4
Lycksele	LY164	18.8	64.6
Lycksele	LY164	18.8	64.6